

**IDENTIFYING IMAGING BIOMARKERS FOR MANGANESE TOXICITY
IN OCCUPATIONALLY EXPOSED WELDERS**

by

David A. Edmondson

A Dissertation

Submitted to the Faculty of Purdue University

In Partial Fulfillment of the Requirements for the degree of

Doctor of Philosophy



School of Health Sciences

West Lafayette, Indiana

May 2019

**THE PURDUE UNIVERSITY GRADUATE SCHOOL
STATEMENT OF COMMITTEE APPROVAL**

Dr. Ulrike Dydak, Chair

School of Health Sciences

Dr. Jason Cannon

School of Health Sciences

Dr. Sébastien Hélie

Department of Psychological Sciences

Dr. Karmen Yoder

Department of Radiology and Imaging Sciences

Dr. Wei Zheng

School of Health Sciences

Approved by:

Dr. Shuang Liu

Head of the Graduate Program

Dedicated to my son, Iain Miles Edmondson

ACKNOWLEDGMENTS

I would like to take this moment to give hearty thanks to all of those that helped me over the nearly 5 years I have spent in West Lafayette, Indiana. I want to thank all of the faculty that had a large impact on my advancement in the fields of toxicology and imaging sciences. First, and foremost, I would like to thank my adviser, Dr. Ulrike Dydak, for providing me all the opportunities to pursue interesting and innovative research in the field of Mn toxicity. Without your commitment to my endless ambitions for new research, this thesis would not exist. I would also like to thank Dr. Karmen Yoder for taking me in as an adjunct member of her IU lab in Indianapolis as well as invite me to attend weekly PET “classes”. Her help was invaluable for getting my second aim off the floor. Dr. Sébastien Hélie was enormously helpful with my last-minute desire to learn programming and machine learning. Your knowledge and advice was unbelievably on point for the development of my third aim and completion of my NIEHS F31 goals. Finally, I’d want to thank Dr. Jason Cannon and Dr. Wei Zheng for encouraging me to consider myself a toxicologist.

I could not have survived my first couple years at Purdue had it not been for the friendships I fostered with past labmates, Dr. Emily Ma and Dr. Chien-Lin Yeh. Your encouragement and recognition of my true talents was invaluable for my progress in my PhD. It is simply amazing how important it is to be told what you’re good at – introspection is often difficult in a PhD program. For my last couple years, I must thank Liesl Krause and Nicole Vike for their friendship. Thank you both for being so enthusiastic about MRI. Together, we made a very nice student group (Purdue Association for Magnetic Resonance) and I truly hope it flourishes into something amazing (beyond what it already is).

Finally, I must thank my family, specifically my wife, Katherine McGuire. While it was your fault (partially) we ended up in Indiana rather than staying in California (I swore I’d never return to Indiana...), you were nonetheless my rock that I could scream obscenities to whenever I was angry about something at work. Unfortunately, since having Iain, I have to be a little quieter now. Without you, I’m not sure completion of this PhD could have been possible.

TABLE OF CONTENTS

LIST OF TABLES	8
LIST OF FIGURES	9
LIST OF ABBREVIATIONS.....	11
ABSTRACT.....	13
1. INTRODUCTION	16
1.1 Manganese	16
1.2 Occupational Mn Exposure as a Risk Factor for Parkinsonism	16
1.3 Mn Brain Transport.....	17
1.3.1 Measuring Mn Accumulation	19
1.4 Using Imaging for Manganese Toxicology	20
1.4.1 Mechanisms of Manganese Toxicity.....	20
1.4.2 Neurodegeneration.....	21
1.4.3 Basal Ganglia.....	22
1.4.4 Mn Effects on GABA/Glutamate	23
1.4.5 Mn Effects on Dopamine.....	25
1.5 The Search for Biomarkers Using Imaging in Mn Toxicity	26
2. REVERSIBILITY OF NEUROIMAGING MARKERS INFLUENCED BY LIFETIME OCCUPATIONAL MANGANESE EXPOSURE.....	28
2.1 Introduction.....	28
2.2 Methods.....	30
2.2.1 Recruitment.....	30
2.2.2 Exposure Assessment	31
2.2.3 Toenails.....	32
2.2.4 MR Spectroscopy.....	32
2.2.5 Relaxometry.....	33
2.2.6 UPDRS	34
2.2.7 Quality Assurance.....	35
2.2.8 Statistical Analysis.....	35
2.3 Results.....	36

2.3.1	Changes in workplace were reflected by changes in measured exposure and imaging parameters.....	36
2.3.2	Correlations with changes in exposure	39
2.3.3	Linear relationships between Mn exposure and GABA but not R1	40
2.3.4	Cumulative Mn interacts with the effect of short-term Mn exposure on R1	41
2.3.5	UPDRS remained stable across both scans	42
2.4	Discussion.....	42
3.	CHRONIC OCCUPATIONAL MANGANESE EXPOSURE EFFECT ON STRIATAL DOPAMINE: A PILOT [¹¹ C]-RACLOPRIDE PET STUDY	48
3.1	Introduction.....	48
3.2	Methods.....	51
3.2.1	Recruitment.....	51
3.2.2	Exposure & UPDRS	52
3.2.3	PET and MRI.....	52
3.2.4	Data Analysis.....	54
3.2.5	Statistical Analysis.....	55
3.3	Results.....	55
3.3.1	Subjects.....	55
3.3.2	Change in DA levels (Δ BP _{ND}) and baseline BP _{ND} indistinguishable between Welders and Controls.....	56
3.3.3	Correlations between BP _{ND} , UPDRS motor performance scores, and Mn exposure	56
3.4	Discussion.....	57
3.5	Conclusion	61
4.	WHOLE-BRAIN R1 PREDICTS EXPOSURE GROUPS IN WELDERS: AN APPLIED USE OF SUPPORT VECTOR MACHINES IN NEUROIMAGING.....	62
4.1	Introduction.....	62
4.2	Methods.....	65
4.2.1	Relaxometry.....	65
4.2.2	GABA	66
4.2.3	UPDRS	67
4.2.4	Exposure Assessment	67

4.2.5	Biokinetic Model	67
4.2.6	Data Processing	70
4.2.7	Model Testing & Scoring	71
4.3	Results.....	73
4.3.1	PCA.....	73
4.3.2	SVM Models.....	75
4.3.2.1	Study Group.....	75
4.3.2.2	Air Mn Exposure	75
4.3.2.3	Excess Brain Mn.....	76
4.3.2.4	Total Welding Years.....	76
4.3.2.5	Age.....	76
4.3.2.6	Thalamic GABA.....	77
4.3.2.7	UPDRS Score	77
4.4	Discussion.....	82
5.	CONCLUSIONS	86
5.1	Overview.....	86
5.2	Advances.....	86
5.2.1	Changes in R1 are not linearly proportional with changes in Mn exposure.....	86
5.2.2	Machine learning can improve <i>in vivo</i> toxicology studies using medical imaging...	87
5.2.3	Evidence of regions in the brain with increased susceptibility to Mn.....	88
5.2.3.1	Striatal Mn susceptibility.....	88
5.2.3.2	Pallidal & Substantia Nigral Mn Susceptibility	89
5.3	Limitations and Future Directions	90
5.3.1	Limitations.....	90
5.3.2	Measuring the Effect from Mixtures	91
5.4	Summary.....	92
	REFERENCES	93

LIST OF TABLES

Table 1 Subject Exposure Assessment	36
Table 2 Spearman partial correlation (controlling for Mn-CEI _{Life}) results (Spearman's ρ).....	40
Table 3 PET Participant Demographics.....	56
Table 4 Results for Principle Component Analysis of Whole-Brain R1	74

LIST OF FIGURES

Figure 1 Basal Ganglia Flowpath. See text for description.	22
Figure 2 GABA/Glu Cycle. See text for description.	24
Figure 3 MRS voxel placement and spectrum. A) Shows the thalamic voxel of interest (VOI) in blue and the striatal voxel in yellow. B) Representative difference spectrum for quantifying GABA in the thalamic VOI. GABA is indicated by the doublet at around 3.0 ppm.	33
Figure 4 Changes in welders between Scan 1 (S1) and Scan 2 (S2). A) Changes in air Mn concentration ($[Mn]_{Air}$), past three months CEI ($Mn-CEI_{3M}$), past year CEI ($Mn-CEI_{12M}$), and toenail Mn concentration ($[Mn]_{Toenail}$). B) Changes in R1 in four different regions of interest in the brain: caudate nucleus, frontal white matter, globus pallidus, and substantia nigra. C) Changes in GABA levels in two regions of the brain: striatum and thalamus. D) Less changes are observed in UPDRS scores.	38
Figure 5 Correlations. A) A significant correlation ($\rho = 0.50$, $p = 0.05$) exists between the changes in R1 in the substantia nigra ($\Delta R1_{SN}$) versus the change in Mn exposure at three months prior to scan ($\Delta Mn-CEI_{3M}$) but no linear relationship. Whereas in (B) there is not only a significant correlation ($\rho = 0.66$, $p = 0.001$), but also a linear relationship between the change in thalamic GABA ($\Delta GABA_{Thal}$) and $\Delta Mn-CEI_{3M}$ ($\beta = 14.7$, $p = 0.02$). C. Depicts a significant correlation ($\rho = 0.64$, $p = 0.006$) between the change in toenail concentration ($\Delta [Mn]_{Toenail}$) and the change in Mn exposure at 7-12 months prior to scan ($\Delta Mn-CEI_{7-12M}$).....	39
Figure 6 Interactions. A) The effect of $\Delta [Mn]_{Air}$ on $\Delta R1_{SN}$ is affected significantly by $Mn-CEI_{Life}$. Subjects with lower levels of $Mn-CEI_{Life}$ ($\leq 3.15 \text{ mg/m}^3 \times \text{Year}$) have larger $\Delta R1_{SN}$ (red, - - Line represents the line of regression for $n = 13$). Subjects with higher levels of $Mn-CEI_{Life}$ ($> 3.15 \text{ mg/m}^3 \times \text{Year}$) have smaller $\Delta R1_{SN}$ (red, -- line represents the line of regression for $n = 4$). B) The effect of $\Delta Mn-CEI_{3M}$ on $\Delta GABA_{Thal}$ is not significantly impacted by $Mm-CEI_{Life}$	42
Figure 7 Schematic of PET study mechanism. A) Normal: Some proportion of synaptic dopamine (DA) binds to available receptors. B) +RAC: Radioactive RAC, a competitive dopamine D_2/D_3 receptor antagonist, enters the synapse after IV injection and binds to available receptors in trace quantities. The quantity “ BP_{ND} ” refers to the estimation of receptor availability. C) +RAC + AMPH: Amphetamine causes an increase of endogenous DA in the synapse, which displaces RAC from receptors and lowers the measurable radioactive signal.	53
Figure 8 [^{11}C]raclopride Binding Potential (BP_{ND}) during baseline (“1”) and an amphetamine challenge (“2”). Data from welders are in black; controls are in grey.	57
Figure 9 Correlations between BP_{ND} , ΔBP_{ND} , $Mn-CEI_{Life}$, and UPDRS Score. A) Right putamen ΔBP_{ND} (Black) is positively correlated with UPDRS motor score. B) Right pre-commissural caudate baseline BP_{ND} is positively correlated with $Mn-CEI_{Life}$. C) Right ventral striatum baseline BP_{ND} is significantly correlated with $Mn-CEI_{Life}$	58

Figure 10 Distribution of R1 in a Region of Interest. Shows the distribution of R1 in the Right Caudate of one welder (orange) and one control (blue). There is a shift to the right and slightly wider variance for the welder compared to the control. Rather than use a single point estimate of the distribution, we chose to select five different parameters that described the R1 distribution. For each ROI, we calculated the median, variance, skew, 10-percentile, and 90-percentile. 66

Figure 11 Biokinetic model of Mn. This model is derived from a previously published model. Respirable Mn was assumed to be transported into the plasma compartment with 100% efficiency. The model then describes through a series of compartments how Mn disperses itself throughout the body. This study used values of excess brain Mn that was calculated from the brain compartment. 68

Figure 12 Example Results from Mn Biokinetic Model. A) Shows the trend of Mn accumulation in 6 regions of the body: brain, cortical bone surface, cortical bone volume, trabecular bone surface, trabecular bone volume, and blood plasma. Welder worked for 2 years with an average air Mn exposure concentration of 0.088 mg/m^3 . B) This welder worked in three jobs over 10 years. The first job was for 5 years with an air concentration of 0.14 mg/m^3 . Second job was welding aluminum, and thus no Mn exposure. The third job lasted for 3 years prior to their participation in a previous study and were exposed to 0.24 mg/m^3 . As can be seen by the R1 images on the right, taken from the same location and with the same contrast, the subject in B has much brighter white matter – indicative of higher R1 due to Mn accumulation..... 69

Figure 13 Confusion Matrix and Scoring. Shows a typical confusion matrix and the calculation for true positive (TP), false positive (FP), false negative (FN), and true negative (TN). 72

Figure 14 SVM Model Accuracy. Show accuracy of the combined, or bagged, SVM model as well as the individual statistics that went into the combined model for all 6 targets: Air Mn Exposure, Excess brain Mn, Total Welding Years, Age, Thalamic GABA, and UPDRS Score. 78

Figure 15 SVM Model Scoring. Shows accuracy and recall for the combined, or bagged, SVM model for all 6 targets: Air Mn Exposure, Excess brain Mn, Total Welding Years, Age, Thalamic GABA, and UPDRS Score. 79

Figure 16 SVM Model Class Imbalance. Shows class balance for each threshold for the combined, or bagged, SVM model for all 6 targets: Air Mn Exposure, Excess brain Mn, Total Welding Years, Age, Thalamic GABA, and UPDRS Score..... 80

Figure 17 SVM Model Prediction Error Balance. Shows how balanced prediction error was for each threshold for the combined, or bagged, SVM model for all 6 targets: Air Mn Exposure, Excess brain Mn, Total Welding Years, Age, Thalamic GABA, and UPDRS Score. 81

LIST OF ABBREVIATIONS

ACGIH	American Conference of Governmental Industrial Hygienists
AMPH	Amphetamine
BBB	Blood-Brain Barrier
BCB	Blood-CSF Barrier
BP _{ND}	Binding Potential Nondisplaceable
CN	Caudate Nucleus
CSF	Cerebrospinal Fluid
DMT1	Divalent Metal Transport – 1
DA	Dopamine
D ₂ R	D ₂ Receptor
FN	False Negative
FP	False Positive
GABA	Gamma-aminobutyric Acid
Glc	Glucose
Gln	Glutamine
Glu	Glutamate
GP	Globus Pallidus
iPD	Idiopathic Parkinson's Disease
Mn	Manganese
Mn-CEI _{3M}	Cumulative Exposure Index of Manganese in 3 Month Window
Mn-CEI _{12M}	Cumulative Exposure Index of Manganese in 1 Year Window
Mn-CEI _{Life}	Cumulative Exposure Index of Manganese over Lifetime
[Mn] _{Air}	Air Mn Exposure Concentration
[Mn] _{Toenail}	Toenail Mn Concentration
MRI	Magnetic Resonance Imaging
MRS	Magnetic Resonance Spectroscopy
PCA	Principle Component Analysis
PD	Parkinson's Disease
PET	Positron Emission Tomography

R1	MRI Relaxation Rate
RAC	[¹¹ C]-Raclopride
ROI	Region of Interest
SN	Substantia Nigra
SNC	Substantia Nigra Pars Compacta
SNr	Substantia Nigra Pars Reticulata
SVM	Support Vector Machine
T1	MRI Relaxation Time
TN	True Negative
TP	True Positive
TLV	Threshold Limit Value
UPDRS	Unified Parkinson's Disease Rating Scale
VOI	Volume of Interest

ABSTRACT

Author: Edmondson, David, A. PhD

Institution: Purdue University

Degree Received: May 2019

Title: Identifying Imaging Biomarkers for Manganese Toxicity in Occupationally Exposed Welders

Committee Chair: Ulrike Dydak, PhD

Manganese (Mn) is an essential element and, at high doses, a neurotoxin that many workers are exposed to daily. Increased Mn body burden due to occupational exposures leads to a parkinsonian disorder that features symptoms such as mood disturbances, cognition deficits, and motor dysfunction. To understand exposed workers' risk, biomarkers of exposure have been developed using blood, hair, bone, and toenails. None of these biomarkers take into account how much Mn is in the brain and instead rely on the assumption that Mn uptake in these materials is proportional and related to the levels in the brain. One way to measure Mn in the brain is through neuroimaging modalities, such as magnetic resonance imaging and positron emission tomography, however there remains a need to establish reliable neuroimaging biomarkers for Mn exposure and its toxicological effects. This thesis addresses this need.

First, we hypothesized that changes in Mn exposure would be reflected by changes in the MRI relaxation rate R1 and thalamic γ -aminobutyric acid (GABA). As part of a prospective cohort study, 17 welders were recruited and imaged on two separate occasions approximately two years apart. MRI relaxometry was used to assess changes of Mn accumulation in the brain. Additionally, GABA was measured using magnetic resonance spectroscopy (MRS) in the thalamic and striatal regions of the brain. Air Mn exposure ($[Mn]_{air}$) and cumulative exposure indexes of Mn (Mn-CEI) for the past three months (Mn-CEI_{3M}), past year (Mn-CEI_{12M}), and lifetime (Mn-CEI_{Life}) were calculated using personal air sampling and a comprehensive work

history, while toenails were collected for analysis of internal Mn body burden. Finally, welders' motor function was examined using the Unified Parkinson's Disease Rating Scale (UPDRS). Mn-CEI_{12M} decreased significantly between the first and second scan (Wilcoxon Signed Rank, $p = 0.02$). Δ Mn-CEI_{3M} were correlated with R1 in the substantia nigra (spearman partial correlation, $\rho = 0.50$, $p = 0.036$) and thalamic GABA ($\rho = 0.66$, $p = 0.001$), but only GABA significantly decreased linearly with Mn-CEI_{3M} (quantile regression, $\beta = 15.22$, $p = 0.02$). Finally, Mn-CEI_{Life} influences the change in R1 in the substantia nigra with Δ [Mn]_{Air}, where higher Mn-CEI_{Life} lessened the Δ R1 per Δ [Mn]_{Air} (F-test, $p = 0.005$). While R1 and GABA changed with Mn exposure, UPDRS was unaffected.

Secondly, we hypothesized that occupational exposure to Mn would lead to disturbances in dopamine release (DA), as measured with PET. Excess exposure to manganese (Mn) can lead to symptoms similar to Parkinson's disease (PD). While symptoms of PD are due to loss of nigrostriatal dopaminergic neurons, there is no DA neuron loss with Mn toxicity. To assess how DA release may be affected by Mn exposure, 6 subjects (3 welders, 3 controls) were scanned with positron emission tomography and [¹¹C]raclopride (a DA D₂/D₃ receptor antagonist displaceable by endogenous DA) at baseline and during an amphetamine challenge. There were no apparent differences in amphetamine-induced striatal DA release between groups. However, UPDRS motor scores were positively linearly related to [¹¹C]raclopride binding potential (BP_{ND}) in the putamen, whereas Mn-CEI_{Life} was negatively related to baseline pre-commissural caudate and ventral striatum BP_{ND}. The pilot results suggest that [¹¹C]raclopride PET might delineate the cause of mood and motor dysfunction in subjects exposed to Mn.

Third, we hypothesized that advanced data analysis techniques, such as machine learning, would increase our power in finding differences between groups of welders and controls based

on exposure and biological outcomes. This study used data from previous studies in occupationally exposed welders and controls. Whole brain relaxometry using MRI measuring the relaxation rate R1 was acquired in 52 welders and 37 controls. Because measures of R1 in selected regions of the brain have been previously found to be proportional to Mn, we hypothesized that an advanced model taking into account the whole brain might be more predictive for Mn exposure. Additionally, because R1 is proportional to Mn in the region, we used a biokinetic model to estimate the amount of excess Mn in the brain from occupational exposures. Support vector machines (SVM) with a linear kernel were trained using leave-one-out cross-validation. Results indicated that models had recall and accuracy better than chance targeting air Mn exposure, years welding, age, and thalamic GABA. In comparison to all models, R1 appears to reliably predict thalamic GABA across all thresholds, which was previously shown to change with increased Mn exposure. This suggests that while R1 may be proportional to Mn, some Mn may not be free to contribute to signal, and instead thalamic GABA might better reflect the overall amount of free Mn in the brain.

Collectively, this thesis is a successful step towards establishing neuroimaging biomarkers of effect from occupational Mn exposure. The MRI relaxation rate R1, with adequate modeling, could eventually be used to measure total Mn brain burden while thalamic GABA might represent a better metric for measuring the neurochemical effects from recent exposures. However, future research should incorporate more endpoints, such as motor tests, mood assessments, and behavior assessments.

1. INTRODUCTION

1.1 Manganese

Manganese (Mn) is an essential nutrient that is commonly found in the environment and in many foods, including fruits, grains, nuts, and tea (Tuschl, Mills, & Clayton, 2013). It also acts as a cofactor for many enzymes including superoxide dismutase, arginase, pyruvate decarboxylase, and glutamine synthetase (Marta Sidoryk-Wegrzynowicz & Aschner, 2013). Due to the relative abundance of this metal in most diets, malnutrition due to a Mn deficiency is rare. However, excess Mn has complications that can arise, for instance in people with chronic liver disease leading to the inability for the liver to remove Mn from the blood. Excess Mn in the body can also be due to occupational exposures, such as from metalworking (e.g. welding and smelting). The safe exposure level of airborne Mn in the workplace is unknown. While the American Conference of Governmental Industrial Hygienists (ACGIH)'s recommended threshold limit value (TLV) of 0.02 mg/m³ for respirable Mn is significantly lower than it has been in the past, it is still uncertain whether this level is low enough to prevent the negative consequences of Mn intoxication.

1.2 Occupational Mn Exposure as a Risk Factor for Parkinsonism

Excess Mn exposure can lead to Manganism, a parkinsonian disorder characterized by behavioral, movement, and cognitive impairments. First described in cases of excess occupational Mn exposure in 1837 (Couper, 1837), Mn toxicity continues to be commonly studied in welders, who are exposed to Mn-containing welding fumes (Bowler et al., 2006; Cook, Fahn, & Brait, 1974; Long, Jiang, et al., 2014; Mena, Marin, Fuenzalida, & Cotzias, 1967; Racette, Aschner, et al., 2012). Manganism progressively increases in severity over time. The first symptoms begin as cognitive and emotional impairment as well as minor fine motor

dysfunction. End-stage symptoms then include dystonia, tremor, rigidity, and a cock-walk gait (Tuschl et al., 2013). While some of these symptoms are similar to idiopathic Parkinson's Disease (PD), patients with Manganism, or simply Mn toxicity, typically do not improve with levodopa treatment (Perl & Olanow, 2007), nor has any other form of treatment been established to date.

Epidemiology studies have been conducted to determine whether welding is a risk factor for PD. A meta-analysis of available literature concluded that welding poses no additional risk to developing PD (Mortimer, Borenstein, & Nelson, 2012). However, there is a greater risk for developing parkinsonism with increased years welding (Racette, Criswell, et al., 2012). Studies have also measured the effects of Mn exposure on motor performance by using neurological and neuropsychological exams. In general, studies show that the more years a worker welds, the greater their deficits in motor tests, as measured through neuropsychological testing (Bowler et al., 2006; R. M. Park, Bouchard, Baldwin, Bowler, & Mergler, 2014). Therefore, it is apparent that excess Mn exposure leads to symptoms in humans that range from minor to severely debilitating. To fully understand how to protect workers, it is advantageous to first understand how Mn moves through the human body, how this might lead to symptoms, and whether there are any options for prevention besides complete cessation of Mn exposure

1.3 Mn Brain Transport

After being inhaled, Mn passes through the lungs into the pulmonary veins, then back to the heart to be distributed throughout the body. Because inhaling bypasses the "first pass effect" through the liver, where Mn can be biotransformed and regulated by the body, Mn is freely available for uptake in the brain. In order for Mn to enter the brain, it must go through one of three routes: through the blood brain barrier (BBB), through the blood-cerebrospinal fluid (CSF)

barrier (BCB), or through the olfactory nerve. The BBB and BCB have specific transporters that have an affinity for Mn. Mn exists predominantly in two oxidation states, +2 and +3 (Karki, Lee, & Aschner, 2013). Mn can enter the central nervous system through various means, either as a free ion or bound to a protein. In blood, Mn^{3+} is commonly found bound to transferrin (O'Neal & Zheng, 2015) and is then transported into the brain through the BBB via transferrin receptors (TfR) in a similar manner as iron-bound transferrin.

The majority of Mn^{2+} is likely transported through the BBB and BCB as a free ion, while some might be bound to citrate. Divalent metal transporter 1 (DMT1) is a highly prevalent transporter found along the BBB and BCB and is thought of as a primary method for Mn transport into the brain (Bornhorst et al., 2012). However, transport of Mn through DMT-1 along the BBB is contested by data that shows that the pH of blood may negatively impact the ability of Mn to transfer and DMT-1 might not express along the capillary endothelial cells that make up the BBB (Tuschl et al., 2013). Other transporters of note include ZIP8/14, glutamate receptors, voltage-regulated Ca^{2+} channels, store-operated Ca^{2+} channels, citrate shuttles, and ferroportin (O'Neal & Zheng, 2015).

Considering the physical location of the choroid plexus with blood supply directly from the anterior and posterior choroidal arteries, branches of the internal carotid artery, and the posterior cerebral arteries, the apparent distribution of Mn along nuclei close to ventricles (Bock, Paiva, Nascimento, Newman, & Silva, 2008), and potentially stronger sensitivity for Mn in the BCB versus BBB as shown from an *in vitro* study (Bornhorst et al., 2012), it is possible that the primary method of Mn transport into the brain is through the BCB, which is then distributed throughout the CNS by the CSF. Additionally, upon being taken up in neurons, Mn can also be transported anterograde down axons to regions of the brain downstream (Saleem et al., 2002),

which may be what occurs after uptake in the olfactory bulb. Therefore, while Mn may accumulate in one location, it can end up in other regions of the brain via projecting neurons.

1.3.1 Measuring Mn Accumulation

Mn accumulates in regions of the brain with high concentrations of transporters that Mn has a strong affinity towards, as well as close proximity to ventricles (Bock et al., 2008), such as the globus pallidus (GP), striatum, and substantia nigra (SN). Manganese has been used for decades in preclinical studies as a T1 contrast agent for tracing neuronal pathways, but due to its toxicity, that has not frequently been used in humans (one rare exception being the use of TESLASCAN™, a marketed Mn-containing contrast agent that was eventually pulled from market due to symptoms (Pan, Schmieder, Wickline, & Lanza, 2011)). Mn is a paramagnetic metal which, when exposed to a magnetic field, will distort the local field and affect the T1 of hydrogen atoms near it. T1, or the relaxation time, refers to how much time it takes for hydrogen atoms to return to their low energy state within a magnetic field. In humans, the most plentiful source of hydrogen atoms is water, which makes up over 70% of our body mass. Mn, therefore, acts as a contrast by decreasing the T1, thus the signal coming from water with Mn present will increase. In welders, or other people with high Mn uptake (such as with chronic liver disease), T1 hyperintensities can be seen in the GP. However, the use of the inverse of T1 ($R1 = 1/T1$), or the relaxation rate, is standard for measuring the effect of a contrast agent.

The oxidation state affects how strong of an effect a contrast agent will have on an image. Mn can exist in multiple oxidation states, but in the body, the majority will be in either 2+ or 3+. Because Mn^{2+} has 5 unpaired electrons while Mn^{3+} has four, Mn^{2+} has a higher effective magnetic moment and thus, provides more contrast (García-Hevia, Bañobre-López, & Gallo, 2019). Therefore, while we cannot be certain of the distribution between Mn^{3+} and Mn^{2+} in the

body, the existence of Mn^{2+} would likely be the source of any image contrast, especially since Mn^{3+} would likely be bound to transferrin, thus limiting Mn's ability to provide contrast in the local environment.

1.4 Using Imaging for Manganese Toxicology

Studies have been conducted using magnetic resonance imaging (MRI), spectroscopy (MRS), and positron emission tomography (PET), but many of them have been more interested in looking for biomarkers of exposure, rather than biological effects and progression of symptoms of Mn toxicity. With neuroimaging, quantification of these effects can be carefully done non-invasively in humans with neurological and neuropsychological effects being tested simultaneously within the study to look for differences in motor and cognitive function.

1.4.1 Mechanisms of Manganese Toxicity

The mechanisms by which neurotoxicity from Mn exposure occurs is largely still unknown. Because Mn exposure leads to symptoms similar but not identical to PD, there has been much attention paid to determining whether the etiology of symptoms is the same. In PD, nigrostriatal dopaminergic neurons degenerate in the substantia nigra, thus leading to a loss of dopaminergic modulation of signals in the striatum. There is ample evidence that the same does not occur after exposure to Mn (Guilarte & Gonzales, 2015b). However, neurotransmitters, such as dopamine (DA), γ -aminobutyric acid (GABA), and glutamate (Glu), are altered with Mn exposure. In animal studies using rats, exposure to Mn led to increased DA in the striatum, which corresponded with increases in DA metabolites such as 3,4-dihydroxyphenylacetic acid (DOPAC) and homovanilic acid (HVA). Rats also had increased GABA in the hippocampus (O'Neal, Lee, Zheng, & Cannon, 2014). Therefore, while dopaminergic nigrostriatal

neurodegeneration may not be occurring as a result of Mn exposure, neurotransmitter alteration may be caused from other sources of neurodegeneration.

1.4.2 Neurodegeneration

Neurodegeneration is the progressive loss of function or structure in neurons.

Neurodegeneration and gliosis due to Mn has been found in the basal ganglia, primarily in the GP, substantia nigra pars compacta (SNc), and the striatum (Olanow, 2004). Although, there are mixed results as to which cells are dying due to Mn. Astrocytes are one possible target (Hazell, 2002; Marta Sidoryk-Wegrzynowicz & Aschner, 2013) where Mn can accumulate in the mitochondria by entering through a calcium uniporter and then set off a chain reaction leading to cell death. Mn has been found to inhibit F1-ATPase and complex 1 of the electron transport chain, thus destabilizing and affecting the ability of the cell to produce ATP (J. Y. Chen, Tsao, Zhao, & Zheng, 2001). Additionally, Mn has been shown to produce reactive oxygen species (ROS), leading to the production of the highly reactive molecule, superoxide (Martinez-Finley et al, 2003). This oxidative stress can further lead to apoptosis and thus neurodegeneration.

Mn-induced neuroinflammation is a more recent discovery. The presence of Mn has been shown to cause the activation of microglia (J. Chen, Su, Luo, & Chen, 2018; Liu et al., 2009). Once activated, microglia will release cytokines that lead to neuroinflammation. Excessive activation of microglia can therefore cause excess releases of pro-inflammatory cytokines that may eventually lead to injury and cell death.

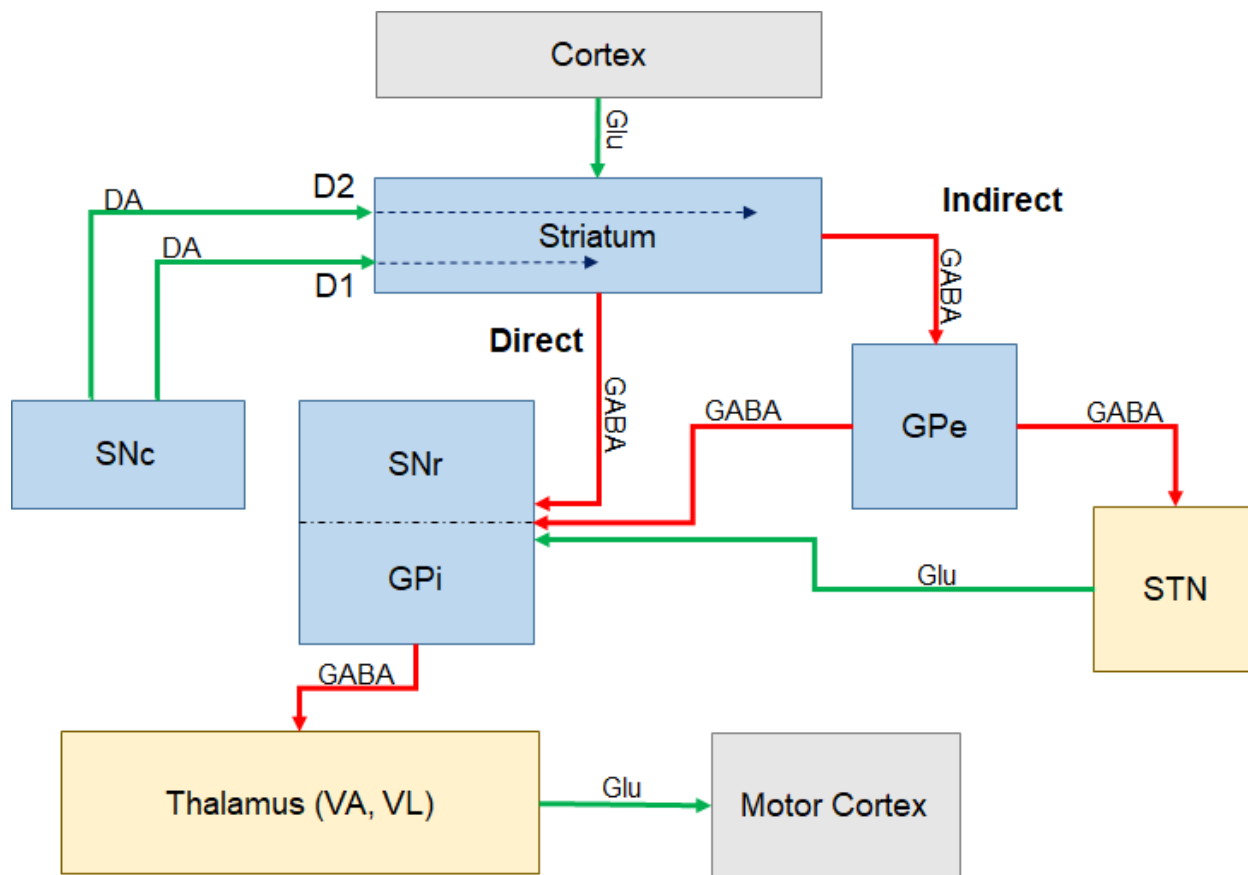


Figure 1 Basal Ganglia Flowpath. See text for description.

1.4.3 Basal Ganglia

Due to the apparent accumulation of Mn in the basal ganglia and the resulting motor dysfunction from exposure, research has focused on the effects on Mn within nuclei of the basal ganglia starting from the SN to the thalamus. The basal ganglia is a series of nuclei that are largely involved with controlling voluntary motor movement as well as the limbic system and memory.

The normal flow path of information in the basal ganglia (Figure 1) begins with dopaminergic neurons projecting from the SNc into the striatum and release DA which modulate neurons in the striatum (Gerfen & Bolam, 2016). From here, there are two pathways for

information to flow, a direct and an indirect pathway which work against one another to precisely control motor movement originating in the motor cortex. The direct pathway excites thalamic neurons and begins with GABAergic neuronal projections to the GP internal (GPi) which then inhibit glutamatergic neurons in the thalamus that project into the cortex. The indirect pathway inhibits thalamic neurons and begins with GABAergic neuronal projections to the globus pallidus external that inhibit glutamatergic projections into the SN pars reticulata (SNr). This inhibition of excitatory neurons then depresses the inhibition of GABAergic neurons projecting into the thalamus, thus allowing glutamatergic neurons in the thalamus to excite neurons in the cortex (Guilarte & Gonzales, 2015a). Effectively, the direct and indirect pathways have opposing actions that collectively allow the basal ganglia to perform an executive role in motor action selection. Any dysfunction in either of these pathways will lead to an imbalance of neurotransmitters and potentially resulting motor symptoms.

1.4.4 Mn Effects on GABA/Glutamate

Whether through cell death or injury, it has been shown that Mn exposure leads to a disruption in the γ -aminobutyric acid (GABA)/Glu cycle (Erikson & Aschner, 2003; Fitsanakis, Au, Erikson, & Aschner, 2006; M. Sidoryk-Wegrzynowicz & Aschner, 2013). Neurons do not have the capacity to convert Glu and GABA from glucose (Glc), rather this occurs in astrocytes where the requisite enzymes are located (Marta Sidoryk-Wegrzynowicz & Aschner, 2013). Glu is taken into an astrocyte where glutamine synthase converts Glu to Glutamine (Gln). Gln is released by the astrocyte and taken up by a neuron which then converts it either to GABA via glutamic acid dehydrogenase or to Glu through Glutaminase. The release of these

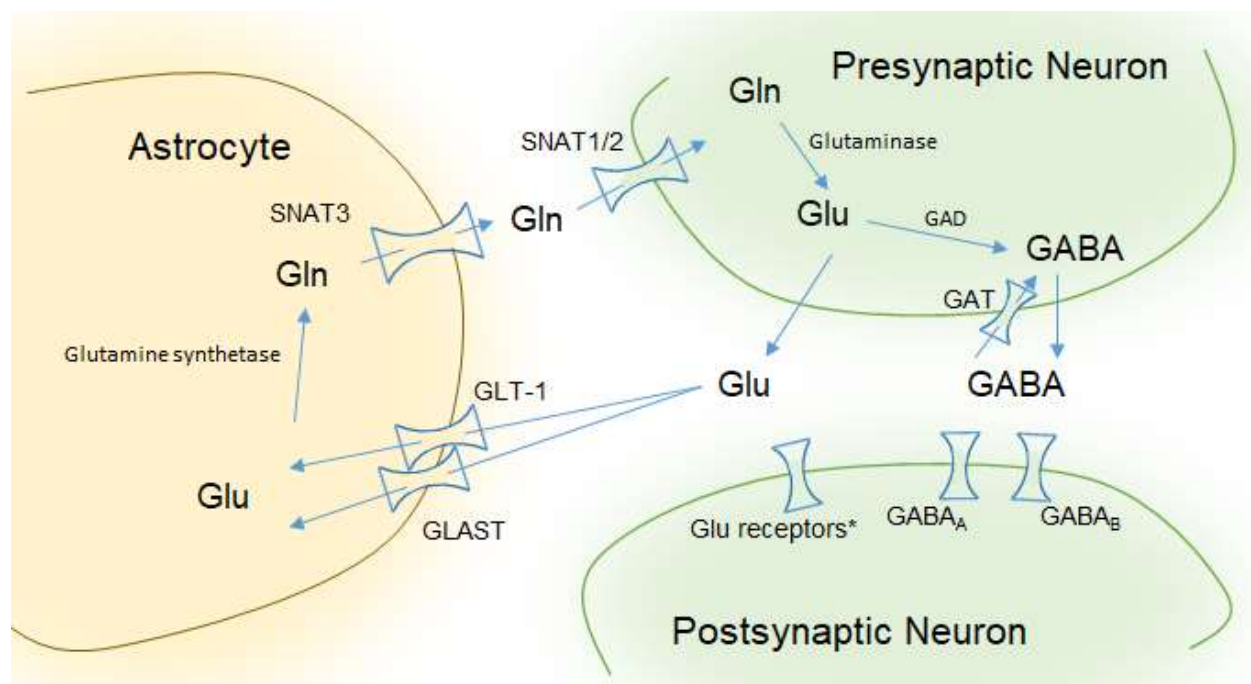


Figure 2 GABA/Glu Cycle. See text for description.

neurotransmitters are then taken back up in an astrocyte and the cycle repeats itself (Fitsanakis et al., 2006). GABA is converted back to Glu via GABA-transaminase (Erikson & Aschner, 2003).

If Mn has any deleterious effect to astrocytes, receptors, or transporters, this cycle will be disrupted. Studies have shown that Mn can inhibit the release of GABA (Cotman, Haycock, & White, 1976), the transport of GABA (P. C. L. Wong, Lai, Lim, & Davison, 1981), and GABA binding to receptors (Fishman, McGinley, & Gianutsos, 1987). Additionally, decreases in GABA and Glu have been reported in rats which may be due to decreased Glu uptake in astrocytes (Erikson & Aschner, 2003). Consequently, depending on where in the basal ganglia injury due to Mn occurs, this could also have downstream effects on concentrations of GABA or Glu which may then lead to symptoms.

Using neuroimaging, higher levels of the inhibitory neurotransmitter GABA have been found as measured by MRS in the thalamus of Mn exposed welders compared to non-exposed

controls (Dydak et al., 2011; Edmondson et al., 2015; Long, Li, et al., 2014), a finding also found in PD patients (Dharmadhikari, Ma, Yeh, Snyder, et al., 2015; O’Gorman Tuura, Baumann, & Baumann-Vogel, 2018). In welders, higher GABA has been found to be related to fine motor dysfunction (Long, Li, et al., 2014). Together, higher GABA might be suggestive of an increase in inhibition tone in the thalamus that is due to upstream neuronal dysfunction in the basal ganglia that leads to decreased motor and cognitive performance.

1.4.5 Mn Effects on Dopamine

In neurons, the generation of dopamine (DA) begins with tyrosine (Tyr). Tyr is converted to Dihydroxyphenylalanine (DOPA) by Tyrosine hydroxylase (TH) which is then converted to DA by Aromatic amino acid decarboxylase. The amount of DA in the brain is significantly less than GABA, and thus signal for this molecule cannot be feasibly measured with MRS. Therefore, measuring DA in vivo must be done through indirect methods, primarily with positron emission tomography (PET).

In 1995, a PET study in monkeys using three different tracers ($[^{18}\text{F}]$ -6-fluoro-L-dopa, $[^{11}\text{C}]$ -raclopride (RAC), and $[^{18}\text{F}]$ -fluorodeoxyglucose) had shown evidence that Mn exposure causes motor deficits through a different mechanism than PD. In other words, no effects were found in the nigrostriatal pathway (Shinotoh et al., 1995). Since then, studies have been conflicted. Other monkey studies appear to disagree with the early 1995 study using RAC (Guilarte et al., 2008) while studies in humans using $[^{18}\text{F}]$ -6-fluoro-L-dopa found reduction in caudate K_i , indicative of presynaptic nigrostriatal dysfunction (Racette et al., 2011). So, rather than no effect nor degeneration of dopaminergic neurons, Mn may be causing dopamine release dysfunction, a potential explanation for why levodopa does not work as a treatment for symptoms of Mn toxicity. This is further supported by Guilarte et al. (2008) which saw less DA

release in monkeys exposed to Mn compared to controls while still having intact nigrostriatal dopaminergic neurons (Guilarte et al., 2008).

1.5 The Search for Biomarkers Using Imaging in Mn Toxicity

Research in Mn toxicity has focused on identifying accurate biomarkers for Mn exposure, with a critical gap in the literature on biomarkers of adverse outcomes. Some biomarkers have been found. Mn concentrations in toenails correlate with exposure as measured 7-9 months prior to clipping (Grashow et al., 2014). Mn levels in hair were also shown to correlate with accumulated exposure 30 days prior to sampling (Reiss et al., 2015). While these biomarkers are potentially useful, they do not measure any biological effect. We will address this knowledge gap by performing MRI, MRS, and PET that focus on different physiological outcomes of Mn exposure. We will utilize a longitudinal cohort study of occupationally exposed welders from a local manufacturing plant to provide greater insight into the effects of Mn over time. This effort will provide key information about the behavior of Mn in the body and the natural history of disease for Mn toxicity in humans. Therefore, the objective of this thesis is to develop imaging biomarkers of effects from Mn exposure as measured by changes in imaging parameters and neurochemistry. I hypothesize that occupational Mn exposure leads to unique and measureable changes as detected by medical imaging, specifically MRI, MRS, and PET. To test this hypothesis, I will focus on three specific aims.

Aim 1: To measure the effects of Mn on GABA availability by quantifying changes in neurochemistry in the basal ganglia as measured by MRS with changing Mn exposure.

Aim 2: To measure the effects of Mn on dopamine availability by measuring response to amphetamine-induced striatal dopamine release with PET in welders and controls.

Aim 3: To model Mn deposition and accumulation within the brain using MRI relaxometry, biokinetic modeling, and machine learning.

2. REVERSIBILITY OF NEUROIMAGING MARKERS INFLUENCED BY LIFETIME OCCUPATIONAL MANGANESE EXPOSURE

2.1 Introduction

Excess Mn exposure can lead to a parkinsonian disorder called Manganism, a disease similar to idiopathic Parkinson's disease. It is characterized by behavioral, movement, and cognitive impairments and was first described in cases of chemical plant workers (Couper, 1837). Recently, the threshold limit value (TLV) for airborne Mn, as recommended by the American Conference of Governmental Industrial Hygienists (ACGIH), was set to 0.02 mg/m³. However, it is still unclear whether subclinical health effects could occur due to chronic Mn exposure lower than this threshold. One population that continues to be exposed to Mn are welders, who are exposed to Mn-containing fumes (Bowler et al., 2006; Cook et al., 1974; Long, Jiang, et al., 2014; Mena et al., 1967; Racette, Aschner, et al., 2012). It has been observed that once motor symptoms due to overexposure appear, they remain even after exposure ends and typically do not improve with levodopa treatment (Perl & Olanow, 2007). No alternate form of treatment has been established to date. Therefore, it is necessary to determine whether welders are at risk of Mn toxicity before any symptoms develop.

Having a method that can quantify brain Mn would be ideal as a metric for assessing how Mn contributes to a welder's risk (Meyer-Baron et al., 2013). One possible method uses magnetic resonance imaging (MRI). Due to the paramagnetic properties of Mn, the metal acts as a contrast agent, much like gadolinium, a commonly used contrast agent for diagnostic medical MRI scans. Areas with a higher concentration of Mn will show up brighter on a T1-weighted image. Previous studies have shown that brain MRIs of Mn-exposed subjects show increased T1-weighted intensities in the basal ganglia, reflecting Mn accumulation (Chuang, Koretsky, &

Sotak, 2009; Criswell et al., 2012; Dorman, 2006; Dydak et al., 2011; Long, Jiang, et al., 2014). However, while the increased intensity is believed to be proportional to Mn accumulation (Dorman, 2006), the ability to fully elucidate the relationship has been difficult. Recently, the change in the relaxation rate R1 (where, $R1 = 1/T1$) was found not to be linearly proportional to lower occupational levels of Mn exposure (Lee et al., 2015), and reflective of short-term exposure (Lewis et al., 2016).

Magnetic resonance spectroscopy (MRS) measures biochemical concentrations *in vivo*. γ -aminobutyric acid (GABA), the primary inhibitory neurotransmitter of the central nervous system, has been measured using MRS and was found to be higher in the thalamus of Mn exposed welders when compared to non-exposed controls (Edmondson et al., 2015; Long, Li, et al., 2014; Ma et al., 2017). A similar result was also found in idiopathic Parkinson's disease (PD) patients (Dydak, Dharmadhikari, Snyder, & Zauber, 2015; O'Gorman Tuura et al., 2018). Because of the similarity in symptoms between patients with Mn toxicity and PD patients, there is some debate about how nigrostriatal dopaminergic neurons are affected by Mn (Guilarte & Gonzales, 2015b). It is possible that Mn has an effect on these neurons which may trigger an imbalance of neurotransmitters in the basal ganglia (Dharmadhikari, Ma, Yeh, Stock, et al., 2015; Dydak et al., 2015; Guilarte et al., 2008; Long, Li, et al., 2014; Racette, Criswell, et al., 2012; Racette et al., 2011), but the effect could also be further downstream in other basal ganglia nuclei. Nonetheless, with work history indicating exposure to Mn, an increase in GABA could potentially be a reliable marker for Mn toxicity. Yet, the GABA levels appear to be dynamic, just as is the exposure, and a single GABA level at one time point does not provide enough information about the effect of Mn exposure on the neurotransmitter levels.

Our initial study (Ma et al., 2017) found significantly higher thalamic GABA in highly exposed welders (air exposure $> 0.24 \text{ mg Mn/m}^3$) compared to lower exposed welders (mean air exposure 0.13 mg Mn/m^3) and controls. Additionally, R1 was higher in the globus pallidus (GP), substantia nigra (SN), frontal white matter (FWM), and caudate nucleus (CN) in highly exposed welders compared to lower exposed welders and controls. While thalamic GABA ($\text{GABA}_{\text{Thal}}$) was correlated with past three-months and past year Mn exposure windows, R1 was not, thus suggesting that the relationship between R1 and Mn exposure may be complicated by a non-linear relationship between Mn exposure and Mn accumulation in the brain. To get a better understanding of the dynamic effects of low-level chronic Mn exposure in the workplace, we therefore conducted a longitudinal follow-up study.

2.2 Methods

This study is a follow-up study of a previous study as described in Ma et al, 2017. This study was approved by the Biomedical Institutional Review Board at Purdue University. Written informed consent forms were obtained from all subjects prior to the participation in the study.

2.2.1 Recruitment

Subjects were recruited from the same U.S. truck trailer manufacturer cohort as in Ma et al, 2017. Of 32 welders in the first study, 17 male welders ($N=17$) elected to participate in a follow-up study. All subjects visited the MRI facility for approximately four hours on a weekend. During this time, they were interviewed about their medical history, work history, and health-related habits (e.g. diet, smoking, and drinking). Additionally, they were given a neurological exam from a qualified neurologist and received an MRI scan lasting approximately 1 hour in length.

2.2.2 Exposure Assessment

Exposure assessment was performed in the welders' workplace with the identical procedure as described in Ma et al. 2017 and Ward et al. 2017. Briefly, an exposure model using each participant's individual work history combined with air sampling data was used to estimate each participant's Mn cumulative exposure index (Mn-CEI). Average air Mn concentrations for each factory department were estimated using an average of all personal air samples collected from each department. Each personal air sample was collected over the duration of a full work shift (8 h). Our sampling methods used SKC aluminum cyclones with a cut-point of 4 μm , which collects the respirable particles capable of penetrating to the alveolar regions of the lungs, as well as deposit in the brain via the olfactory pathway. The samples were collected inside the welding helmet for welders and on the shoulder in the personal breathing zone for control subjects.

For each participant, the Mn-CEI was calculated as a summation of the individual exposure from the current employer, past employers, and off the job welding for the given exposure window in (mg/m^3) years (Ward et al., 2017). Mn-CEIs were calculated for the following exposure time windows: exposure over the past three months (before the MRI measurement), exposure over the past year, and cumulative exposure over their working lifetime (back to age 18). The Mn-CEI for the current employer was then calculated by summing over the measured average respirable Mn exposure for each department an individual has worked in during the respective time window, multiplied by the time worked at this department. For cumulative exposure including past employers or for off-the-job welding, the exposure model utilizes additional information from a detailed work history questionnaire, as well as weighting factors accounting for ventilation, welding frequency, welding type, base metals and use of respirator to better estimate the individual's past exposure based on personal history

(Laohaudomchok et al., 2011). For our study, the different exposure windows can be conceptualized (in order of closest to the scan) as recent ($[\text{Mn}]_{\text{Air}}$, Mn-CEI_{3M}) and distant (Mn-CEI_{12M}, cumulative lifetime Mn exposure Mn-CEI_{Life}).

2.2.3 Toenails

Toenail clippings were acquired at the first scan (S1) and second scan (S2) and placed in small envelopes for storage. Analysis of clippings was performed as described in Ward et al., 2018, but briefly described here. External contamination was removed using a surfactant solution (1% Triton X-100) for 20 minutes. After being rinsed with distilled de-ionized water, the toenails were dried, weighed, and then dissolved by microwave nitric-acid digestion. The digested samples were then analyzed using inductively-coupled plasma mass spectroscopy (ICP-MS). Toenail Mn concentrations ($[\text{Mn}]_{\text{Toenail}}$) are reported in units of $\mu\text{g/g}$.

2.2.4 MR Spectroscopy

All MRI acquisitions were obtained using a 3T GE Signa MRI scanner with an 8-channel head coil. We obtained GABA-edited spectra using MEGA-PRESS (TR/TE = 2000/68 ms, 256 Averages) (Mullins et al., 2014) in two volumes of interest (VOI), thalamic (25mm x 30mm x 25mm) and striatal (25mm x 30mm x 25mm) regions of the brain. Spectra were quantified using LCModel V6.3-1B (Provencher, 1993) and a basis set generated by density matrix simulation using GABA coupling constants from Kaiser et al. (2008). The GABA signal in these spectra also includes contributions from co-edited macromolecules and homocarnosine and is therefore commonly referred to as GABA⁺. However, for the sake of simplicity, we refer to the measure as GABA. The thalamus VOI was centered on the right thalamus while the striatal VOI was centered over the striatum, but included parts of the globus pallidus, putamen, caudate nucleus, and thalamus (Figure 1). This overlap was intentional in order to detect any possible contribution

of striatal GABA signal in the large thalamus VOI. Water reference scans without water suppression were used for phase and frequency correction. Cerebrospinal fluid (CSF) correction was performed by first segmenting 3D T1-weighted images into three components: grey matter (GM), white matter (WM), and CSF (SPM8, Wellcome Department of Imaging Neuroscience, London, United Kingdom). Percentages of each component were calculated for the VOIs using a home-made Matlab code and then GABA levels were corrected for CSF to obtain corrected GABA concentrations (Chowdhury et al., 2014).

2.2.5 Relaxometry

We used MRI relaxometry to assess relative brain Mn accumulation *in vivo*. Whole brain

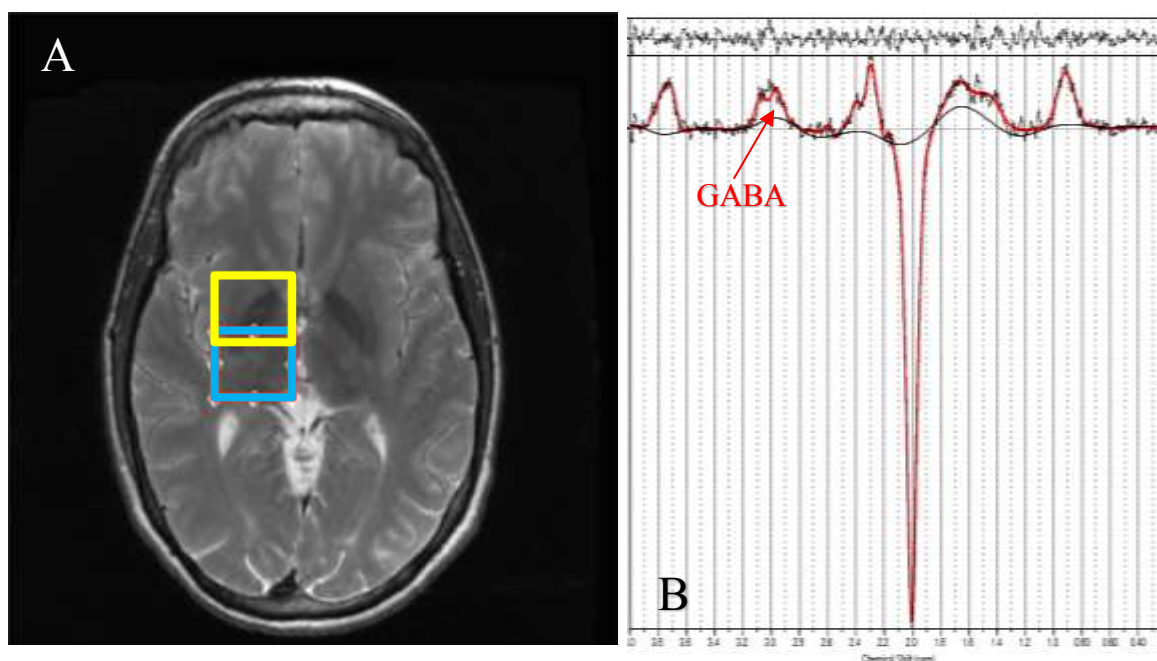


Figure 3 MRS voxel placement and spectrum. A) Shows the thalamic voxel of interest (VOI) in blue and the striatal voxel in yellow. B) Representative difference spectrum for quantifying GABA in the thalamic VOI. GABA is indicated by the doublet at around 3.0 ppm.

3D T1 relaxation time mapping was performed using a dual flip angle (3° and 17°) technique (Christensen, Grant, Schulman, & Walling, 1974) consisting of two spoiled gradient echo images

(SPGR, TR/TE = 6.36/1.76 ms, bandwidth = 224 Hz/pixel, matrix dimension = 256 x 192, resolution = 1mm x 1mm x 2mm). Whole brain T1 maps were then generated using an in-house program written in Matlab (The MathWorks, Natick, MA, USA). T1 was calculated for each pixel based on repetition time (TR), flip angle (α) and a factor that is proportional to the equilibrium longitudinal magnetization (M_0) (Sabati & Maudsley, 2013). T1 values were calculated in brain regions of interest (ROIs) chosen based on prior studies (Criswell et al., 2012) that showed high Mn deposition in the globus pallidus (GP), substantia nigra (SN), caudate nucleus (CN), and frontal white matter (FWM). Circular ROIs with an area of 30 mm² were measured bilaterally on T1 maps, using the ROI tool in Matlab and Osirix (Pixmeo, Switzerland). R1 values were then calculated as the inverse T1 relaxation time ($R1 = 1/T1$) and then averaged over left and right hemispheres.

2.2.6 UPDRS

Subjects' motor abilities were examined by a certified neurologist using the MDS-Unified Parkinson's Disease Rating Scale Part III (UPDRS-III) (Goetz et al., 2007). Rigidity scores were calculated as the summation of 5 items: rigidity in the neck, in the left and right upper extremities and in the left and right lower extremities. Tremor scores were calculated as the summation of 7 items: left and right kinetic tremor of the hands, rest tremor amplitude in lip/jaw, and rigidity in the right, left, upper and lower extremities. Bradykinesia scores were calculated as the summation of 5 terms: right and left finger-tapping, right and left hand movements, right and left pronation-supination movements of hands, right and left toe tapping, and right and left leg agility. A higher UPDRS score indicates a worse motor performance with UPDRS scores 15 or below being considered non-symptomatic.

2.2.7 Quality Assurance

In an effort to ensure all measurements were reliable and stable across both scans, quality assurance (QA) measurements were performed frequently and consistently. These included repeating the MRI and MRS procedures detailed above in phantoms and volunteers. For testing R1, we used a spherical phantom filled with a solution doped with Mn whereas for testing MRS, we used a spherical phantom filled with a 2.0 mM GABA solution. QA testing showed that R1 measurements in phantoms had a mean of 0.63 s^{-1} with a coefficient of variability (CV) of 15.5%, while R1 in volunteers had a mean of 0.64 s^{-1} with a CV of 8%. For GABA, phantoms showed a CV of 2.5% while volunteers had a CV of 15%.

2.2.8 Statistical Analysis

All statistical tests were performed within the R environment (R Core Team, 2013). Due to our small sample size, Wilcoxon Signed Rank nonparametric tests were used to measure differences in parameters between S1 and S2. Spearman partial correlation tests were used to assess correlations between different parameters, such as R1, GABA, and exposure.

For our study we chose to control for cumulative exposure as measured at S2, rather than age at S2. Spearman partial correlation results using age rather than cumulative exposure were virtually identical, with the correlations controlling for cumulative exposure being slightly more significant. Therefore, controlling for cumulative exposure is roughly equivalent to controlling for age, but more relevant in the context of this study.

Due to the small number of subjects and high potential for outliers to affect the results, we assessed linear relationships through nonparametric means using quadratic regressions by estimating the median. To assess interactions, a multiple quantile regression model was used with the included interaction term. For the interaction analysis, the best model was determined

by using an F-test. Multiple quantile regressions were performed using the *quantreg* package in R.

2.3 Results

Exposure assessment for the 17 subjects recruited for a second scan from the original cross-sectional cohort of welders from a local factory (Ma et al., 2017) are shown in Table 1. Welders had an average age of 40.9 (SD = 9.7) years at S1 and 42.4 (SD =9.7) years at S2.

Table 1 Subject Exposure Assessment

	Scan 1	Scan 2
N	17	17
Average Air Mn (mg/m^3)	0.099 (0.043)	0.077 (0.04)
Toenail Mn ($\mu\text{g}/\text{g}$)	6.93 (3.46)	5.73 (1.93)
Mn-CEI _{3M} (mg/m^3)	0.035 (.024)	0.017 (0.013)
Mn-CEI _{7-12M} (mg/m^3)	0.086 (0.111)	0.034 (0.027)
Mn-CEI _{12M} (mg/m^3)	0.19 (0.17)	0.068* (0.053)
Mn-CEI _{Life} (mg/m^3)	1.51 (1.47)	1.69 (1.48)

* $p < 0.05$

2.3.1 Changes in workplace were reflected by changes in measured exposure and imaging parameters

For the average welder, Mn exposure over the time window 3 months prior to scan, (Mn-CEI_{3M}) decreased by 50% from $0.035 \frac{\text{mg}}{\text{m}^3} * \text{Year}$ to $0.017 \frac{\text{mg}}{\text{m}^3} * \text{Year}$ ($p = 0.07$); and Mn exposure over the time window 1 year prior to scan (CEI_{12M}) changed from $0.187 \frac{\text{mg}}{\text{m}^3} * \text{Year}$ to $0.068 \frac{\text{mg}}{\text{m}^3} * \text{Year}$ ($p = 0.03$). Finally, toenail Mn concentration ($\Delta[\text{Mn}]_{\text{Toenail}}$) dropped significantly from 6.93 to $5.73 \frac{\mu\text{g}}{\text{g}}$ ($p = 0.02$) (Figure 4). These significant decreases in Mn exposure are partially due to welders taking more precautionary actions by wearing respiratory protection, thus lowering their inhaled Mn exposure. Additionally, many welders went from

welding stainless steel to aluminum, thus lowering their Mn exposure virtually to zero.

Depending on when this change happened within the two years between S1 and S2, it is reflected in the exposure windows of 3 months prior to scan, 7-12 months prior to scan, and past year prior to scan.

Between S1 and S2, R1 values in regions of interest changed dramatically as well.

Average R1 lowered in the caudate nucleus (CN) from 0.765 s^{-1} to 0.725 s^{-1} ($p = 0.057$), lowered in the globus pallidus (GP) from 0.959 s^{-1} to 0.908 s^{-1} ($p = 0.03$), lowered in the substantia nigra (SN) from 0.871 s^{-1} to 0.721 s^{-1} ($p < 0.0001$), but increased in the frontal white matter (FWM) from 1.22 s^{-1} to 1.44 s^{-1} ($p = 0.001$). Results are suggesting there was less Mn in most of these regions in S2 compared to S1, with the exception of FWM. Finally, we found that $\text{GABA}_{\text{Thal}}$ decreased significantly ($p = 0.0005$) on average from 2.012 mM to 1.206 mM while no significant decrease in striatal GABA could be measured. Taking into account the normal variance in our acquisitions as tested by our phantoms and controls, the changes in $\text{GABA}_{\text{Thal}}$ (40%) and R1 in the SN (17.3%) and FWM (15.3%) between S1 and S2 were all outside of normal variance expected.

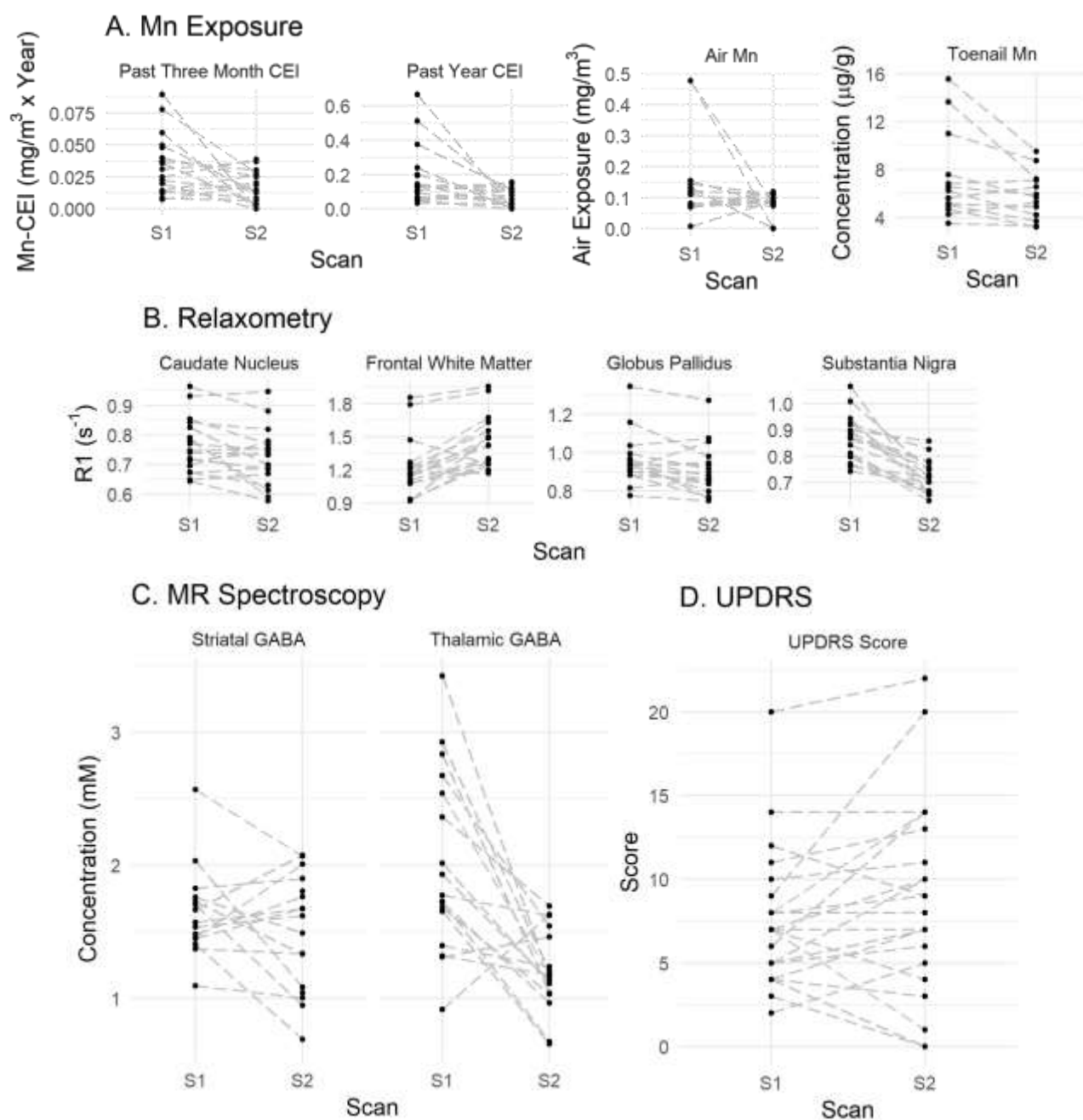


Figure 4 Changes in welders between Scan 1 (S1) and Scan 2 (S2). A) Changes in air Mn concentration ($[\text{Mn}]_{\text{Air}}$), past three months CEI ($\text{Mn-CEI}_{3\text{M}}$), past year CEI ($\text{Mn-CEI}_{12\text{M}}$), and toenail Mn concentration ($[\text{Mn}]_{\text{Toenail}}$). B) Changes in R1 in four different regions of interest in the brain: caudate nucleus, frontal white matter, globus pallidus, and substantia nigra. C) Changes in GABA levels in two regions of the brain: striatum and thalamus. D) Less changes are

2.3.2 Correlations with changes in exposure

MRS was used to measure changes in neurochemistry in two separate voxels within the basal ganglia. In the thalamus voxel, ΔGABA was strongly correlated ($\rho = 0.77$, $p < 0.0001$) with change in air concentration ($\Delta[\text{Mn}]_{\text{Air}}$), with the change in exposure 3 months prior to scan ($\Delta\text{Mn-CEI}_{3\text{M}}$) ($\rho = 0.66$, $p = 0.001$) (Figure 5B), and past year ($\Delta\text{Mn-CEI}_{12\text{M}}$) ($\rho = 0.70$, $p = .0004$), all suggesting that with greater positive changes in Mn exposure, there are

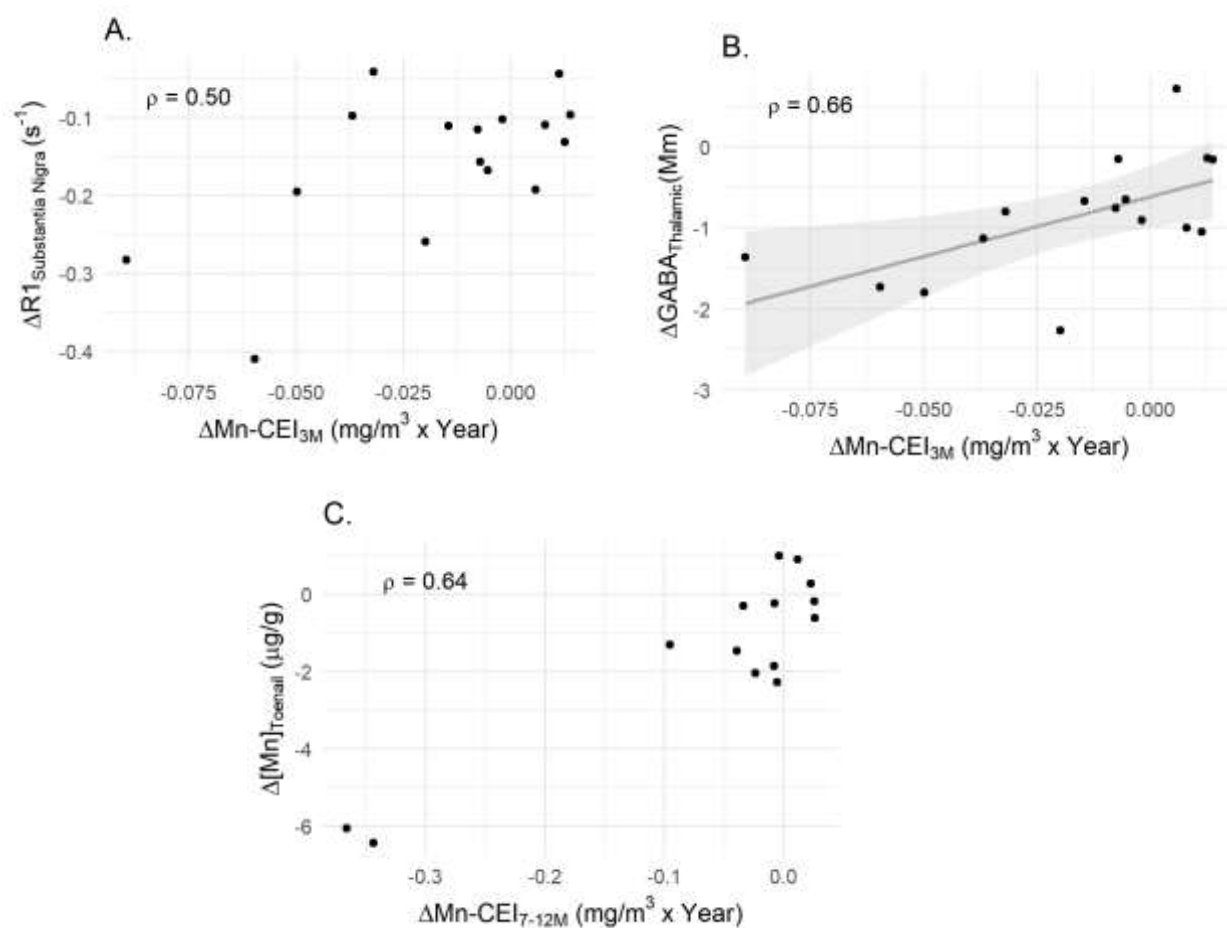


Figure 5 Correlations. **A)** A significant correlation ($\rho = 0.50$, $p = 0.05$) exists between the changes in R1 in the substantia nigra ($\Delta\text{R1}_{\text{SN}}$) versus the change in Mn exposure at three months prior to scan ($\Delta\text{Mn-CEI}_{3\text{M}}$) but no linear relationship. Whereas in **(B)** there is not only a significant correlation ($\rho = 0.66$, $p = 0.001$), but also a linear relationship between the change in thalamic GABA ($\Delta\text{GABA}_{\text{Thal}}$) and $\Delta\text{Mn-CEI}_{3\text{M}}$ ($\beta = 14.7$, $p = 0.02$). **C.** Depicts a significant correlation ($\rho = 0.64$, $p = 0.006$) between the change in toenail concentration ($\Delta[\text{Mn}]_{\text{Toenail}}$) and the change in Mn exposure at 7-12 months prior to scan ($\Delta\text{Mn-CEI}_{7-12\text{M}}$).

corresponding greater positive changes in GABA. In the striatal voxel, Δ GABA was not significantly correlated with any changes in Mn exposure.

To assess whether the change in exposure had any relationship with the observed differences in R1 between S1 and S2, we performed Spearman partial correlations, controlling for cumulative Mn exposure (Mn-CEI_{Life}) at S2. While there were significant differences in R1 in specified regions between S1 and S2, only the substantia nigra (SN) had a significant correlation with Δ Mn-CEI_{3M} after controlling for cumulative exposure at the S2 ($\rho=0.50$, $p = 0.036$) (Table 2).

Δ [Mn]_{Toenail} was significantly correlated ($\rho = 0.64$, $p = 0.006$) with the change in Mn exposure 7-12 months prior to scan (Δ Mn_{7-12M}) (Figure 5C). Δ [Mn]_{Toenail} was not significantly correlated with Δ R1 in any region of interest or Δ GABA in either the thalamic or striatal areas.

Table 2 Spearman partial correlation (controlling for Mn-CEI_{Life}) results (Spearman's ρ)

Δ Mn Exposure	Δ Mn _{Toenail}	Δ R1				Δ GABA	
		GP	SN	FWM	CN	Thalamus	Striatum
[Mn] _{Air}	0.18	0.05	0.23	0.22	0.08	0.77****	-0.07
Mn-CEI _{3M}	0.10	0.28	0.50*	0.32	0.16	0.66**	-0.10
Mn-CEI _{7-12M}	0.64**	0.04	0.12	0.05	-0.15	0.43	0.33
Mn-CEI _{12M}	0.36	0.07	0.23	0.08	-0.13	0.70****	0.02

* $p < 0.05$, ** $p < 0.01$, *** $p < 0.001$, **** $p < 0.0001$

2.3.3 Linear relationships between Mn exposure and GABA but not R1

For relationships that were significantly correlated, quantile regressions were performed to see if the relationship was linear. Of all significant correlations, only Δ GABA_{Thal} ($\beta = 15.22$ (7.45 – 26.01), p -value = 0.02) was *linearly* related to Δ Mn-CEI_{3M} where for every $0.01 \frac{mg}{m^3} *$ *year* change in Δ Mn-CEI_{3M} leads to a 0.15 mM median increase in Δ GABA_{Thal} concentration. Δ GABA_{Thal} was also linearly related to air concentration ($\beta = 1.27$ (0.87 – 8.22), p -value = 0.04).

For every $0.1 \text{ mg/m}^3 \Delta[\text{Mn}]_{\text{Air}}$, we see a 0.13 mM median increase in $\Delta\text{GABA}_{\text{Thal}}$ concentration. We found no other linear relationships between exposure measurements and ΔR1 , including toenails.

2.3.4 Cumulative Mn interacts with the effect of short-term Mn exposure on R1

To explore whether a welder's $\text{Mn-CEI}_{\text{Life}}$ affected the relationship between more recent exposures and R1, GABA, or $[\text{Mn}]_{\text{Toenail}}$, interaction analyses were performed using quantile regression analysis with $\text{Mn-CEI}_{\text{Life}}$ at S2 included as an interaction term. Using the F-test method to compare regressions with an interaction term and regressions without, we found that for three regions of the brain, $\text{Mn-CEI}_{\text{Life}}$ had a significant interaction with $\Delta[\text{Mn}]_{\text{Air}}$ where, as $\text{Mn-CEI}_{\text{Life}}$ increased, the effect of $\Delta[\text{Mn}]_{\text{Air}}$ on R1 decreased. In the SN, the median slope of R1 vs. $\Delta[\text{Mn}]_{\text{Air}}$ differed by -0.18 ($p = 0.005$), by -0.45 in FWM ($p = 0.04$), and by -0.15 in CN ($p = 0.009$) for one unit change in $\text{Mn-CEI}_{\text{Life}}$ as measured at S2 (Figure 6). The median slope of R1 vs $\Delta[\text{Mn}]_{\text{Air}}$ was estimated to differ by $-0.16 \text{ s}^{-1}/(\text{mg}/\text{m}^3)$ ($p = 0.59$), but this was not significant. Interactions between $\Delta\text{GABA}_{\text{Thal}}$ and $\text{Mn-CEI}_{\text{Life}}$ at S2 was also tested. While not statistically significant, $\text{Mn-CEI}_{\text{Life}}$ may interact with $\Delta\text{Mn-CEI}_{3\text{M}}$, changing the median slope of $\Delta\text{GABA}_{\text{Thal}}$ vs. $\Delta\text{Mn-CEI}_{3\text{M}}$ by $-4.31 \text{ mM}/(\text{mg}/\text{m}^3)$ ($p = 0.10$) for one unit change in $\text{Mn-CEI}_{\text{Life}}$. Finally, there were no interactions between $\text{Mn-CEI}_{\text{Life}}$ and $\Delta\text{Mn-CEI}_{7-12\text{M}}$ for describing $\Delta[\text{Mn}]_{\text{Toenail}}$ with $\Delta\text{Mn-CEI}_{7-12\text{M}}$. The same interaction tests with age found no significant interaction.

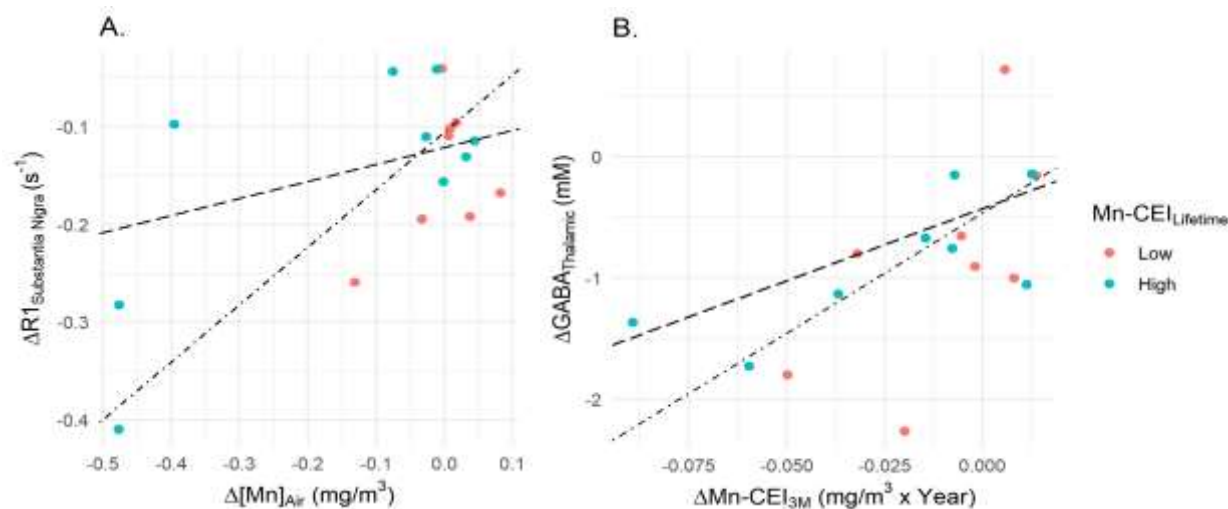


Figure 6 Interactions. A) The effect of $\Delta[Mn]_{\text{Air}}$ on $\Delta R1_{\text{SN}}$ is affected significantly by $Mn-CEI_{\text{Lifetime}}$. Subjects with lower levels of $Mn-CEI_{\text{Lifetime}} (\leq 3.15 \text{ mg/m}^3 \times \text{Year})$ have larger $\Delta R1_{\text{SN}}$ (red, -- Line represents the line of regression for $n = 13$). Subjects with higher levels of $Mn-CEI_{\text{Lifetime}} (> 3.15 \text{ mg/m}^3 \times \text{Year})$ have smaller $\Delta R1_{\text{SN}}$ (red, -- line represents the line of regression for $n = 4$). **B)** The effect of $\Delta Mn-CEI_{3M}$ on $\Delta GABA_{\text{Thal}}$ is not significantly impacted by $Mn-CEI_{\text{Lifetime}}$.

2.3.5 UPDRS remained stable across both scans

While average UPDRS total scores increased between S1 and S2 (7.76 to 8.88), variability within the scores also increased (standard deviation 4.6 to 6.06). Consequently, no correlations or relationships were found between the overall score or measured sub-scores (e.g. bradykinesia, tremor, and rigidity).

2.4 Discussion

Our study measured Mn exposure directly in the workplace, thus we were able to successfully quantify Mn exposure to each participant and measure how exposure levels were changing over time. Significant decreases in Mn exposure are partially due to welders reporting that they were taking more precautionary actions such as by wearing respiratory protection, thus lowering their inhaled Mn exposure. Additionally, many welders went from welding stainless

steel to aluminum, thus lowering their occupational Mn exposure virtually to zero. Depending on when this change happened within the two years between S1 and S2, it is reflected in Mn-CEI_{3M}, Mn-CEI_{7-12M}, and Mn-CEI_{12M}. Particularly, we quantified how Mn exposure changed when subjects moved from one department that welded carbon steel in a confined space to another that welded in open air, thus lowering overall exposure due to better ventilation.

A sub-group of our cohort, three participants, had previously welded in confined tanks with minimal air flow. About 6 months after the first round of scanning, two of the three participants went from working in that high Mn environment to welding aluminum, thus dropping their Mn exposure to zero, whereas the third participant only cut his exposure by approximately one-fifth. The two that started welding aluminum had two of the largest decreases in GABA_{Thal} as well as in SN R1. The participant that continued to be exposed to manganese had lower SN R1 as well, but change was far less than for the other two. Relationships between Δ GABA_{Thal} and Δ [Mn]_{Air} and Δ Mn-CEI_{12M} remained significant even after removing these three subjects, however the statistical significance of relationships between Δ GABA_{Thal} and Δ Mn_{3M} and between Δ R1_{SN} and Δ Mn_{3M} disappeared. While these results suggest reversibility, UPDRS increased for the two participants that switched to aluminum, whereas the third participant's UPDRS score decreased. Potentially, this could be an effect of age, as the third participant was almost 15 years younger and had less Mn-CEI_{Life} than the other two.

The results of this study are consistent with another study which showed that changes in welding hours within 90 days from a scan was associated with changes in R1 after correcting for age, baseline R1, hours worked 90 days before scan, and blood Mn values (Lewis et al., 2016). With the exception of SN, most regions did not have a directional relationship with exposure. While we found that Δ GABA_{Thal} is linear to Δ Mn-CEI_{3M}, there is no linear relationship between

$\Delta R1$ and any measure of $\Delta \text{Mn-CEI}$ or $\Delta [\text{Mn}]_{\text{Air}}$. The same group found that R1 had a nonlinear relationship with hours worked, but that R1 only changed after 300 hours welding, or approximately 12 work weeks (Lee et al., 2015), similar to our calculated $\text{Mn-CEI}_{3\text{M}}$.

We can understand how R1 changes over time by taking into account how Mn exists in two different binding states in tissue, bound (Mn-B) and free (Mn-F), as shown in biological models (Nong, Taylor, Clewell, Dorman, & Andersen, 2009; Nong, Teeguarden, Clewell, Dorman, & Andersen, 2008; Ramoju et al., 2017; Schroeter et al., 2012; Taylor et al., 2012; Teeguarden et al., 2007). Mn-B has been taken up into a cell, and thus is less able to diffuse out of a particular region in the brain and affect R1. Mn-F is able to diffuse in and out of the region, and readily interact with the hydrogen spins in water that were excited by MRI, thus increasing the relaxation rate R1. Therefore, the R1 changes based on the amount of Mn-F available and the amount of binding sites available for binding Mn-F in each region. During times of higher exposure, more Mn will accumulate in the brain, with higher preference towards the inner-brain regions such as the basal ganglia and brainstem (Bock et al., 2008). Therefore, because of higher amounts of Mn-susceptible transporter proteins in the SN, such as divalent metal transporter 1 (DMT1), Mn will accumulate in the neurons and glia there (Au, Benedetto, & Aschner, 2008b). Eventually, the number of available binding locations will be occupied by Mn-B, forcing additional Mn to exist in a free state. This Mn-F leads to higher R1 in the region. When Mn-F leaves the region, the R1 decreases proportionately, but Mn-B remains, potentially returning to a free state, thus complicating the relationship between $\Delta R1$ and changes in Mn exposure.

These different states of Mn may explain why we found that at higher levels of cumulative exposure, there is less $\Delta R1$ with the $\Delta [\text{Mn}]_{\text{Air}}$ in all regions except for the GP. Past studies do not implicate previous exposures to Mn as a risk factor to the effects from current

exposure. One explanation could be that occupational Mn exposure over a lifetime could potentially change expressions of proteins within the astrocytes and other glial cells, thus affecting the exchange of Mn-B to Mn-F. Changes in protein expression have been shown to occur with higher doses in cell lines, where Mn and Fe dosing caused higher expression of DMT1 (Au, Benedetto, & Aschner, 2008a). Once transported into the cell, Mn is bound into endosomes for future use. The GP is highly concentrated with another transporter known to accumulate Mn, voltage activated Ca^{2+} channels, and thus there is no interaction of Mn-CEI_{Life} with the effect of more recent windows of exposure on $\Delta R1$, or at least not at the exposure levels we studied.

We also found that $\Delta[\text{Mn}]_{\text{Toenail}}$ changed proportionately with the $\Delta\text{Mn-CEI}_{7-12\text{M}}$, further validating the use of toenails as a biomarker for exposure in that 7-12 months window prior to clipping. Since there were no statistically significant relationships between $\Delta[\text{Mn}]_{\text{Toenail}}$ and R1 in any region or GABA, this suggests that the accumulation of Toenail Mn over a given time not only represents a different mechanism of Mn absorption compared to the brain, but also represents a separate time window of exposure compared to either R1 or GABA. Additionally, we found that the relationship between $\Delta[\text{Mn}]_{\text{Toenail}}$ and $\Delta\text{Mn-CEI}_{7-12\text{M}}$ was not affected by Mn-CEI_{Life}, suggesting that the process by which Mn accumulates in toenails is different than how it accumulates in brain regions, or affects R1.

$\Delta R1_{\text{FWM}}$ performed the opposite of what was expected, with R1 increasing for many people between S1 and S2 rather than going down proportionally to the change in exposure. Mn has been used for decades now in Mn-enhanced MRI, or MEMRI, as a contrast agent in preclinical studies particularly for tracing neurons due to anterograde Mn transport along axons. In a recent study using whole-brain R1 mapping to compare welders and controls, R1 is

significantly higher for welders compared to controls along white matter tracks (Yeh et al., 2016). Since the striatum has many neuronal projections to the frontal cortex, the excess Mn may have migrated to the FWM. Anterograde transport of Mn to the FWM would cause an increase in R1 that cannot be accounted for by the differences in recent Mn exposure due to our two time-points being approximately two years apart.

We also found that GABA changes proportionately with Mn exposure. $\Delta\text{GABA}_{\text{Thal}}$ correlated with all measurements of $\Delta[\text{Mn}]_{\text{Air}}$ or $\Delta\text{Mn-CEI}$ after correcting for $\text{Mn-CEI}_{\text{Life}}$ at S2. Additionally, there was a significant linear relationship between $\Delta\text{GABA}_{\text{Thal}}$ and changes in $[\text{Mn}]_{3\text{M}}$. Therefore, $\Delta\text{GABA}_{\text{Thal}}$ could be considered reflective of changes in the workplace environment's Mn exposure levels. For instance, as participants were exposed to less Mn in the air, by the time of S2, their $\text{GABA}_{\text{Thal}}$ subsided to levels similar to controls in our previous study (Ma et al., 2017). In that study, it was concluded that higher levels of $\text{GABA}_{\text{Thal}}$ in welders likely represented a dysregulation of neurotransmitters in the basal ganglia. While we see reversal of GABA levels coexisting with lower exposure levels, UPDRS scores did not change proportionately, suggesting that while $\text{GABA}_{\text{Thal}}$ is reversible, neurological dysfunction is not.

One possibility for why $\text{GABA}_{\text{Thal}}$ changes with Mn exposure is that upstream Mn accumulation in the GP or SN could be causing downstream effects in the thalamus. There has been evidence that Mn inhibited calcium-dependent release of GABA (Cotman et al., 1976) and increased GABA has been reported in earlier articles after exposure to Mn (Bonilla, 1978). Since the GP has a higher concentration of Ca^{2+} channels, this could be the initial point of toxicity. Mn may impact inhibition of GABAergic neurons projecting from the GP, leading to an increase in GABA in the thalamus.

While this study had a small sample size of 17, the strength of our longitudinal design allowed for each of our welders to effectively be their own control. Additionally, this study design removed the need to account for potential confounders, such as diet or smoking, making this study much stronger than an observational study design. One limitation, though, is that our CEIs become less precise the further their windows extend into the past. Additionally, we are limited by the resolution of MRS to obtain meaningful GABA concentrations in regions of the basal ganglia, besides the thalamus.

In conclusion, our study shows that dynamic effects from Mn exposure can be measured using a longitudinal study design incorporating MRI and MRS. We show that changes in levels of GABA_{Thal} and region-specific R1 are largely proportional to environmental exposure to Mn. When exposure decreases, GABA decreases as well – showing that the change in GABA is a potential biomarker for the effects of Mn exposure. As the exposure decreases, R1 also decreases in most regions, except for FWM. While the change is not linearly proportional to the change in Mn exposure, an appropriate model might be able to explain the changes. But, the model will need to take into account Mn-CEI_{Life}, as we have some evidence that this influences the turnover rate of Mn in the brain.

3. CHRONIC OCCUPATIONAL MANGANESE EXPOSURE EFFECT ON STRIATAL DOPAMINE: A PILOT [¹¹C]-RACLOPRIDE PET STUDY

3.1 Introduction

Manganese (Mn) is a known neurotoxic agent that many metalworking (e.g. welding, smelting) and mining workers around the world are exposed to every day. Since the disease was first described by Couper in 1837 and called “manganism” (Couper, 1837), Mn has been linked with parkinsonism. However, the connection between Mn and idiopathic Parkinson’s disease is controversial, particularly with the putative relationship between iPD and occupational Mn exposure. Previous studies have shown a relatively high association between parkinsonism and welding (Racette, Criswell, et al., 2012). Additionally, the same group found that continued exposure to Mn over time yields an average increase in the Unified Parkinson’s Disease Rating Scale (UPDRS) III scale of 0.24 for each mg Mn/m³-year of exposure (Racette et al., 2017). Combined, these results suggest that excess Mn exposure is a risk factor for iPD, and could potentially be a cause of the disease.

Yet, there are some differences between symptoms of iPD and those typically associated with chronic exposure to Mn. IPD is diagnosed when a patient exhibits bradykinesia and at least one of three other core symptoms: rigidity, unilateral tremor, and postural instability (Jankovic, 2008; Massano & Bhatia, 2012). The diagnosis is further supported by a response to L-DOPA therapy (although this is not a diagnostic requirement). Additionally, the degeneration of nigrostriatal neurons and the resulting depletion of available dopamine (DA) in the striatum is the primary source of the symptoms manifested in iPD, and nuclear medicine scans to determine integrity of dopaminergic innervation are helpful in confirming a diagnosis of iPD (Massano & Bhatia, 2012). Exposure to Mn is known to cause parkinsonian-like symptoms including rigidity,

bradykinesia, and disturbed gait. To date, no etiology for the symptoms of Mn toxicity has been found, and unlike iPD, Mn-intoxicated patients appear to have normal substantia nigra, suggesting that the nigrostriatal neurons are intact (Yamada et al., 1986). Additionally, gliosis and neuronal cell loss in the globus pallidus has been found in patients exposed to Mn (Perl & Olanow, 2007), suggesting an alternate mechanism for the motor symptoms.

Given that conclusive neuropathological evidence of whether motor symptoms are due to iPD or Mn toxicity is only available *post mortem*, other *in vivo* methods have been employed to determine the etiology of Mn toxicity. One method, positron emission tomography (PET), has been used to study the effects of Mn on humans with some success. One radiotracer, 6-^[18F]fluoro-L-dopa (FDOPA, a radioactive analogue to L-DOPA, the precursor of dopamine (DA), and a marker for dopamine neuron integrity), has been used to measure differences in FDOPA uptake. Recently, Criswell et al. found lower FDOPA uptake in the caudate in welders versus controls (Criswell, Nielsen, et al., 2018), which built upon their previous study (Racette et al., 2011). Lower FDOPA uptake may indicate presynaptic dysfunction, which could suggest functional impairment of the nigrostriatal dopaminergic neurons, with or without degeneration (Criswell, Nielsen, et al., 2018). However, these results are contrary to previous reports, which did not find differences in FDOPA uptake after Mn intoxication (Shinotoh et al., 1997).

Another radiotracer, ^[13C]raclopride (RAC, a DA D₂/D₃ receptor antagonist), has been used to measure differences in dopamine receptor availability in the striatum. While there has been some significant advancement in Mn toxicity research using RAC PET, it has only been applied to animal models. In the earliest nonhuman primate study with RAC PET and Mn toxicity, one monkey was injected subcutaneously with 0.4g Mn on 11 occasions over 16 months. RAC binding showed a transient decrease after 3 months, which returned to normal

levels after 16 months of exposure (Eriksson et al., 1992). The authors' conclusion was that the reduction in D₂/D₃ receptor availability was due to a decrease in D₂ dopamine receptors (D2R), possibly an effect resulting from an increased Mn body burden (Seth & Chandra, 1984). The authors contended, however, that there was no support for depletion of D2R from low doses of Mn exposure (Eriksson et al., 1992). In a later study, three adult rhesus monkeys weighing 12 to 18kg were injected intravenously with doses of 10-14 mg/kg MnCl₂, or 0.12-0.25g of MnCl₂, weekly for seven weeks. At this dose, which was lower than in Eriksson et al. (1992), two of the monkeys had no visible change in RAC binding, and one monkey had a transient change in RAC signal that reverted back to normal (Shinotoh et al., 1995), analogous with the Eriksson study.

More recently, another pair of studies assessed the impact of chronic Mn exposure in non-human primates using RAC PET during a d-amphetamine (AMPH) challenge. The first study used 12 macaques that were given 3.26-4.89 mg Mn/kg intravenous injections once per week over approximately 40 weeks. No changes in initial binding potential (BP, a measure related to the number of receptors available for binding) were found, but the AMPH challenge elicited a 42% decrease in BP at the first timepoint tested, and a subsequent 61% decrease at the second scan at a later date (Guilarte et al., 2006). This suggested that continued Mn exposure may alter the amount of DA released by AMPH. In the second study, which was a continuation of the first, the authors included 9 additional non-human primates and showed similar results. They also reported a small, but significant decrease in baseline striatal BP at the later scan (Guilarte et al., 2008). Additionally, a post-mortem analysis found no degradation of nigrostriatal neurons, suggesting that Mn toxicity does not share the same mechanism as iPD; instead, Mn likely affects other regions of the basal ganglia (Guilarte & Gonzales, 2015b).

To our knowledge, RAC PET has not been used to assess either baseline striatal D₂/D₃ receptor availability or relative DA release with an AMPH challenge in humans exposed to Mn. RAC PET has, however, been used in many studies in humans exposed to common toxins, such as alcohol (Yoder et al., 2007, 2005) and cannabis (Albrecht et al., 2013), so its use to study the striatal dopamine system in welders exposed to chronic low-levels of occupational exposure to Mn is reasonable. Consistent with the studies described above done by Guilarte, this study aimed to determine: a) if baseline BP changes with Mn exposure in a dose-dependent manner, b) if DA released, inferred from an AMPH challenge, is lower in welders versus controls, and c) if baseline BP (D₂/D₃ receptor availability) in welders is related to motor dysfunction, as measured by UPDRS scores.

3.2 Methods

3.2.1 Recruitment

Three welders and three non-welder controls were recruited from a local cohort that had participated in prior neuroimaging studies. All but one subject, a control, worked for the same company. Subjects were evaluated for potential health complications (e.g. EKG, medical history), as part of our exclusion criteria, and were cleared for participation in the study by the study physician. Exclusion criteria for potential heart complications included more than one risk factor for coronary artery disease and any history of hypertension. We also excluded subjects that had a history of neurological illness, insulin-dependent diabetes, illicit drug use, use of medication which would affect DA transmission, blood donation within 8 weeks of the study, history of taking blood thinners, or prior participation in a study or medical procedure in the past year in which any additional dose of ionizing radiation would exceed yearly dose limits for normal volunteers.

This study was approved by the Indiana University School of Medicine Institutional Review Board and the Radioactive Drug Research Committee, and all subjects provided written informed consent prior to participating in the study.

3.2.2 Exposure & UPDRS

Cumulative Exposure Indices (CEI) for Mn were calculated for two time windows, Past Year (Mn-CEI_{12M}), and Lifetime (Mn-CEI_{Lifet}), using personal air sampling and a comprehensive work history questionnaire. For a detailed explanation of these methods, please see Ma et al., (2017) and Ward et al., (2017) (Ma et al., 2017; Ward et al., 2017). Prior to the scans, a neurological test commonly used for assessing iPD progression, The Unified Parkinson's Disease Rating Scale (UPDRS III), was administered by a trained neurologist (EZ) to determine the level of motor dysfunction in all subjects.

3.2.3 PET and MRI

As mentioned above, RAC PET was used to determine baseline D₂/D₃ receptor availability, indexed by the parameter binding potential (BP) (Innis et al., 2007). RAC is a D₂/D₃ receptor antagonist that is sensitive to changes in endogenous dopamine (Dewey et al., 1992; Seeman, Guan, & Niznik, 1989). Here, we used d-amphetamine, a dopamine releasing agent, as a pharmacological challenge to probe relative dopamine release capacity between groups (Breier et

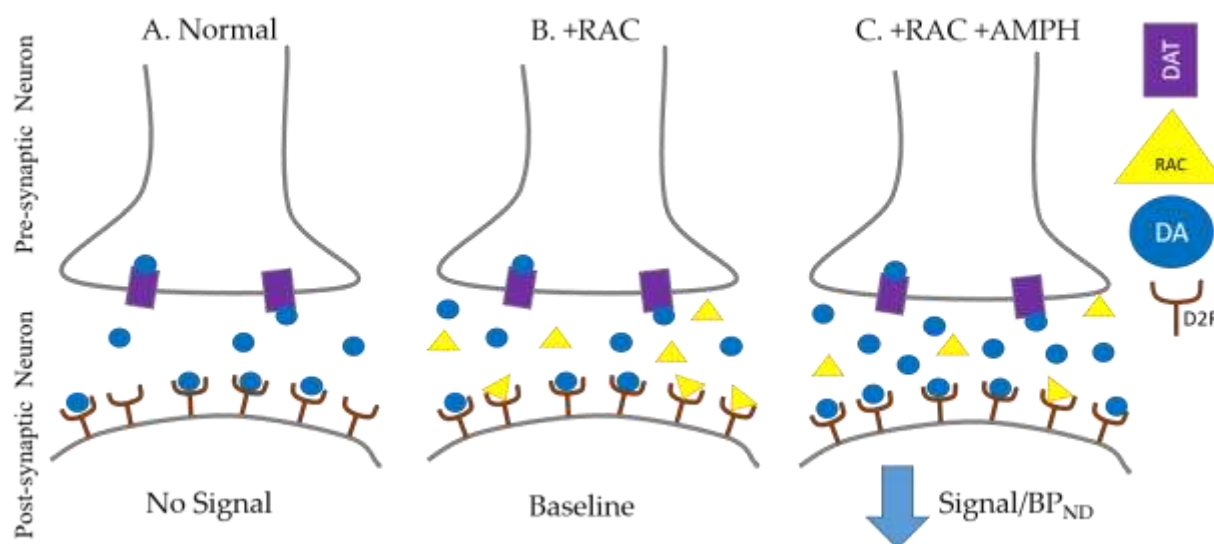


Figure 7 Schematic of PET study mechanism. **A)** Normal: Some proportion of synaptic dopamine (DA) binds to available receptors and reuptake is performed through the dopamine transporter (DAT). **B)** +RAC: Radioactive RAC, a competitive dopamine D₂/D₃ receptor antagonist, enters the synapse after IV injection and binds to available receptors in trace quantities. The quantity “BP_{ND}” refers to the estimation of receptor availability. **C)** +RAC + AMPH: Amphetamine causes an increase of endogenous DA in the synapse, which displaces RAC from receptors and lowers the measurable radioactive signal.

al., 1997), for review, see (K. Yoder, A. Kareken, & D. Morris, 2011) and (Laruelle, 2000).

Figure 7 provides a schematic of this concept.

Subjects received two RAC PET scans, one at baseline and another one hour after oral ingestion of 0.4mg/kg *d*-amphetamine (Cárdenas, Houle, Kapur, & Busto, 2004; Laruelle, 2000; Zhou et al., 2006). The PET scans were acquired on a Siemens mCT CT/PET Scanner (Siemens, Knoxville TN, USA). Scan order was fixed in order to avoid residual effects of AMPH on the baseline condition. Scans took place in the late morning and/or afternoon with a minimum of 2 hours between tracer injections. A low-dose CT scan was acquired for attenuation correction. RAC PET scans were initiated with a bolus IV infusion of 14.6 (SD = 0.42) mCi RAC over 1.5 min. Scan acquisition separated into 10 frames for 30s each, followed by 40 frames for 60s each, for a total acquisition time of 45 minutes. After the AMPH challenge and the second scan, the

subject's vitals (heart rate, blood pressure) were monitored until a medical professional approved it safe for the subject to leave. Data were reconstructed with Siemens software using Filtered Backprojection and a 5 mm Hanning filter.

High resolution T1-weighted structural magnetic resonance imaging (MRI) images were previously acquired for a previous study for each subject (Ma et al., 2017) on a 3T GE Signa MRI (FSPGR, TR/TE = 6.26/2.67 ms, resolution = 1 x 1 x 1 mm³) with an 8 channel head coil.

3.2.4 Data Analysis

Data pre-processing was done in SPM12. For each subject, each dynamic PET frame was coregistered to a mean image created from the first 10 minutes of data. PET data were coregistered to the subject's T1-weighted structural MRI image using the normalized mutual information algorithm in SPM12 (for additional details, please see (Yoder et al., 2016)). Regions of interest (ROIs) were drawn on the subject's T1 image using MRICron (<http://www.sph.sc.edu/comd/rorden/mricron/>). Striatal ROIs consisted of the left and right ventral striatum (VST), pre-commissural dorsal caudate, post-commissural caudate, anterior putamen, and posterior putamen (Martinez et al., 2003). Cerebellar gray matter (minus the vermis) served as the receptor-free reference region. Time-activity curves (TACs) for each ROI were extracted from the dynamic RAC PET data using the MarsBaR toolbox for SPM12 (<http://marsbar.sourceforge.net/>). For each striatal ROI, D₂/D₃ receptor availability was indexed with BP_{ND}, which estimates receptor availability as specifically bound tracer concentration relative to non-displaceable tracer concentration (Innis et al., 2007). Estimations of BP_{ND} were conducted with the multilinear reference tissue model (MRTM) (Ichise et al., 2003). Percent change in BP_{ND} relative to baseline ($\Delta BP_{ND} = (1 - BP_{ND,2} / BP_{ND,1})$) (E. Morris, Lucas, & Cosgrove, 2013) was used to infer AMPH-induced changes in synaptic DA levels.

3.2.5 Statistical Analysis

Statistical tests were performed in the R environment (R Core Team, 2013). Paired student's t-tests were used to test differences in BP_{ND} between both scans. Independent samples student's t-tests were used for comparisons of baseline BP_{ND} and ΔBP_{ND} between welders and controls. Pearson's product-moment correlation tests were performed to assess relationships between variables over all subjects. Statistical significance was set at $p < 0.05$.

3.3 Results

3.3.1 Subjects

A summary of subject demographics is shown in Table 3. Welders were 39.0 ± 9.6 years old; controls were 46.7 ± 3.1 years old. This difference in age was due to an outlier in the welder group, who was 28 years old at the time of the study. While our exclusion criteria were meant to prevent subjects with motor dysfunctions from being included, we did not conduct a pre-study UPDRS. All subjects had a UPDRS score of less than 15, which was considered not symptomatic of a parkinsonian disorder. Nonetheless, one control had an abnormally high UPDRS of 14. Additionally, the same control also had some previous exposure to Mn from a previous non-welding job. $Mn-CEI_{Life}$ for all controls was nearly 10x less than the lowest welder exposure.

Table 3 PET Participant Demographics

	Age	Sex	Height	Weight (kg)	Race	AMPH Dose (mg/kg)	UPDRS	Years Welding	Past Year Mn CEI (mg/m ³ *year)	Cumulative Mn CEI (mg/m ³ *year)
W1	43	M	5'11	116.2	White	0.34	7	18	0.499	2.4736
W2	28	M	5'7	80	African-American	0.375	12	2.5	0.0347	0.348
W3	46	M	6'2	101.7	White	0.39	7	18.5	0.102	2.581
C1	50	M	5'10	84	White	0.36	14	0	0.0042	0.6634
C2	44	M	5'11.5	80	African-American	0.375	1	0	0.0021	0.0588
C3	46	M	6'4"	98	White	0.36	1	0	0	0

3.3.2 Change in DA levels (ΔBP_{ND}) and baseline BP_{ND} indistinguishable between Welders and Controls

A summary of BP_{ND} in all ROIs is in Figure 8. Welders had significantly lower BP_{ND} in the second scan compared to the first, indicative of more DA release in response to AMPH, in the left hemisphere Precommissural Caudate (paired t-test, $p = 0.02$) and left ventral striatum ($p = 0.02$). Controls had no significant differences between first scan and second scan. Between welders and controls, there was a trend towards significance in ΔBP_{ND} in the left pre-commissural caudate ($p = 0.055$) where welders had a higher average ΔBP_{ND} (0.13 ± 0.05 vs -0.13 ± 0.26). No other regions had significant differences in baseline BP_{ND} or ΔBP_{ND} .

3.3.3 Correlations between BP_{ND} , UPDRS motor performance scores, and Mn exposure

UPDRS scores were significantly correlated with right putamen BP_{ND} ($r = 0.86$, $p = 0.03$) (Figure 9A), and while the correlation was of the same sign with the left putamen ($r = 0.44$), this relationship was not significant.

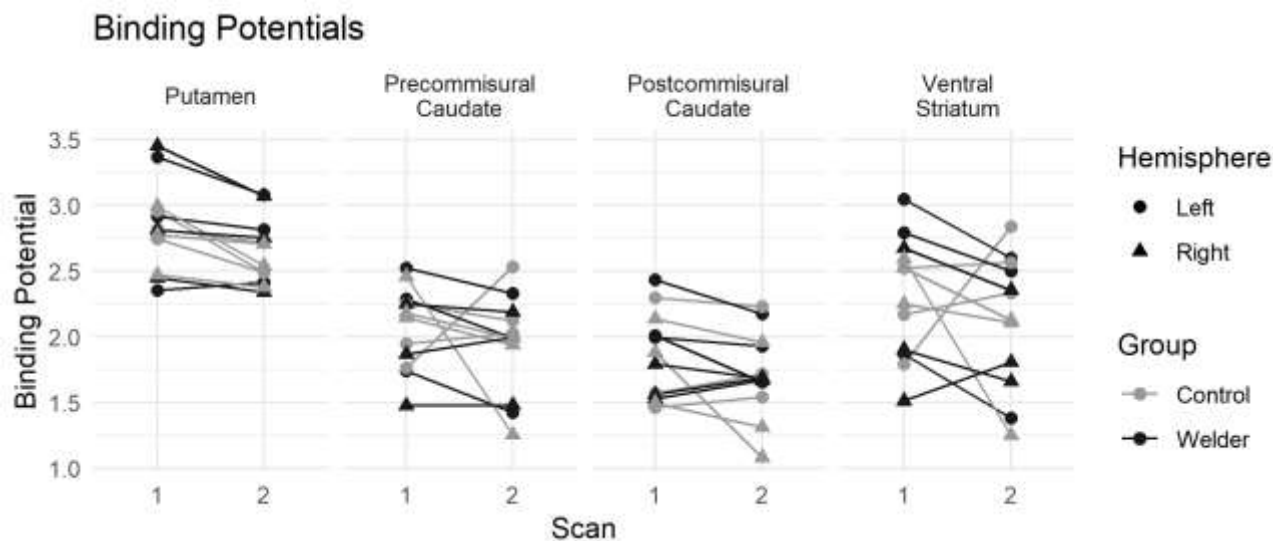


Figure 8 [¹¹C]raclopride Binding Potential (BP_{ND}) during baseline (“1”) and an amphetamine challenge (“2”). Data from welders are in black; controls are in grey.

Baseline BP_{ND} in the right pre-commissural caudate was highly negatively correlated with Mn-CEI_{Life} ($r = -0.88$, $p = 0.02$) (Figure 9B). However, while the left hemisphere had the same sign correlation ($r = -0.20$), this was not significant. Baseline BP_{ND} in the right ventral striatum was also negatively correlated with Mn-CEI_{Life} ($r = -0.88$, $p = 0.02$) (Figure 9C), as well as Mn-CEI_{3M} ($r = -0.85$, $p = 0.03$), and Mn-CEI_{12M} ($r = -0.86$, $p = 0.03$). Baseline BP_{ND} in the left ventral striatum was not significantly correlated with any measure of Mn exposure.

3.4 Discussion

In summary, our preliminary results show that AMPH-induced BP_{ND} was positively associated with UPDRS scores in the putamen, whereas there was a negative relationship between BP_{ND} and Mn exposure in the pre-commissural caudate and ventral striatum.

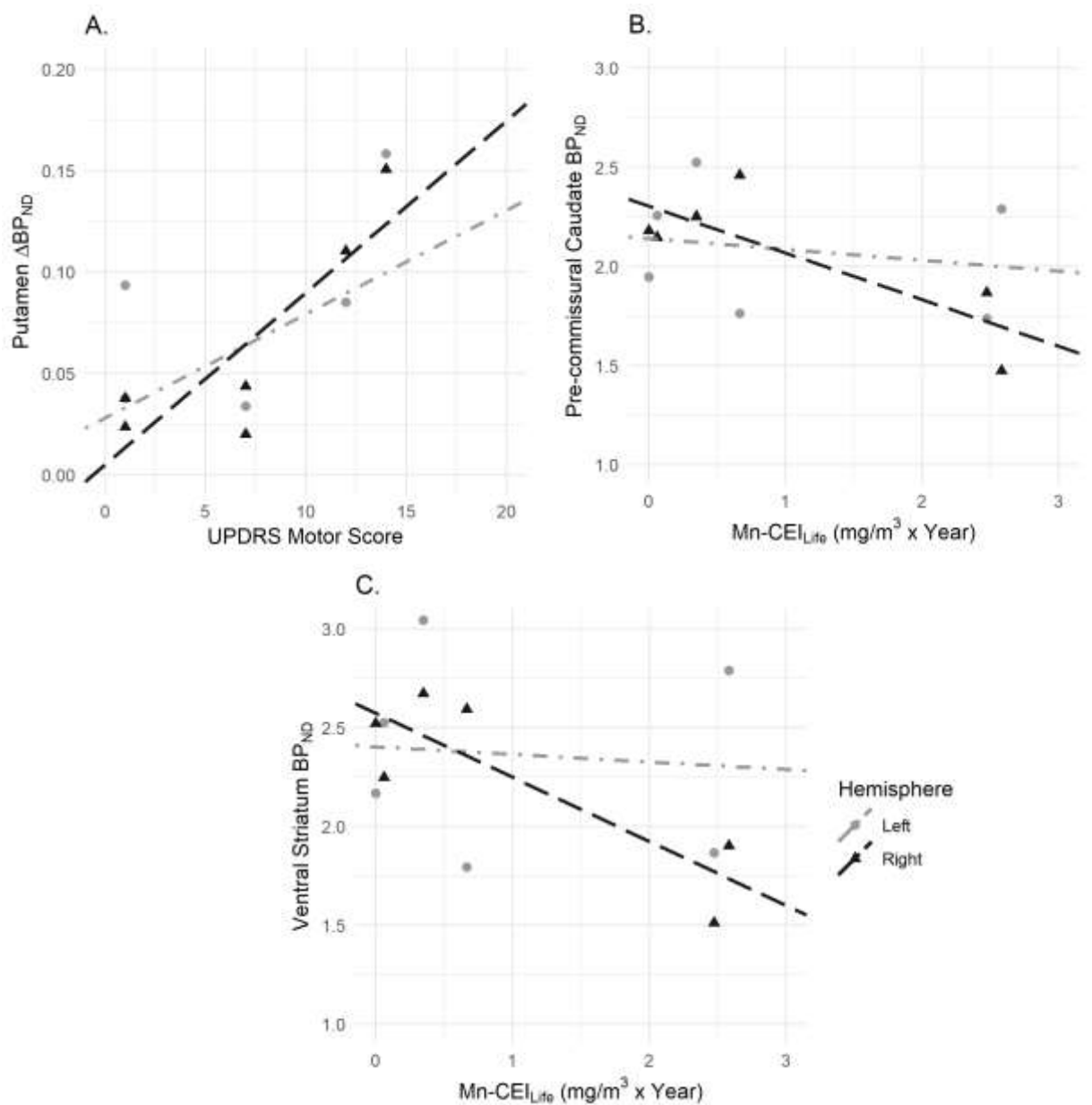


Figure 9 Correlations between BP_{ND} , ΔBP_{ND} , Mn-CEI_{Life}, and UPDRS Score. A) Right putamen ΔBP_{ND} (black) is positively correlated with UPDRS motor score. B) Right pre-commissural caudate baseline BP_{ND} is positively correlated with Mn-CEI_{Life}. C) Right ventral striatum baseline BP_{ND} is significantly correlated with Mn-CEI_{Life}.

The positive relationship between UPDRS and BP_{ND} suggests that subjects with higher UPDRS scores have greater AMPH-induced DA release in the right putamen. This may suggest that dopaminergic function in the putamen may be related to parkinsonian-like symptoms.

There are some limitations with this interpretation. First, across all the subjects, UPDRS scores were not high enough to be considered parkinsonian. Finally, while the correlation was statistically significant, the small average change in BP_{ND} of ~5 % is well within the test-retest variability of pharmacological challenges that increase synaptic dopamine (Wang et al., 1999). Given the small sample size, further investigation is needed to determine the veracity of this result.

It should be noted that the results from this study showed a more attenuated response to the AMPH challenge than anticipated; there is typically a 10-15% reduction in BP_{ND} after a similar oral dose of AMPH (Narendran et al., 2009) (for review, see Laruelle et al. 2000). There may be several factors that explain the data. First, this was a small pilot sample, and additional subjects would likely have decreased the overall variability. It is also possible that differences in the pharmacokinetics of amphetamine across subjects may have obscured our ability to reliably detect AMPH-induced DA release. If the peak timing of the amphetamine effect differed across subjects, then this would cause differential estimations of the relative magnitude of DA release (Yoder, Wang, & Morris, 2004). Along these lines, the subjects' weight may have had an impact on total dose received. The target dose for each subject was 0.4 mg/kg, however, some subjects weighed more than 100 kg, yet we were limited to a total maximum dose to 40 mg because of our safety protocol. Thus, two subjects, both welders, did not receive the full relative dose of AMPH.

In welders there was also a significant negative relationship between baseline BP in the right pre-commissural caudate and $Mn-CEI_{Life}$. Guilarte et al. (2008) reported a similar finding of reduced striatal baseline BP in macaques after extended exposure to Mn (Guilarte et al., 2008). A clinical report on Taiwanese smelters also reported lower caudate BP (Huang, 2005). Given that

BP is a complex index that is influenced by both receptor density and endogenous DA levels, there are two potential interpretations of our data. First, that Mn exposure decreases D₂/D₃ receptor density, or that it somehow increases synaptic DA levels. However, the latter interpretation is inconsistent with prior work in animal and in vitro models (Burton & Guilarte, 2009; Seth & Chandra, 1984; Tran, Chohanadisai, Crinella, Chicz-DeMet, & Lönnerdal, 2002). Therefore, this result points towards a loss of receptors. However, a recent study on workers exposed to Mn found higher D₂/D₃ receptors in the basal ganglia (Criswell, Warden, et al., 2018). Additional work is needed to understand the consequences of Mn exposure on the dopaminergic system in humans may be needed.

Additionally, we found a significant negative correlation between Mn-CEI_{Life} and baseline BP_{ND} in the right VST. This relationship may suggest a loss in D₂/D₃ receptors in this region that is known to be associated with reward circuitry while dysfunctions are associated with mood disorders (Caseras, Lawrence, Murphy, Wise, & Phillips, 2013; Drevets, Price, & Furey, 2008; Yip, Worhunsky, Rogers, & Goodwin, 2015). One of the first reported symptoms of Mn toxicity is mood disturbance (Bowman, Kwakye, Herrero Hernández, & Aschner, 2011; Olanow, 2004). Welders (Bowler et al., 2011) and munition workers (Bowler et al., 2001) have reported depression and anxiety at a greater rate than controls. Other mood disturbances include fatigue, impulsive or compulsive behavior, psychotic experiences, and hostility (Bowler, Mergler, Sassine, Larribe, & Hudnell, 1999). At the present, no mechanism for why mood disturbances occur in Mn intoxicated workers exists.

Our comparisons between welders and controls were limited by several factors. First, recruitment was difficult due to the health considerations that had to be taken into account for an AMPH challenge, e.g., high blood pressure or heart conditions; these exclusion criteria

eliminated much of the available welding population. Therefore, to complete the study, we recruited outside of the intended age range and outside the place of employment. This potentially complicated our results, as BP is known to be affected by age (Antonini et al., 1993; E. D. Morris et al., 1999; D. F. Wong et al., 1984) and the one welder (Welder 2) was nearly 20 years younger than the rest of the subjects. We also did not take into account potential movement disorders prior to recruitment, and one control (Control 1) had a much higher UPDRS score than the other subjects. Nonetheless, the pilot results suggest that there are putative relationships between Mn exposure and the dopamine system.

3.5 Conclusion

This study establishes feasibility for a PET study incorporating an AMPH challenge into the study of Mn exposure. Although this is a pilot study, some general trends between dopaminergic parameters and UPDRS and Mn exposure were noted in the data that may inform future work. There were no initial differences in AMPH-induced DA release between controls and welders. Given the pilot study results, we are optimistic that RAC PET may provide insight as to mechanisms behind the mood and motor impairments of Mn toxicity.

4. WHOLE-BRAIN R1 PREDICTS EXPOSURE GROUPS IN WELDERS: AN APPLIED USE OF SUPPORT VECTOR MACHINES IN NEUROIMAGING

4.1 Introduction

Manganese (Mn) is a neurotoxic metal that is a common constituent of welding fume which thousands of welders inhale every day in the manufacturing industry. Symptoms of excessive Mn exposure are similar to Parkinson's disease and include bradykinesia, dystonia, postural tremor and rigidity (Guilarte & Gonzales, 2015a; Racette, Aschner, et al., 2012; Tsuboi, Uchikado, & Dickson, 2007). These symptoms do not recede upon cessation of exposure (Guilarte, 2013), nor are symptoms alleviated with the standard treatment for PD, levodopa (Olanow, 2004). Therefore, preventing symptoms is the primary goal when it comes to risk assessment. The primary method of risk assessment comes from exposure monitoring through air sampling where 0.02 mg/m^3 was determined to be the recommended threshold limit value (Ward et al., 2017). While having a low limit is a conservative method of minimizing risk, it is unknown whether this level is too low or low enough to prevent symptoms from eventually occurring. Some have recommended raising the occupational exposure level to 0.1 to 0.14 mg/m^3 based on studies that adequately accounted for exposure levels in the work place (Bailey, Kerper, & Goodman, 2018). Yet, it is unknown whether continued low levels of exposure lead to accumulative effects.

Because the symptoms of Mn toxicity are neurological, understanding how Mn affects the brain is of vital importance. But, to do so, we need to have an idea of how much Mn is in the brain for a given exposure. When Mn is inhaled into the lungs, it is readily absorbed into the bloodstream (Leggett, 2011) and into the pulmonary veins. Inhaled Mn therefore bypasses the

first pass effect of the liver and is transported to the brain. There are two primary barriers that Mn must then pass before entering the brain, the blood brain barrier (BBB) and the blood CSF (cerebral spinal fluid) barrier (BCB). Mn can cross the BBB while bound to transferrin via transferrin transporters and ZIP8 transporters (Aschner & Aschner, 1991). Mn can also penetrate the BCB via divalent metal transporter 1 (DMT1) (Yokel, 2009). Mn competes with Iron for DMT1, but it has been found that there is preferential uptake for Mn in the choroid plexus, site of the BCB (Bornhorst et al., 2012).

Once Mn is in the brain, it disperses. It can be taken into glial cells through transporters and into neurons through Ca^{2+} voltage-gated transporters (Bedenk et al., 2018; Leuze et al., 2012). Once in cells, Mn tends to be taken into endosomes or the mitochondria (Borg & Cotzias, 1958). Mn can also travel anterograde along axons. Using the MRI relaxation rate R1, which is proportional to Mn in the region, we can measure Mn uptake, accumulation, and dispersion in the brain (Yeh et al., 2016). This has been done to great effect in studies involving rats (Lehallier, Coureaud, Maurin, & Bonny, 2012), monkeys (Dorman, 2006; J. D. Park et al., 2007; Shinotoh et al., 1995), and humans (Lee et al., 2015; Lee, Flynn, Lewis, Mailman, & Huang, 2018; Lewis et al., 2016; Long et al., 2015; Ma et al., 2017), but understanding the characteristics of this relationship is still ongoing. For instance, in monkeys, there was a strong correlation and linear relationship between R1 and Mn in the various regions of the brain (Dorman, 2006). However, in humans, R1 has been found to be higher in subjects with higher exposure versus controls with lower exposure, but there was no linear relationship between R1 and exposure (Ma et al., 2017). However, there appears to be a non-linear relationship which may suggest a physiological threshold (Lee et al., 2015), therefore complicating the ability to use R1 as a measure of Mn content in the brain and as a potential biomarker. Additionally, dispersion

of Mn appears to be different in rats compared to monkeys or humans (Bock et al., 2008). Taken together, this suggests that getting a better estimate of Mn content in the brain, rather than exposure, may be a better metric for assessing risk. To do this, a biological model could be employed to estimate Mn in the brain. Biological modeling is used to simulate how a specific xenobiotic will disperse throughout the body. By accounting for this, the model can estimate how much Mn will be in a part of the body at a given time after exposure.

Finally, the amount of Mn in the brain is hypothesized to have direct effects on motor dysfunction. Assessment of motor impairment is done using the Unified Parkinson's Disease Rating Scale (UPDRS) (Goetz et al., 2008). Given by a certified neurologist, this series of tests looks at a variety of symptoms of Parkinson's disease including bradykinesia, tremor, and postural gait. Higher scores are reflective of higher levels of dysfunction with scores greater than 15 being indicative of a parkinsonian disorder. Additionally, neurochemistry has been found to be affected by increased Mn exposure, and thus increased Mn accumulation. Previously, γ -aminobutyric acid (GABA), the primary inhibitory neurotransmitter in the central nervous system, had been shown to be higher in the thalamus in groups exposed to higher levels of Mn (Ma et al., 2017).

If we can track changes in Mn levels in the brain over time, we may be better equipped to predict outcomes for workers. Our hypothesis is that whole-brain R1 measures will reflect Mn uptake, accumulation, and dispersion within the brain and largely depends on the cumulative effect of exposure levels over a worker's lifetime. These measures will then be readily identified as a reproducible pattern using advanced data analysis tools, such as machine learning. To this end, we employed a data analysis pipeline that used whole-brain R1 MRI data, transformed it into its most representative brain structures, and then used that to predict groups at different

thresholds of air Mn exposure, excess brain Mn, and total years welding. Using R1 as a proxy for Mn, we also assessed whether whole-brain R1 data could predict groups at different thresholds of UPDRS score and thalamic GABA.

4.2 Methods

Data used in this study was compiled from 89 subjects (52 welders, 37 controls) in previous studies (Edmondson et al., 2015; Ma et al., 2017; Ward et al., 2017). All subjects gave informed consent at that time. The methods used for data acquisition (Relaxometry, Spectroscopy, UPDRS, and Exposure Assessment) from these studies is briefly summarized below. Methods specific to this study are elaborated, as needed.

4.2.1 Relaxometry

MRI was performed on a 3T GE Signa MRI scanner using an 8-channel head coil. A high-resolution 3D T1-weighted structural image (FSPGR, TR/TE = 6.26/2.67 ms, resolution: 1 x 1 x 1 mm³) was taken for use in segmentation. Segmentation was performed using Freesurfer (surfer.nmr.mgh.harvard.edu) which parsed the brain into 192 separate regions of interest (ROI) as masks. To produce T1 relaxation time maps, we acquired a spoiled gradient echo imaging sequence (SPGR, TR/TE = 6.36/1.76 ms, resolution: 1 x 1 x 2 mm³) using two different flip angles (3°, 17°). A 3D T1 relaxation time map was generated using the images from these two flip angles

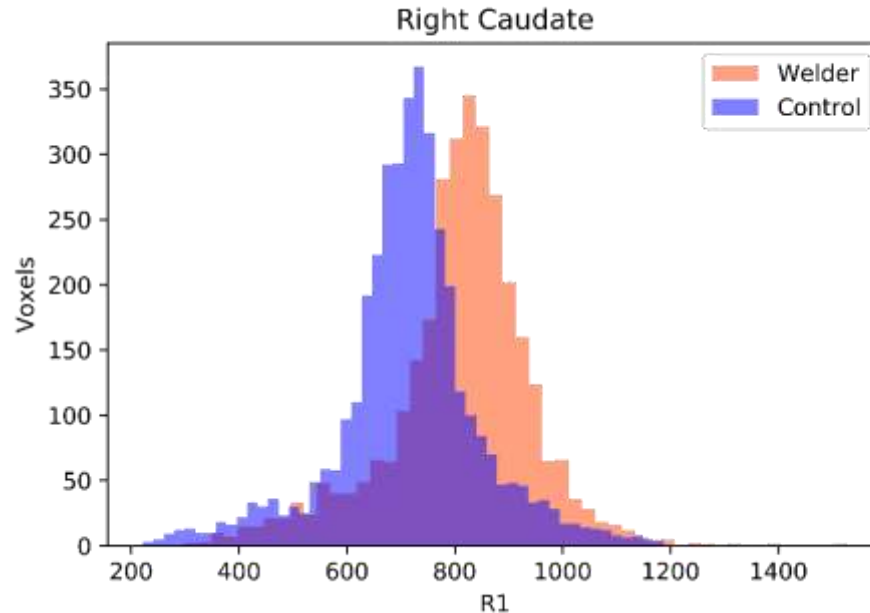


Figure 10 Distribution of R1 in a Region of Interest. This histogram shows the distribution of R1 in the right caudate of one welder (orange) and one control (blue). There is a shift to the right and slightly wider variance for the welder compared to the control. Rather than using a single point estimate of the distribution, we chose to select five different parameters that described the R1 distribution. For each ROI, we calculated the median, variance, skew, 10-percentile, and 90-percentile.

(Christensen et al., 1974). To correct for inhomogeneity in the radiofrequency field, we acquired an inversion recovery SPGR with the same parameters as the SPGR images (Deoni, 2007). R1 in each voxel was then calculated as inverse T1 relaxation time where $R1 = 1/T1$. Finally, the segmented masks were used to extract R1 from each ROI. R1 values for every voxel in each ROI were used to calculate five different statistics: median, variance, skew, 10-percentile, and 90-percentile. These statistics were chosen to best describe the overall histogram in each ROI (Figure 10).

4.2.2 GABA

GABA concentrations in the thalamus were obtained from spectra acquired using magnetic resonance spectroscopy (MRS). Using MEGA-PRESS localization (TR/TE = 2000/68

ms, 256 Averages) (Mullins et al., 2014), a volume of interest (VOI) was placed over the right thalamus (25mm x 30mm x 25mm). Spectra were quantified using LCModel V6.3-1B (Provencher, 1993). Reported GABA concentrations were CSF-corrected to account for CSF volume in the VOI. See Ma et al. for more details.

4.2.3 UPDRS

Motor dysfunction was measured using the Unified Parkinson's Disease Rating Scale Part III (UPDRS-III) (Goetz et al., 2007). A certified neurologist tested each subject and rated them based on their motor performance in tasks measuring symptoms such as tremor and bradykinesia. A higher score represented worse performance. A score of 15 or below is considered asymptomatic for Parkinsonism, whereas greater than 15 suggests a disease state.

4.2.4 Exposure Assessment

Air Mn exposure was determined by performing personal air sampling of respirable Mn on subjects in the workplace. The air exposure values were averaged to respirable Mn concentrations per worksite in the factory. Personal air sampling was obtained over 8 hours, a standard time period of measure. Air filters for sampling were placed inside the welding helmet for welders and on the shoulder in the personal breathing zone for control subjects to be as close as possible to actual breathing exposure levels.

4.2.5 Biokinetic Model

A biokinetic model was used to determine the amount of Mn accumulation due to occupational exposure in the brain above normal amounts (Figure 11). The model was created with a home-made script using SciPy's ordinary differential equation module based on the Leggett 2011 model (Leggett, 2011). Air Mn exposure was the input. To determine how much

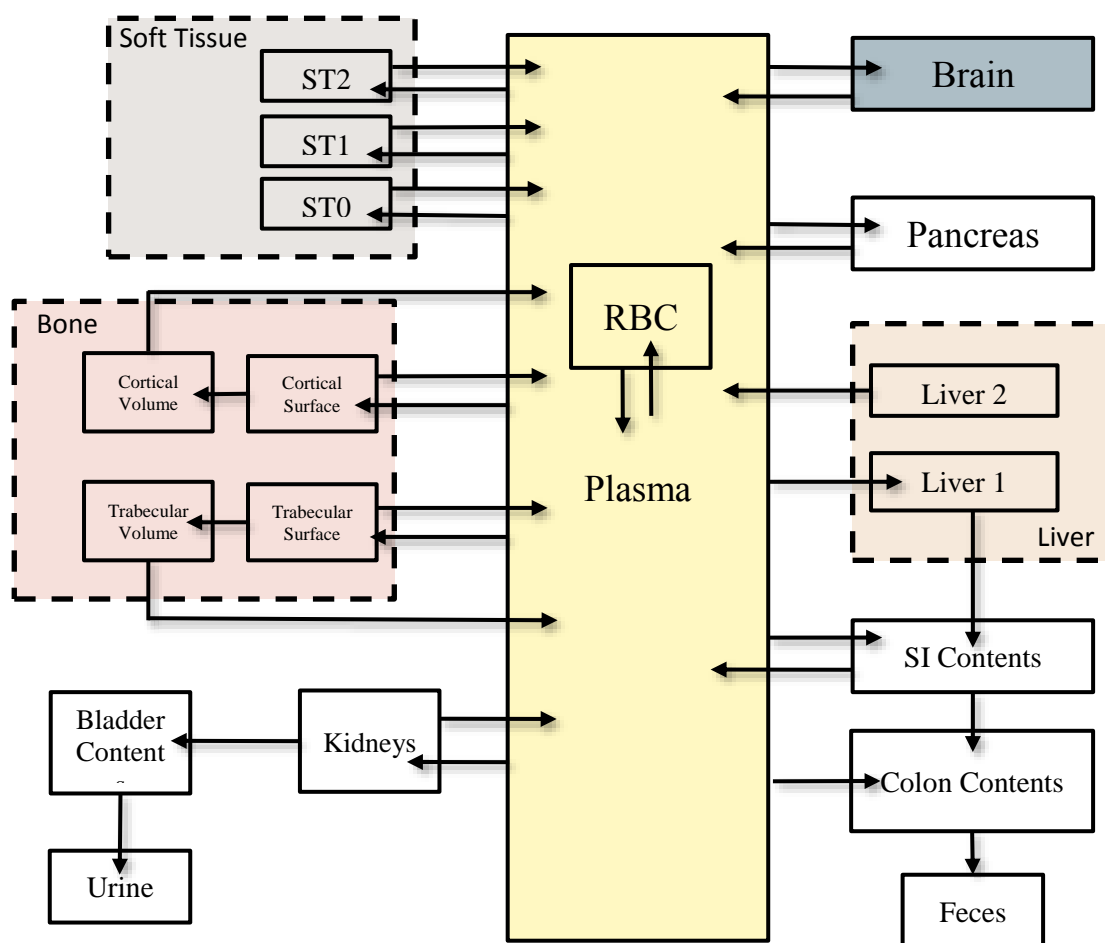


Figure 11 Biokinetic model of Mn. This model is derived from a previously published model.

Respirable Mn was assumed to be transported into the plasma compartment with 100% efficiency. The model then describes through a series of compartments how Mn disperses itself throughout the body. This study used values of excess brain Mn that was calculated from the brain compartment.

Mn was inhaled each day, the air Mn exposure value was adjusted for the total amount of air inhaled over the 8 hour workday. This amount of Mn was then assumed to be 100% taken into the blood compartment. ODEs were used to calculate the amount of Mn in each compartment on a given day. Using each subject's work-history, a timeline of Mn accumulation was created with the final data point representing the amount of Mn in the brain on the day of scanning. We called this value Excess brain Mn. To simplify the model, we assumed every person worked 8 hours a day, 7 days a week. This is largely because the welders in our cohort were known to work up to 7

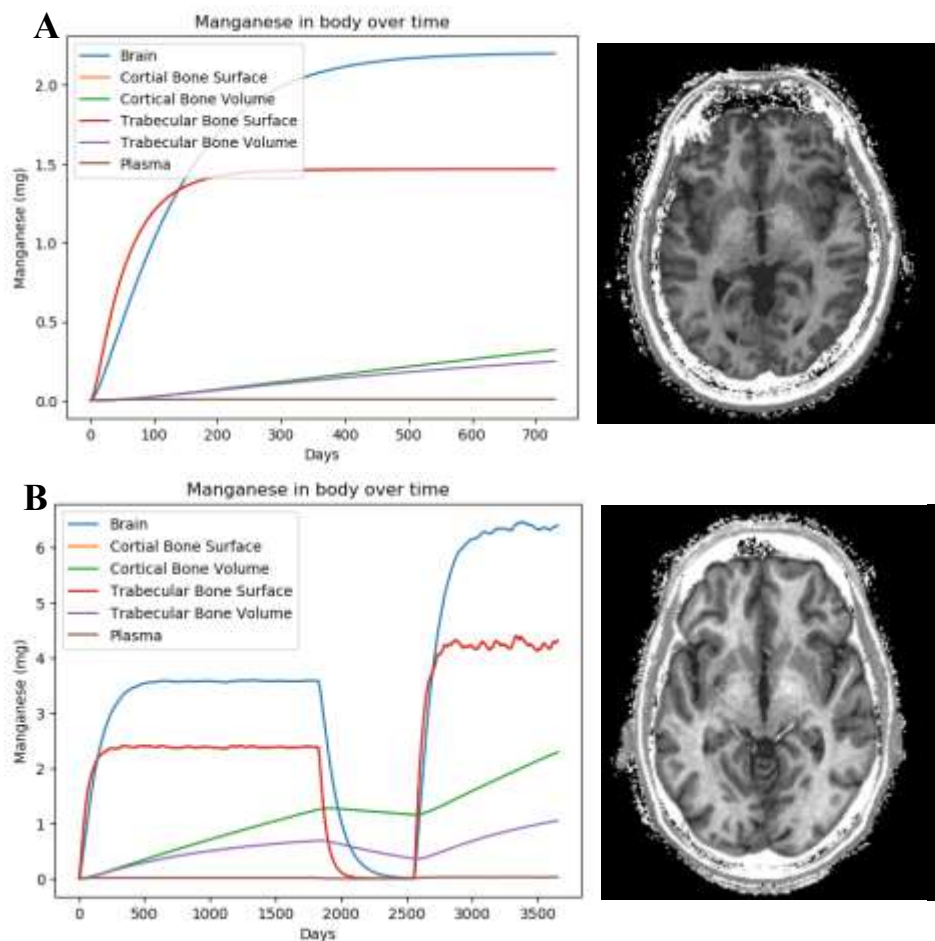


Figure 12 Example Results from Mn Biokinetic Model. **A)** Shows the trend of Mn accumulation in 6 regions of the body: brain, cortical bone surface, cortical bone volume, trabecular bone surface, trabecular bone volume, and blood plasma. This welder worked for 2 years with an average air Mn exposure concentration of 0.088 mg/m^3 . **B)** Another welder worked in three jobs over 10 years. The first job was for 5 years with an air concentration of 0.14 mg/m^3 . The second job was welding aluminum, and thus no Mn exposure. The third job lasted for 3 years prior to his participation in a previous study and were exposed with an exposure level of 0.24 mg/m^3 . As can be seen by the R1 images on the right, taken from the same location and with the same contrast, the subject in B has much brighter white matter – indicative of higher R1 due to Mn accumulation.

days a week and up to 10 hour days. To account for this, we assumed the same with a relatively conservative estimate of time spent working. These values were then used as inputs to the biokinetic model. Excess brain Mn was extracted according to the differential equation:

$$\frac{dN}{dt} = \lambda_{Blood \rightarrow Brain} N_{Blood} - \lambda_{Brain \rightarrow Blood} N_{Brain}$$

Where N is the amount of Mn in the compartment and λ is the rate of transfer from one compartment to the other. Finally, we used the final day's value for excess brain Mn (Figure 13).

4.2.6 Data Processing

All models were built using Scikit-Learn, a machine learning package developed in Python (Pedregosa et al., 2012). Data was standardized using the StandardScaler method in Scikit Learn. This method removes the mean and scales to unit variance over the whole brain where each sample score is calculated as a z -score:

$$z = \frac{x - u}{s}$$

Where x is the sample, s is the standard deviation of all samples, and u is the mean of all samples.

Principle component analysis (PCA) was then performed on the standardized data. PCA is performed by calculating the covariance matrix of the data and then extracting the eigenvalues and eigenvectors that explain up to a set threshold of variance in the data. For this study, we chose 90% variance as the cut-off. In PCA, each eigenvector contains the weights to produce a linear combination of each ROI while the normalized eigenvalues are the percent of total variance explained by the eigenvector. Once the number of eigenvectors is chosen, they are used to transform the data.

A support vector machine (SVM) was created for each target, threshold, and statistic. A target is the variable that the SVM is going to predict. In this study, targets include: air Mn exposure, excess brain Mn, total welding years, age, thalamic GABA, and UPDRS score. For each target, thresholds were created based on its range of values ensuring that at least one subject

was in the minority group. A linear kernel was used with a penalty term (C) equal to 1 which was adjusted based on class imbalance and calculated for each threshold. Due to our relatively low sample size, a linear kernel was chosen to avoid overfitting the data and remain readily interpretable. SVM was implemented using the LIBLINEAR library (Fan, Rong-En, 2008). In simplest terms, SVM models our data in terms of a hyperplane boundary created by maximizing the distance, the margin, between data points that are nearest to the hyperplane (support vectors).

4.2.7 Model Testing & Scoring

For each SVM model created for a target, statistic parameter, and threshold, leave one-out cross validation (LOO-CV) was used to estimate generalizability performance. Classes were determined by the threshold where Class 0 was less than or equal to the threshold and Class 1 was greater than the threshold. This was done by creating the SVM model with N-1 subjects and then use the model to predict the class for the remaining subject. This was done of all subjects before aggregating all predictions to assess scoring in a process called “bagging”. Bagging is the process of using multiple machine learning models to improve overall performance. In this case, class predictions from all five statistic SVM models are determined and then the best prediction is chosen based on a majority rule.

A confusion matrix (Figure 13) was created by calculating the true positives (TP), true negatives (TN), false positives (FP), and false negatives (FN). SVM models were scored using accuracy $\left(\frac{TP+TN}{TP+TN+FP+FN}\right)$ and recall $\left(\frac{TP}{TP+FN}\right)$. Accuracy depicts the total number of correct predictions and describes how correct the model is when accounting for all possible outcomes while recall focuses on the total number of correct predictions for class 1 out of all possible class 1 available (i.e. the proportion of subjects with Mn levels above threshold that are correctly

		Predicted	
		Yes (1)	No (0)
Actual	Yes (1)	TP	FN
	No (0)	FP	TN

Figure 13 Confusion Matrix and Scoring. Shows a typical confusion matrix and the calculation for true positive (TP), false positive (FP), false negative (FN), and true negative (TN).

identified) and only measures how well a model can identify one group, in our case, subjects with high Mn exposure. Superior model performance is considered from a combination of high accuracy with high recall.

Without appropriate precautions, a SVM model will be biased towards the majority class to maximize accuracy of the model potentially leading to always predicting the majority class. To measure how far away from equal distribution of classes, a 95% confidence interval was calculated using a test of proportions. Therefore, we accounted for this with a penalty term that takes into account the imbalance of the classes:

$$a = \frac{n}{(m * q)}$$

Where n is the number of samples, m is the number of classes and q is the number of subjects in the class. To measure how well our model is performing, taking into account class imbalance, appropriate scoring (Recall) and performing a test of proportions to assess the distribution of errors between FP and FN.

4.3 Results

4.3.1 PCA

Results from PCA are summarized in Table 4. By focusing on only using a number of principle components (PCs) required to explain 90% of the total variance, we effectively eliminated a lot of the noise that might have obscured our results. Median, 10-percentile, and 90-percentile all went from using all 192 ROIs as features to only needing less than 7% total features to represent 90% of the variance in the data. Variance in each statistic also occurred more in different regions. For example, the first PC for median had the highest weighting for the superior temporal sulcus, but it should be noted that most of the ROIs had near equal weightings. The second PC was heavily weighed by variations of median in the ventricle and corpus callosum ROIs while the third was influenced strongly by variations in the postcentral gyrus and other ROIs near there in the brain. Conceptually, the structures with greater variance in R1 could be due to Mn uptake in the regions. Therefore, with PCA, noise is eliminated and regions with greater variance in R1 are used for later analyses.

Table 4 Results for Principle Component Analysis of Whole-Brain R1

R1 Distribution Statistic	# of PCs explaining 90% total Variance	PC1		PC2		PC3	
		% Variance Explained	Highest Weighted ROI	% Variance Explained	Highest Weighted ROI	% Variance Explained	Highest Weighted ROI
Median	6	77%	Superior Temporal Sulcus	6.4%	Ventricle, Corpus Callosum	2.8%	Postcentral Gyrus
Variance	25	41.6%	Cerebral White Matter	11%	Insula	4.9%	Cerebellum White Matter
Skew	49	12.3%	Corpus Callosum	7.8%	Precentral & Postcentral Sulci	5%	Superior Frontal Gyrus
10 percentile	13	72.6%	Parietal Occipital Sulcus	4.8%	Ventricles	2.5%	Precentral & Postcentral Gyri
90 percentile	13	63.8%	Parietal Occipital Sulcus	9.6%	Cuneus & Precuneus Gyri	3.9%	Lateral Ventricles

4.3.2 SVM Models

Results for all SVM models are summarized in Figures 15,16, 17, and 18. Figure 15 shows the prediction accuracy for all models across all thresholds. Figure 16 shows the combined prediction recall and accuracy. Figure 17 shows the proportionality of classes across all thresholds while Figure 18 shows the proportionality of prediction error.

4.3.2.1 Study Group

A SVM model predicting whether a subject is welder or control had an accuracy (57.3%) and recall (57.9%) slightly better than chance. Of the five individual statistic models, both skew (68.5 %) and variance (68.5 %) performed above chance, while the 10-percentile (55%) and 90-percentile (59.6%) performed near chance. Median was the worst performed with an accuracy of 43.8%, suggest middle mass measures of a ROI were not sufficient to discriminate between welders and controls.

4.3.2.2 Air Mn Exposure

Bagged models predicting air Mn exposure performed best with thresholds between 0.16 and 0.25 mg/m³. In this range, accuracy ranged from 83% upwards to 88%. Similarly, recall ranged from 58% to 78% (Figure 15A). While the classes were imbalanced at these higher threshold (Figure 17A), the errors (FN, FP) were distributed evenly (Figure 17A). When looking at the accuracies of specific statistics, skew and variance predict better than the other three in the lower exposure levels, but are quickly taken over by the 10-percentile, which also performs better than the bagged model in some levels (Figure 14A).

4.3.2.3 Excess Brain Mn

Bagged SVM models predicting excess brain Mn performed best with thresholds between 6.5 and 8.5 mg/m³. In this range, accuracy ranged from 79% to 80% while recall ranged from 58% to 60% (Figure 15B). In this range, the groups were imbalanced (Figure 16B), but the prediction errors were within expected distributions (Figure 17B). For specific statistics, median performed very poorly in the earlier ranges and likely negatively impacted the performance of the bagged model, but in later ranges, predicted well and nearly on par with the bagged model.

4.3.2.4 Total Welding Years

Better performance measures were found at later thresholds for the bagged SVM model predicting total welding years. For thresholds of 18-20 years, accuracy and recall were between 80 and 88% (Figure 15C). Below these levels, accuracy and recall were slightly better than chance, on average, but did not perform very well in the lower ranges from 0 to 6 years. Median performed poorly for most thresholds, but increasingly performed better than average above 12.5 years welding (Figure 14C).

4.3.2.5 Age

A bagged SVM model predicting age was effective across all ages with the exception of the later ones where precision and recall went to 0%, suggesting all errors were false negatives with no true positive predictions (Figure 15D). Nonetheless, for threshold ages from 24 to 52 years, accuracy and recall were between 70% and 80%. Individual statistics did not greatly differ from the bagged results, with the exception of the 90-percentile, which may have negatively impacted the bagged results in the lower age thresholds (Figure 14D). Errors are within the expected deviation after 1.5 mM and are favoring Type 1 errors before that threshold (Figure 17D).

4.3.2.6 Thalamic GABA

Bagged SVM models perform reasonably consistent across all thresholds with accuracies ranging between 63% and 81%, significantly above chance (Figure 15E). The model's recall was also between 60% and 75%. But, skew consistently underperformed compared to the other statistics with a strong dip in accuracy at 1.4 mM to 41% (Figure 14E). This likely had a large negative impact on the overall bagged SVM model performance in the lower ranges below 2.0 mM, but also some impact above that threshold. In fact, the median over-performed the bagged SVM model above 2.2 mM with accuracy approaching 90%.

4.3.2.7 UPDRS Score

The bagged SVM model has accuracies that range from 61% to 93%, but recall dramatically drops after a threshold score of 9 to below chance (Figure 15F). This suggests that the model cannot identify any differences between scores above or below these thresholds and is relying upon the majority class for predictions. There is very high accuracy and recall for the SVM model at a threshold of 0 which may indicate a robust signature that separates those with no motor dysfunction with those with even minor dysfunction. But, the class imbalance is very severe in this range and this may be an artifact of this (Figure 16F).

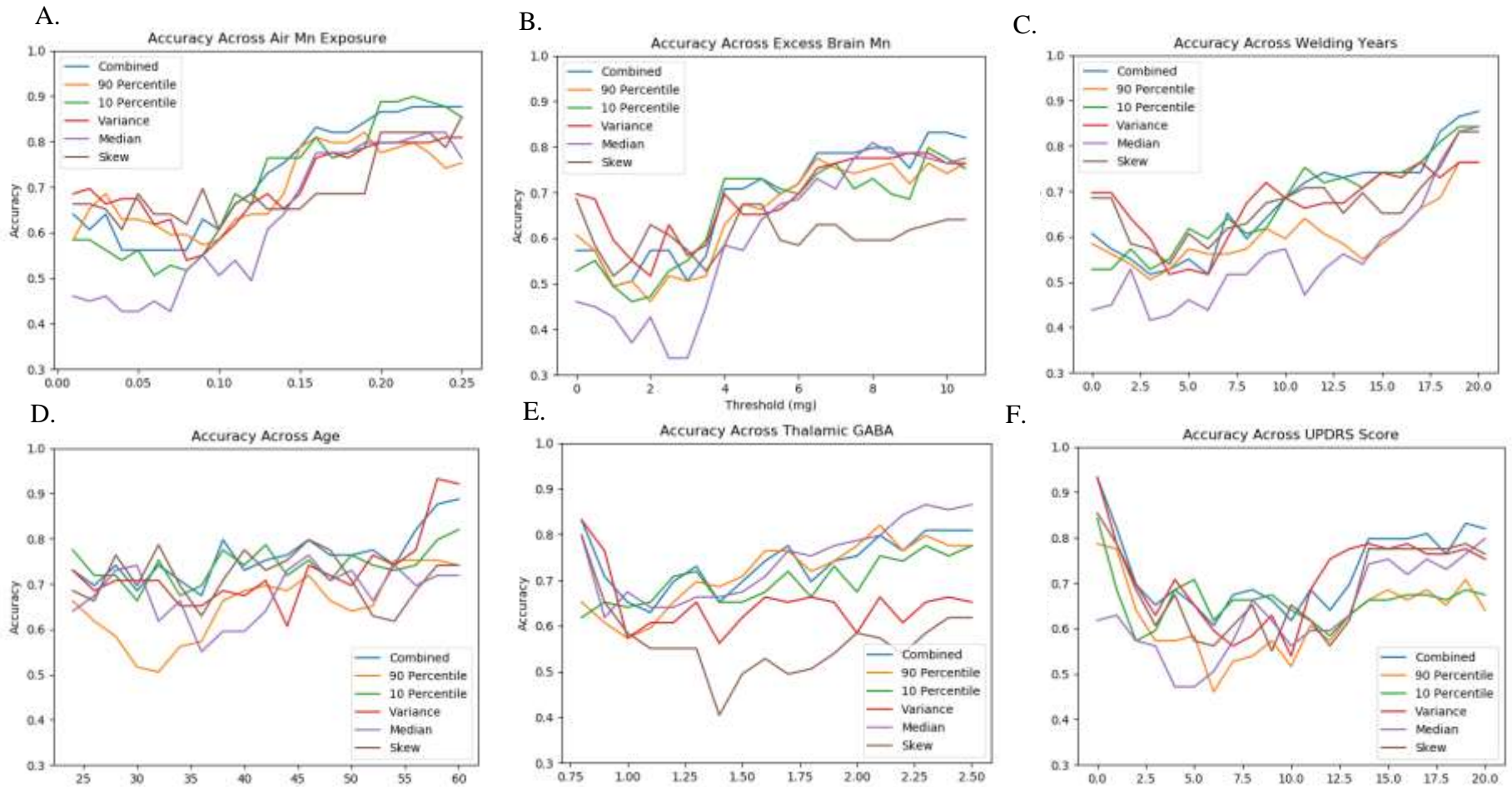


Figure 14 SVM Model Accuracy. Show accuracy of the combined, or bagged, SVM model as well as the individual statistics that went into the combined model for all 6 targets: Air Mn Exposure, Excess brain Mn, Total Welding Years, Age, Thalamic GABA, and UPDRS Score.

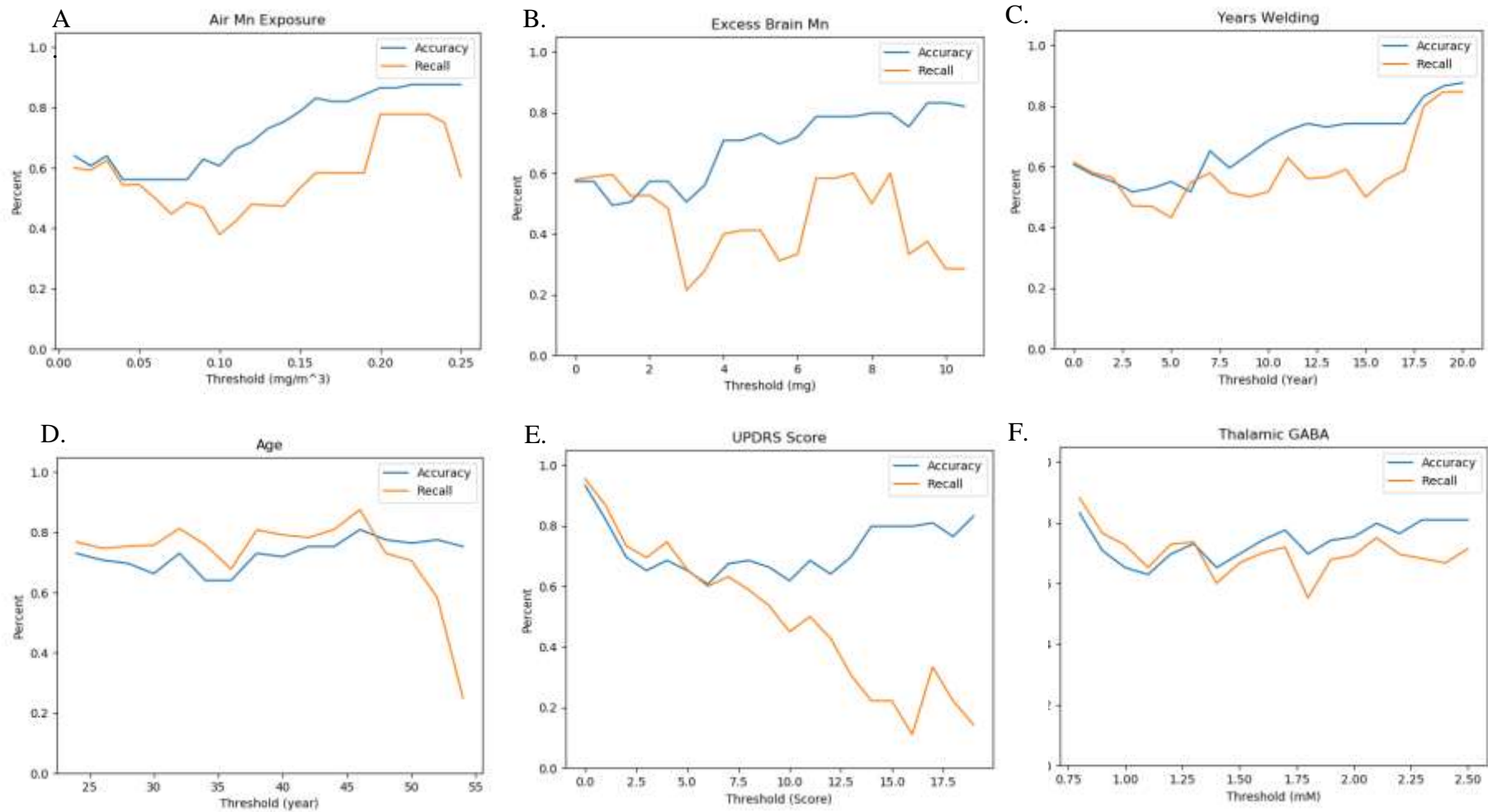


Figure 15 SVM Model Scoring. Shows accuracy and recall for the combined, or bagged, SVM model for all 6 targets: Air Mn Exposure, Excess brain Mn, Total Welding Years, Age, Thalamic GABA, and UPDRS Score.

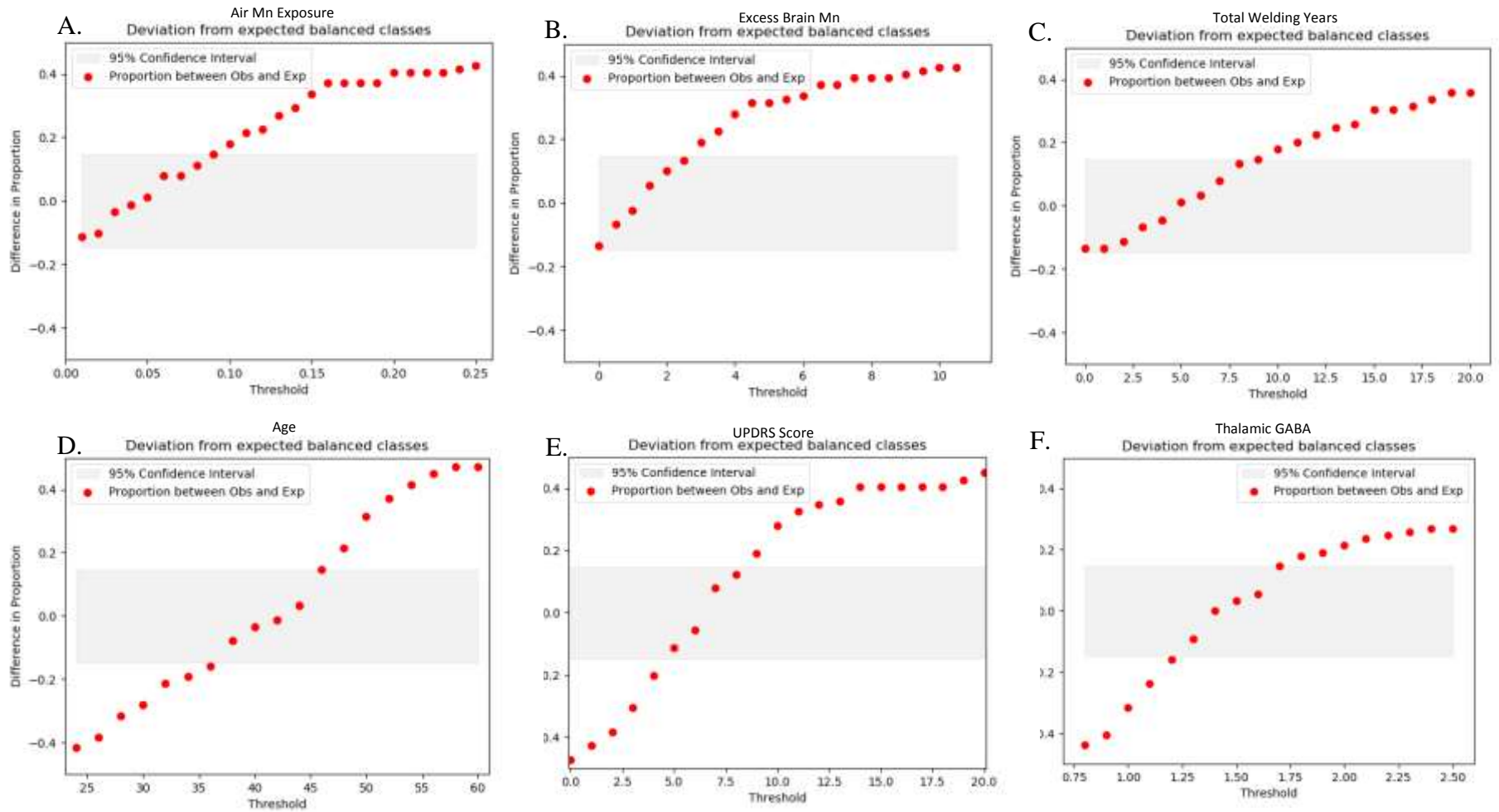


Figure 16 SVM Model Class Imbalance. Shows class balance for each threshold for the combined, or bagged, SVM model for all 6 targets: Air Mn Exposure, Excess brain Mn, Total Welding Years, Age, Thalamic GABA, and UPDRS Score.

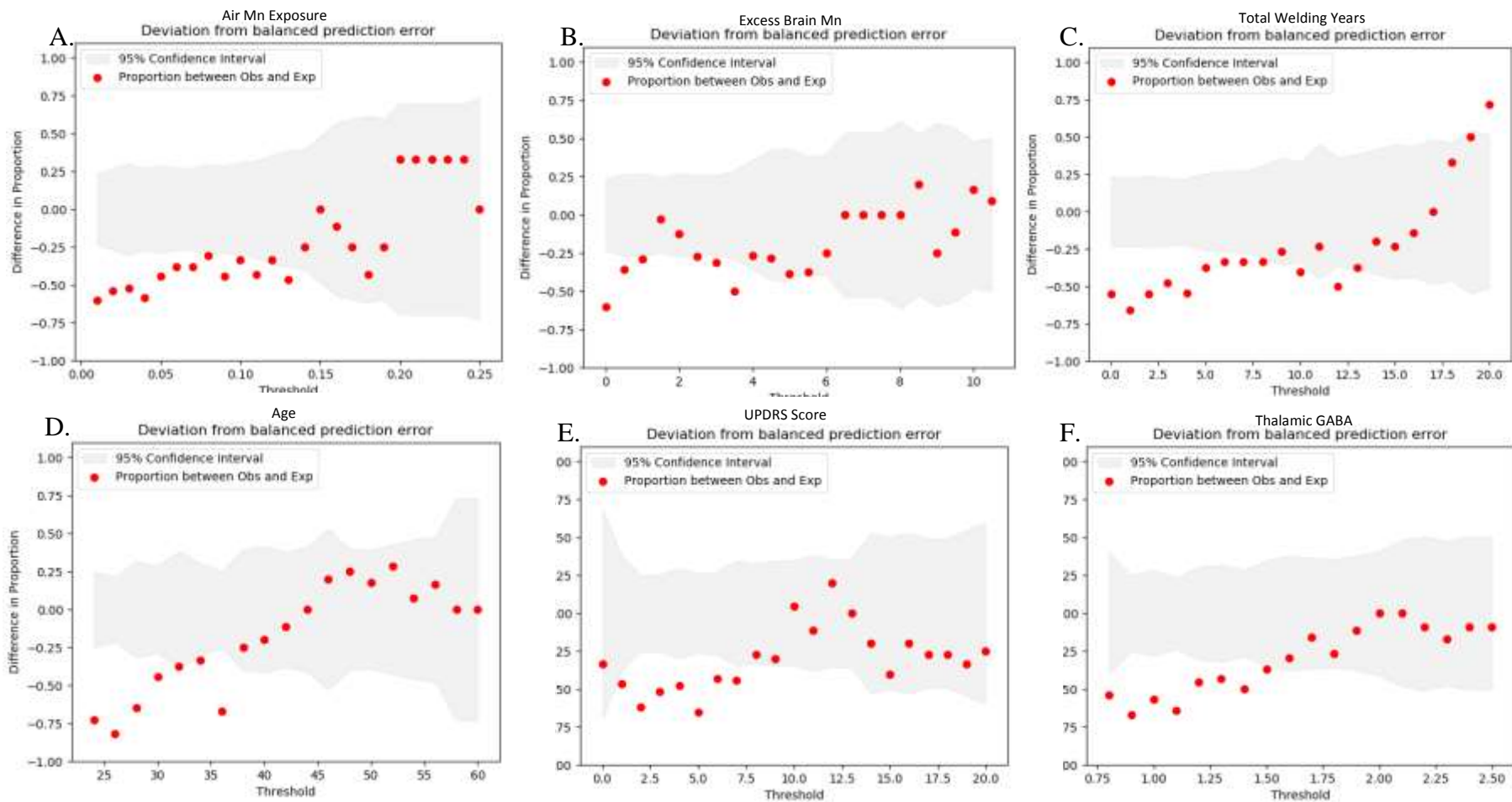


Figure 17 SVM Model Prediction Error Balance. Shows how balanced prediction error was for each threshold for the combined, or bagged, SVM model for all 6 targets: Air Mn Exposure, Excess brain Mn, Total Welding Years, Age, Thalamic GABA, and UPDRS Score.

4.4 Discussion

In this study, we tested a series of SVM models to measure how well R1 predicts groups of different targets: air Mn exposure, excess brain Mn, total years welding, age, UPDRS score, and thalamic GABA. Our results indicate that R1 may be a viable predictor for Mn exposure, Mn accumulation, years welding, and thalamic GABA. While we used four metrics for scoring our bagged SVM models, the focus of the discussion will be on how well each SVM model performed based on accuracy and recall. Accuracy was chosen because it accounts for all correct class 0 predictions, whereas the other metrics do not. We feel this is important to measure because knowing that the model can correctly identify subjects with low to none Mn exposure or accumulation in the brain is important for discerning how Mn affects R1. Recall was chosen to therefore account for how well the model can identify class 1 subjects out of all class 1 subjects available. This measure, therefore, differentiates how well R1 is affected by Mn in the presence of Mn and whether this signature difference is enough to identify subjects with Mn in their brain at certain thresholds.

First, we trained a SVM model to look at whether we could predict whether a subject was a welder or control. This model was accurate slightly better than chance. Because R1 is proportional to Mn in the region, it was hypothesized that getting an estimate for the amount of Mn in the brain would be a better measure for predictions with R1. While the SVM model predicting excess brain Mn was relatively accurate with accuracies greater than 70% above levels of 4mg, recall was around 40%, suggesting that the model was reasonably good at identify subjects below the threshold, but could only get 2 out of 5 subjects greater than the threshold. In comparison to the SVM model predicting air Mn exposure, recall remained better than chance while the model's accuracy increased with greater exposure levels. Therefore, it could be concluded that air Mn exposure at levels around 0.20 mg/m³ might provide identifiable

signatures of R1 that differentiate above and below that threshold. If a new welder worked in a space and breathed 0.20 mg/m^3 every day for 365 days, they would have an excess brain Mn level of approximately 5 mg, whereas a welder that breathed 0.16 mg/m^3 would have a level of approximately 4 mg. Because the biokinetic model takes into account previous exposures, these levels vary, which may be why accuracies and recall are different at these levels between the two models

There could be a couple reasons why this may be occurring. First, the biokinetic model may not be detailed enough to cover all the complexities of how Mn disperses through the brain. Mn which is bound to a protein or stored in an endosome will impact R1 significantly less than Mn that is free. Therefore, a biological model may need to take this into account and only calculate for the free Mn in the brain. A physiologically-based pharmacokinetic model (PBPK) has been developed that accounts for the different states of Mn, but only in select regions of the brain (Schroeter et al., 2011). When performing this study, it was determined that this may not be representative of the whole brain and so we chose to use a less complicated model that only considered the brain as its own compartment.

Additionally, because other Mn toxicity studies using MRI have used some metric of time spent welding as a proxy for exposure, we also trained a model to see if we could predict years welding. Not surprisingly, it performed similarly to our study group model for a threshold of 0 years and also had a recall score equal to accuracy of 61%. Additionally, as the threshold was increased, accuracy plateaued around 75% with recall also trending around 60%. We tested to verify that welding years were not correlated with air Mn exposure or excess brain Mn, and they were not.

We therefore ran a model looking at age as the target and found that the model performed with high 70s percent accuracy and greater than 80% recall across all regions, except for once the threshold was set to 55 years, recall dropped dramatically. This model was one of our strongest performing models, and even though there was a high correlation between years welding and age ($r = 0.73$, $p < 0.0001$, for welders only), this model performed better than the model predicting years welding. One thing this model does not take into account is cumulative Mn throughout a lifespan. In an earlier study, there is some evidence that cumulative Mn exposure may influence how R1 is impacted with additional Mn exposure where higher levels of cumulative Mn exposure will cause lower increases in R1 with current exposure. Recall plummeted for models with thresholds greater than or equal to 50, this may be because the majority of these subjects were welders (16 out of 21) with higher levels of cumulative exposure that prevented R1 from being predictive of the age. R1 may also simply be a better predictor of age for subjects that do not have enough Mn exposure to differentiate them from others in the same age class. Still, the overall improved performance of this model compared to other targets, such as air Mn exposure, needs to be further investigated.

Finally, we looked at two models that predicted biological effects from Mn, UPDRS score and thalamic GABA. Unfortunately, UPDRS scores were correlated with age (Pearson's product-moment correlation, $r = 0.48$, $p = < 0.0001$), so it is not surprising that the model performed similarly to the age model. Thalamic GABA was not correlated with age, but was correlated with air Mn exposure (Pearson's product-moment correlation, $r = 0.33$, $p = 0.001$). Similarly to the air Mn exposure model, accuracy increased with higher thresholds of thalamic GABA, but contrary to the air Mn exposure model, recall remained steadily high around 75%. So, while air Mn exposure was highly predictive at higher thresholds of exposure, generally

speaking, whole-brain R1 might be a better predictor for overall status of biochemical disruption from Mn exposure.

In conclusion, our study shows that R1 may be a viable predictor for assessing Mn exposure and the resulting effects in biochemistry as shown by thalamic GABA. Considering all models together, Mn air exposure may need to be at a higher threshold before it can differentiate subjects better than age. Nonetheless, because sample sizes are much smaller at higher thresholds, more data is needed to further improve these models.

5. CONCLUSIONS

5.1 Overview

Despite the complicated nature of working with large amounts of imaging data, this work shows that medical imaging can be used to explore the mechanism of Mn toxicity in humans.

Imaging is a powerful tool that allows us to observe effects of toxins within the brain.

Specifically, well-planned studies can test hypotheses driven by preclinical research in cell lines and animal models. In this thesis, we did that in all three aims. Specifically with the third aim, I show that there is great promise in using whole-brain MRI data and machine learning to extract more information – especially with metals that can be widespread within the brain.

5.2 Advances

This PhD thesis was successful in expanding on the current knowledge in the field of Mn toxicology. Advances were made in three primary categories: characterizing R1 as a measure of Mn exposure, understanding how symptoms of Mn toxicity are distinct from Parkinson's disease, and the advantage of using machine learning with imaging analysis. These are detailed next.

5.2.1 Changes in R1 are not linearly proportional with changes in Mn exposure

Aim 1 and Aim 3 were concerned with understanding how R1 changes with Mn exposure and Mn accumulation in the brain. Aim 1, as detailed in chapter 2, showed that R1 changes proportionately with Mn exposure while Aim 3, as detailed in chapter 4, showed that R1 is more predictive of subjects with higher levels of Mn exposure, but not quite as predictive for lower levels of estimated excess brain Mn. Together, both might be considered some evidence of a threshold effect, where below a certain exposure level, Mn does not accumulate in large enough

quantities to impact R1 reliably. There are a couple reasons for this threshold that one must consider. First, Mn is known to be heavily regulated by biliary clearance in the liver. While inhaled Mn bypasses the first-pass mechanism of clearance, when Mn is below a certain level, it will be removed from the blood. However, if the concentration of Mn is greater than the biliary clearance rate, it will remain in the blood and remain available for further uptake in the brain. Second, there may be a specific concentration of free Mn necessary to induce R1 contrast that provides signal above noise. Since Mn is readily sequestered in mitochondria and vacuoles, free Mn may not become readily available for contrast unless it reaches a certain concentration.

5.2.2 Machine learning can improve *in vivo* toxicology studies using medical imaging

Aim 3 effectively showed that whole-brain relaxometry could be used to predict classes of exposure or biological effects based on a moving threshold. This is consequential because one of the biggest limitations for toxicological studies using cell lines or animal studies is that their model is not human. Therefore, by maximizing the amount of information we can get out of our imaging, we are able to learn more about how a toxin might be affecting the target model, a human. Further studies could incorporate other types of sequencing, including diffusion weighted or diffusion tensor imaging, susceptibility, resting-state functional MRI, or spectroscopic imaging. With a proper data analysis flow path, the amount of hypothesis testing could be endless within a given study. However, none of this suppresses the need for further preclinical studies, as we simply cannot test some molecular interactions in humans. Nonetheless, reliable and robust methods of data analysis using machine learning could be used for hypothesis testing that comes from these studies. By itself, this is a powerful advancement made by this thesis.

5.2.3 Evidence of regions in the brain with increased susceptibility to Mn

This thesis points to there being three potential locations where Mn accumulation may be leading to the effects measured through PET and MRS, striatum, globus pallidus, and substantia nigra. First, we have evidence that Mn accumulates in all of these regions, but at varying degrees based on density of Mn-affine transporters and other proteins. However, each of these regions have different cells that may be more susceptible to Mn toxicity than others.

5.2.3.1 Striatal Mn susceptibility

In chapter 3 we found a negative correlation between baseline BP_{ND} in the ventral striatum and $Mn-CEI_{Life}$, suggesting a loss of D_2/D_3 receptors. As briefly mentioned in the introduction, Mn may enter the brain through the olfactory nerve and into the olfactory bulb. Consequently, one connection from the olfactory bulb to the ventral striatum is the olfactory tubercle (Xiong & Wesson, 2016). The relationship found in chapter 3 might suggest that this pathway could be more consequential for humans than previously thought. Considering that one of the first symptoms to occur from Mn toxicity is mood disturbances (Olanow, 2004), and that the ventral striatum is thought to play a critical role in the reward system, the loss of these receptors could be one of the early points of Mn susceptibility in the brain. However, since chapter 3 was only a pilot study, further investigation is required to confirm this hypothesis.

Additionally, a similar negative correlation was found between baseline BP_{ND} in the pre-commissural caudate and $Mn-CEI_{Life}$. Besides neurons that project from the striatum to the globus pallidus, there are cholinergic interneurons that also receive DA as an excitatory input, that could be a susceptible target for Mn (Bouabid, Tinakoua, Lakhdar-Ghazal, & Benazzouz, 2016). Mn-induced decreased cholinergic interneuronal activity could not only reduce thalamic

input to the striatum, but also impact emotional response circuits (Finkelstein, Milatovic, & Aschner, 2007).

5.2.3.2 Pallidal & Substantia Nigral Mn Susceptibility

GABAergic neurons in the globus pallidus and substantia nigra pars reticulata are potentially susceptible to Mn toxicity. This thesis also attempted to determine why thalamic GABA changes with changes in exposure. As shown in chapter 2, changes in R1 are representative of changes in short-term exposure windows and that rate of change might be affected by the total burden of Mn in the brain over a lifetime. As stated, R1 might best reflect the total amount of free Mn in the brain, rather than bound Mn. Additionally, in chapter 4, our SVM model using R1 to predict GABA was one of our better performing models across all thresholds of thalamic GABA concentration. Therefore, taken together, since R1 represents free Mn, thalamic GABA concentration may be related to the amount of free Mn available. This becomes consequential because other studies have shown Mn can inhibit GABA release (P. C. L. Wong et al., 1981) and binding of GABA to GABA_A receptors (Fishman et al., 1987). So, thalamic GABA may be a good indicator of how much free Mn is in the brain, reflective of short-term Mn exposure. Unfortunately, while we showed reversibility in thalamic GABA levels and R1 in chapter 2, there still exists the knowledge that overall motor symptoms become irreversible at some point. Therefore, while this may explain why GABA levels will fluctuate with Mn exposure, there remains a need to elucidate the mechanism by which long-term behavioral, cognitive, and motor deficits occur from Mn exposure.

5.3 Limitations and Future Directions

5.3.1 Limitations

Initially, one of the more disappointing results was the inability for the biokinetic model to be a better representation of R1 than air Mn exposure, as described in chapter 4. However, in hindsight, when considering the physics of how Mn influences R1 in the immediate area, this result is reasonable. The majority of the R1 contrast signal will come from free Mn, therefore, since we know Mn will bind to other proteins or be sequestered in vacuoles or the mitochondria, R1 will not represent the total amount of excess Mn in the brain based on exposure. Therefore, a more elaborate physiologically-based pharmacokinetic model should be used, but even now, the one that has been developed recently by Schroeter et al. (2012) only incorporates 3 regions of the brain: pituitary gland, cerebellum, and globus pallidus (Schroeter et al., 2012). Additionally, a model should account for anterograde transport along axons into cortical regions of the brain. If this becomes available, Mn accumulation in the brain may better represent R1 and a SVM model may perform significantly better predicting Mn accumulation than air Mn exposure.

Throughout, a low number of total subjects was an issue for all three studies in this thesis. In the longitudinal study described in chapter 2, there were only 17 subjects that participated in both scanning timepoints. In the PET study described in chapter 3, only 6 subjects participated. However, this was a pilot study and, fortunately, equal numbers of welders and controls participated. In chapter 4 where we used machine learning on whole-brain R1 maps, we used all available data from the first and second rounds of the longitudinal study and ended with 89 total subjects. While this is a reasonably large sample size for human studies, machine learning becomes much more informative when above 100 or even into the 1000s of subjects. While having that many is unlikely, doubling the total number of subjects would have led to significantly more generalizable models.

5.3.2 Measuring the Effect from Mixtures

Welding fume does not contain only Mn, but rather it is a mixture of metal particulate, including copper (Cu), iron (Fe), and zinc (Zn), as well as other trace metals. Fe is the major component in welding fume, making up about 55% of the total particulate. Mixtures have been given a prominent position in toxicological research since almost every toxin is comorbid with other known toxins, and welding fume is no exception. Much discussion has gone into how best to handle mixtures, including using more complicated statistical models, such as a mixed effects model. While this may be perfectly reasonable, the best way to disentangle the effects of different toxins within a mixture is to have a way of identifying each separately. Fortunately, with MRI we can do this with Mn and Fe. Much like Mn, Fe is also a contrast agent, however it is a T2* contrast agent due to its ferromagnetic properties. Briefly, when Fe is exposed to a magnetic field, it generates its own magnetic field which greatly increases the inhomogeneity in the region. However, Fe will still provide some T1 contrast, and as such may contribute to Mn T1 contrast. As mentioned in the introduction, Mn and Fe also compete for the same transporters in the brain.

Therefore, given rates of exposure to Mn and Fe, a future study could see how well R1 and R2* predict these exposure levels. But while there are more complicated PBPK models for modeling Mn uptake in the brain, nothing similar exists for Fe. In fact, most biokinetic models for Fe disregard the brain completely or include it under a miscellaneous tissue category. However, as was shown in chapter 4, R1 was a good predictor for Mn exposure at higher levels, so it is not unreasonable to assume that since Fe contribution in welding fume is 5x greater, R2* could be more sensitive. But, considering Mn has been shown able to out-compete Fe for transporters into neurons and glia, R2* may not reflect exposure at all. Thus, this could represent

some *in vivo* evidence that Mn is out competing Fe in humans suggesting that the primary metal of concern is Mn, and not a mixture.

Finally, while not approached in this thesis, using additional measures of contrast may be prudent for predicting how much exposure a subject has received. Future longitudinal studies might consider measuring three different measures of relaxometry: T1, T2, and T2*. The combined power of these three may lead to improved predictability as these three measures provide a clearer understanding of the microenvironment within each voxel.

5.4 Summary

There is plenty of room for future research using medical imaging to understand the mechanisms of Mn toxicity in humans. Aim 1 showed that R1 and GABA is dependent on Mn exposure and changes proportionately with changes in occupational Mn exposure. Aim 2, while a pilot study, showed that differences in Raclopride binding potential in the striatum might discriminate between motor dysfunction due to PD or Mn exposure. Aim 3 provided evidence that R1 is more predictive of higher levels of free Mn in the brain, reflective of higher Mn exposure and higher GABA levels. Additionally, aim 3 represented a successful implementation of machine learning for effectively maximizing data use provided by imaging to test hypotheses.

REFERENCES

- Albrecht, D. S., Skosnik, P. D., Vollmer, J. M., Brumbaugh, M. S., Perry, K. M., Mock, B. H., ... Yoder, K. K. (2013). Striatal D2/D3receptor availability is inversely correlated with cannabis consumption in chronic marijuana users. *Drug and Alcohol Dependence*, *128*(1–2), 52–57. <https://doi.org/10.1016/j.drugalcdep.2012.07.016>
- Antonini, A., Leenders, K., Reist, H., Thomann, R., Beer, H., & Locher, J. (1993). Effect of Age on D2 Dopamine Receptors in Normal Human Brain Measured by Positron Emission Tomography and 11C-Raclopride. *Archives of Neurology*, *50*(5), 474–480.
- Aschner, M., & Aschner, J. L. (1991). Manganese Neurotoxicity : Cellular Effects and Blood-Brain Barrier Transport. *Neuroscience & Biobehavioral Reviews*, *15*(28), 333–340.
- Au, C., Benedetto, A., & Aschner, M. (2008a). Manganese in Eukaryotes: the role of DMT1. *Neurotoxicology*, *29*(4), 569–576. <https://doi.org/10.1021/nl061786n>.Core-Shell
- Au, C., Benedetto, A., & Aschner, M. (2008b). Manganese transport in eukaryotes: The role of DMT1. *NeuroToxicology*, *29*, 569–576. <https://doi.org/10.1016/j.neuro.2008.04.022>
- Bailey, L. A., Kerper, L. E., & Goodman, J. E. (2018). Derivation of an occupational exposure level for manganese in welding fumes. *NeuroToxicology*, *64*, 166–176. <https://doi.org/10.1016/j.neuro.2017.06.009>
- Bedenk, B. T., Almeida-Corrêa, S., Jurik, A., Dedic, N., Grünecker, B., Genewsky, A. J., ... Wotjak, C. T. (2018). Mn²⁺dynamics in manganese-enhanced MRI (MEMRI): Cav1.2 channel-mediated uptake and preferential accumulation in projection terminals. *NeuroImage*, *169*(August 2017), 374–382. <https://doi.org/10.1016/j.neuroimage.2017.12.054>
- Bock, N. A., Paiva, F. F., Nascimento, G. C., Newman, J. D., & Silva, A. C. (2008). Cerebrospinal fluid to brain transport of manganese in a non-human primate revealed by MRI. *Brain Research*, *1198*, 160–170. <https://doi.org/10.1016/j.brainres.2007.12.065>
- Bonilla, E. (1978). Increased GABA content in caudate nucleus of rats after chronic manganese chloride administration. *Journal of Neurochemistry*, *31*(2), 551–552. <https://doi.org/10.1111/j.1471-4159.1978.tb02672.x>

- Borg, D. C., & Cotzias, G. C. (1958). Manganese Metabolism in Man: Rapid Exchange of MN56 with Tissue as Demonstrated by Blood Clearance and Liver Uptake. *Journal of Clinical Investigation*, 37(9), 1269–1278. <https://doi.org/10.1172/JCI103714>
- Bornhorst, J., Wehe, C. a, Hüwel, S., Karst, U., Galla, H.-J., & Schwerdtle, T. (2012). Impact of manganese on and transfer across blood-brain and blood-cerebrospinal fluid barrier in vitro. *The Journal of Biological Chemistry*, 287(21), 17140–17151. <https://doi.org/10.1074/jbc.M112.344093>
- Bouabid, S., Tinakoua, A., Lakhdar-Ghazal, N., & Benazzouz, A. (2016). Manganese neurotoxicity: behavioral disorders associated with dysfunctions in the basal ganglia and neurochemical transmission. *Journal of Neurochemistry*, 136(4), 677–691. <https://doi.org/10.1111/jnc.13442>
- Bowler, R., Gocheva, V., Harris, M., Ngo, L., Abdelouahab, N., Wilkinson, J., ... Roels, H. A. (2011). Prospective study on neurotoxic effects in manganese-exposed bridge construction welders. *NeuroToxicology*, 32(5), 596–605. <https://doi.org/10.1016/j.neuro.2011.06.004>
- Bowler, R., Gysens, S., Diamond, E., Nakagawa, S., Drezgic, M., & Roels, H. a. (2006). Manganese exposure: Neuropsychological and neurological symptoms and effects in welders. *NeuroToxicology*, 27(3), 315–326. <https://doi.org/10.1016/j.neuro.2005.10.007>
- Bowler, R., Lezak, M., Booty, A., Hartney, C., Mergler, D., Levin, J., & Zisman, F. (2001). Neuropsychological dysfunction, mood disturbance, and emotional status of munitions workers. *Applied Neuropsychology*, 8(2), 74–90. https://doi.org/10.1207/S15324826AN0802_2
- Bowler, R., Mergler, D., Sassine, M., Larribe, F., & Hudnell, K. (1999). Neuropsychiatric effects of manganese on mood. *Neurotoxicology*, 20(2–3), 367–378.
- Bowman, A. B., Kwakye, G. F., Herrero Hernández, E., & Aschner, M. (2011). Role of manganese in neurodegenerative diseases. *Journal of Trace Elements in Medicine and Biology*, 25(4), 191–203. <https://doi.org/10.1016/j.jtemb.2011.08.144>
- Breier, A., Su, T. P., Saunders, R., Carson, R. E., Kolachana, B. S., de Bartolomeis, A., ... Pickar, D. (1997). Schizophrenia is associated with elevated amphetamine-induced synaptic dopamine concentrations: evidence from a novel positron emission tomography method. *Proceedings of the National Academy of Sciences of the United States of America*, 94(6), 2569–2574. <https://doi.org/10.1073/pnas.94.6.2569>

- Burton, N. C., & Guilarte, T. R. (2009). Manganese neurotoxicity: Lessons learned from longitudinal studies in nonhuman primates. *Environmental Health Perspectives*, *117*(3), 325–332. <https://doi.org/10.1289/ehp.080035>
- Cárdenas, L., Houle, S., Kapur, S., & Busto, U. E. (2004). Oral D-Amphetamine Causes Prolonged Displacement of [¹¹C]Raclopride as Measured by PET. *Synapse*, *51*(1), 27–31. <https://doi.org/10.1002/syn.10282>
- Caseras, X., Lawrence, N. S., Murphy, K., Wise, R. G., & Phillips, M. L. (2013). Ventral striatum activity in response to reward: Differences between bipolar I and II disorders. *American Journal of Psychiatry*, *170*(5), 533–541. <https://doi.org/10.1176/appi.ajp.2012.12020169>
- Chen, J., Su, P., Luo, W., & Chen, J. (2018). Role of LRRK2 in manganese-induced neuroinflammation and microglial autophagy. *Biochemical and Biophysical Research Communications*, *498*(1), 171–177. <https://doi.org/10.1016/j.bbrc.2018.02.007>
- Chen, J. Y., Tsao, G. C., Zhao, Q., & Zheng, W. (2001). Differential cytotoxicity of Mn(II) and Mn(III): Special reference to mitochondrial [Fe-S] containing enzymes. *Toxicology and Applied Pharmacology*, *175*(2), 160–168. <https://doi.org/10.1006/taap.2001.9245>
- Chowdhury, F. a., O’Gorman, R. L., Nashef, L., Elwes, R. D., Edden, R. a., Murdoch, J. B., ... Richardson, M. P. (2014). Investigation of glutamine and GABA levels in patients with idiopathic generalized epilepsy using MEGAPRESS. *Journal of Magnetic Resonance Imaging*, *699*, 694–699. <https://doi.org/10.1002/jmri.24611>
- Christensen, K. A., Grant, D. M., Schulman, E. M., & Walling, C. (1974). Optimal determination of relaxation times of fourier transform nuclear magnetic resonance. Determination of spin-lattice relaxation times in chemically polarized species. *The Journal of Physical Chemistry*, *78*(19), 1971–1977. <https://doi.org/10.1021/j100612a022>
- Chuang, K.-H., Koretsky, A. P., & Sotak, C. H. (2009). Temporal changes in the T₁ and T₂ relaxation rates (ΔR_1 and ΔR_2) in the rat brain are consistent with the tissue-clearance rates of elemental manganese. *Magnetic Resonance in Medicine*, *61*(6), 1528–1532. <https://doi.org/10.1002/mrm.21962>
- Cook, D., Fahn, S., & Brait, K. (1974). Chronic manganese intoxication. *Archives of Neurology*, *30*(1), 59–64.

- Cotman, C. W., Haycock, J. W., & White, W. F. (1976). Stimulus- secretion coupling processes in brain: analysis of noradrenaline and gamma- aminobutyric acid release. *The Journal of Physiology*, *254*(2), 475–505. <https://doi.org/10.1113/jphysiol.1976.sp011241>
- Couper, J. (1837). On the effects of black oxide of manganese when inhaled into the lungs. *British Annals of Medicine Pharmacy, Vital Statistics, and General Science*, *1*, 41–42.
- Criswell, S. R., Nielsen, S. S., Warden, M., Perlmutter, J. S., Moerlein, S. M., Flores, H. P., ... Racette, B. A. (2018). [18F]FDOPA positron emission tomography in manganese-exposed workers. *NeuroToxicology*, *64*, 43–49. <https://doi.org/10.1016/j.neuro.2017.07.004>
- Criswell, S. R., Perlmutter, J. S., Huang, J. L., Golchin, N., Flores, H. P., Hobson, A., ... Racette, B. A. (2012). Basal ganglia intensity indices and diffusion weighted imaging in manganese-exposed welders. *Occupational and Environmental Medicine*, *69*(6), 437–443. <https://doi.org/10.1136/oemed-2011-100119>
- Criswell, S. R., Warden, M. N., Searles Nielsen, S., Perlmutter, J. S., Moerlein, S. M., Sheppard, L., ... Racette, B. A. (2018). Selective D2 receptor PET in manganese-exposed workers. *Neurology*, *91*(11), e1022–e1030. <https://doi.org/10.1212/WNL.00000000000006163>
- Deoni, S. C. L. (2007). High-resolution T1 mapping of the brain at 3T with driven equilibrium single pulse observation of T1 with high-speed incorporation of RF field inhomogeneities (DESPOT1-HIFI). *Journal of Magnetic Resonance Imaging*, *26*(4), 1106–1111. <https://doi.org/10.1002/jmri.21130>
- Dewey, S. L., Smith, G. S., Logan, J., King, P. T., Macgregor, R. R., Martin, T. P., ... Joanna, S. (1992). GABAergic Inhibition of Endogenous Dopamine viva with 11C-Raclopride and Positron Emission Release Measured Tomography in. *Receptor*, *12*(October).
- Dharmadhikari, S., Ma, R., Yeh, C.-L., Snyder, S., Zauber, S. E., & Dydak, U. (2015). MRS of basal-ganglia in Parkinson's Disease reveals higher GABA levels. In *23rd Annual Meeting & Exhibition International Society for Magnetic Resonance in Medicine* (p. 23:2209). Toronto, Canada.
- Dharmadhikari, S., Ma, R., Yeh, C.-L., Stock, A.-K., Snyder, S., Zauber, S. E., ... Beste, C. (2015). Striatal and thalamic GABA level concentrations play differential roles for the modulation of response selection processes by proprioceptive information. *NeuroImage*, *120*, 36–42. <https://doi.org/10.1016/j.neuroimage.2015.06.066>

- Dorman, D. C. (2006). Correlation of Brain Magnetic Resonance Imaging Changes with Pallidal Manganese Concentrations in Rhesus Monkeys Following Subchronic Manganese Inhalation. *Toxicological Sciences*, 92(1), 219–227. <https://doi.org/10.1093/toxsci/kfj209>
- Drevets, W. C., Price, J. L., & Furey, M. L. (2008). Brain structural and functional abnormalities in mood disorders: Implications for neurocircuitry models of depression. *Brain Structure and Function*, 213(1–2), 93–118. <https://doi.org/10.1007/s00429-008-0189-x>
- Dydak, U., Dharmadhikari, S., Snyder, S., & Zauber, S. E. (2015). Increased Thalamic GABA Levels Correlate with Parkinson Disease Severity. In *AD/PD Conference*. Nice, France.
- Dydak, U., Jiang, Y., Long, L., Zhu, H., Chen, J., Li, W., ... Zheng, W. (2011). In vivo measurement of brain GABA concentrations by magnetic resonance spectroscopy in smelters occupationally exposed to manganese. *Environmental Health Perspectives*, 119(2), 219–224.
- Edmondson, D., Ma, R., Yeh, C.-L., Ward, E. J., Snyder, S., Zauber, S. E., ... Dydak, U. (2015). Increased GABA levels in manganese-exposed welders correlate with exposure, brain manganese, cognitive function, and motor function. *Neurotoxicology and Teratology*, 49, 121. <https://doi.org/10.1016/j.ntt.2015.04.071>
- Erikson, K. M., & Aschner, M. (2003). Manganese neurotoxicity and glutamate-GABA interaction. *Neurochemistry International*, 43(4–5), 475–480. [https://doi.org/10.1016/S0197-0186\(03\)00037-8](https://doi.org/10.1016/S0197-0186(03)00037-8)
- Eriksson, H., Tedroff, J., Thuomas, K.-Å., Aquilonius, S.-M., Hartvig, P., Fasth, K.-J., ... Heilbronn, E. (1992). Manganese induced brain lesions in *Macaca fascicularis* as revealed by positron emission tomography and magnetic resonance imaging. *Archives of Toxicology*, 66(6), 403–407.
- Fan, Rong-En, et al. (2008). LIBLINEAR: A library for large linear classification. *Journal of Machine Learning Research*, 9(2008), 1871–1874. Retrieved from <http://www.jmlr.org/papers/v9/fan08a.html>
- Finkelstein, Y., Milatovic, D., & Aschner, M. (2007). Modulation of cholinergic systems by manganese. *NeuroToxicology*, 28(5 SPEC. ISS.), 1003–1014. <https://doi.org/10.1016/j.neuro.2007.08.006>

- Fishman, B. E., McGinley, P. A., & Gianutsos, G. (1987). Neurotoxic effects of methylcyclopentadienyl manganese tricarbonyl (MMT) in the mouse: Basis of MMT-induced seizure activity. *Toxicology*, *45*(2), 193–201. [https://doi.org/10.1016/0300-483X\(87\)90105-3](https://doi.org/10.1016/0300-483X(87)90105-3)
- Fitsanakis, V. a, Au, C., Erikson, K. M., & Aschner, M. (2006). The effects of manganese on glutamate, dopamine and gamma-aminobutyric acid regulation. *Neurochemistry International*, *48*(6–7), 426–433. <https://doi.org/10.1016/j.neuint.2005.10.012>
- García-Hevia, L., Bañobre-López, M., & Gallo, J. (2019). Recent Progress on Manganese-Based Nanostructures as Responsive MRI Contrast Agents. *Chemistry - A European Journal*, *25*(2), 431–441. <https://doi.org/10.1002/chem.201802851>
- Gerfen, C., & Bolam, J. (2016). The Neuroanatomical Organization of the Basal Ganglia. In H. Steiner & K. Tseng (Eds.), *Handbook of Basal Ganglia Structure and Function* (2nd ed., pp. 3–31). <https://doi.org/dx.doi.org/10.1016/b978-0-12-802206-1.00001-5>
- Goetz, C. G., Tilley, B. C., Shaftman, S. R., Stebbins, G. T., Fahn, S., Martinez-Martin, P., ... Zweig, R. M. (2008). Movement Disorder Society-Sponsored Revision of the Unified Parkinson's Disease Rating Scale (MDS-UPDRS): Scale presentation and clinimetric testing results. *Movement Disorders*, *23*(15), 2129–2170. <https://doi.org/10.1002/mds.22340>
- Grashow, R., Zhang, J., Fang, S. C., Weisskopf, M. G., Christiani, D. C., & Cavallari, J. M. (2014). Toenail metal concentration as a biomarker of occupational welding fume exposure. *Journal of Occupational and Environmental Hygiene*, *11*(6), 397–405. <https://doi.org/10.1080/15459624.2013.875182>
- Guilarte, T. R. (2013). Manganese neurotoxicity: new perspectives from behavioral, neuroimaging, and neuropathological studies in humans and non-human primates. *Frontiers in Aging Neuroscience*, *5*(June), 23. <https://doi.org/10.3389/fnagi.2013.00023>
- Guilarte, T. R., Burton, N. C., McGlothan, J. L., Verina, T., Zhou, Y., Alexander, M., ... Schneider, J. S. (2008). Impairment of nigrostriatal dopamine neurotransmission by manganese is mediated by pre-synaptic mechanism(s): implications to manganese-induced parkinsonism. *Journal of Neurochemistry*, *107*(5), 1236–1247. <https://doi.org/10.1111/j.1471-4159.2008.05695.x>

- Guilarte, T. R., Chen, M.-K., McGlothan, J. L., Verina, T., Wong, D. F., Zhou, Y., ... Schneider, J. S. (2006). Nigrostriatal dopamine system dysfunction and subtle motor deficits in manganese-exposed non-human primates. *Experimental Neurology*, *202*(2), 381–390. <https://doi.org/10.1016/j.expneurol.2006.06.015>
- Guilarte, T. R., & Gonzales, K. K. (2015a). Manganese-induced parkinsonism is not idiopathic Parkinson's disease: Environmental and genetic evidence. *Toxicological Sciences*, *146*(2), 204–212. <https://doi.org/10.1093/toxsci/kfv099>
- Guilarte, T. R., & Gonzales, K. K. (2015b). Manganese-Induced Parkinsonism Is Not Idiopathic Parkinson's Disease: Environmental and Genetic Evidence. *Toxicological Sciences*, *146*(2), 204–212. <https://doi.org/10.1093/toxsci/kfv099>
- Hazell, A. S. (2002). Astrocytes and manganese neurotoxicity. *Neurochemistry International*, *41*, 271–277.
- Huang, C.-C. (2005). Parkinsonism induced by chronic manganese intoxication--an experience in Taiwan. *Chang Gung Medical Journal*, *30*(5), 385–395. <https://doi.org/10.1212/01.WNL.0000166916.40902.63>
- Ichise, M., Liow, J.-S. S., Lu, J.-Q. Q., Takano, A., Model, K., Toyama, H., ... Carson, R. E. (2003). Linearized reference tissue parametric imaging methods: application to [11C]DASB positron emission tomography studies of the serotonin transporter in human brain. *Journal of Cerebral Blood Flow and Metabolism : Official Journal of the International Society of Cerebral Blood Flow and Metabolism*, *23*(9), 1096–1112. <https://doi.org/10.1097/01.WCB.0000085441.37552.CA>
- Innis, R. B., Cunningham, V. J., Delforge, J., Fujita, M., Gjedde, A., Gunn, R. N., ... Carson, R. E. (2007). Consensus nomenclature for in vivo imaging of reversibly binding radioligands. *Journal of Cerebral Blood Flow and Metabolism*, *27*(9), 1533–1539. <https://doi.org/10.1038/sj.jcbfm.9600493>
- Jankovic, J. (2008). Parkinson's disease: clinical features and diagnosis. *Journal of Neurology, Neurosurgery & Psychiatry*, *79*(4), 368–376. <https://doi.org/10.1136/jnnp.2007.131045>
- K. Yoder, K., A. Kareken, D., & D. Morris, E. (2011). Assessing Dopaminergic Neurotransmission with PET: Basic Theory and Applications in Alcohol Research. *Current Medical Imaging Reviews*, *7*(2), 118–124. <https://doi.org/10.2174/157340511795445694>

- Karki, P., Lee, E., & Aschner, M. (2013). Manganese Neurotoxicity: a Focus on Glutamate Transporters. *Annals of Occupational and Environmental Medicine*, 25(1), 4. <https://doi.org/10.1186/2052-4374-25-4>
- Laruelle, M. (2000). Imaging synaptic neurotransmission with in vivo binding competition techniques: A critical review. *Journal of Cerebral Blood Flow and Metabolism*, 20(3), 423–451. <https://doi.org/10.1097/00004647-200003000-00001>
- Lee, E. Y., Flynn, M. R., Du, G., Lewis, M. M., Fry, R., Herring, A. H., ... Huang, X. (2015). T1 relaxation rate (R1) indicates nonlinear Mn accumulation in brain tissue of welders with low-level exposure. *Toxicological Sciences*, 146(2), 281–289. <https://doi.org/10.1093/toxsci/kfv088>
- Lee, E. Y., Flynn, M. R., Lewis, M. M., Mailman, R. B., & Huang, X. (2018). Welding-related brain and functional changes in welders with chronic and low-level exposure. *NeuroToxicology*, 64, 50–59. <https://doi.org/10.1016/j.neuro.2017.06.011>
- Leggett, R. W. (2011). A biokinetic model for manganese. *The Science of the Total Environment*, 409(20), 4179–4186. <https://doi.org/10.1016/j.scitotenv.2011.07.003>
- Lehallier, B., Coureaud, G., Maurin, Y., & Bonny, J.-M. (2012). Effects of manganese injected into rat nostrils: implications for in vivo functional study of olfaction using MEMRI. *Magnetic Resonance Imaging*, 30(1), 62–69. <https://doi.org/10.1016/j.mri.2011.08.009>
- Leuze, C., Kimura, Y., Kershaw, J., Shibata, S., Saga, T., Chuang, K.-H., ... Aoki, I. (2012). Quantitative measurement of changes in calcium channel activity in vivo utilizing dynamic manganese-enhanced MRI (dMEMRI). *NeuroImage*, 60(1), 392–399. <https://doi.org/10.1016/j.neuroimage.2011.12.030>
- Lewis, M. M., Flynn, M. R., Lee, E. Y., Van Buren, S., Van Buren, E., Du, G., ... Huang, X. (2016). Longitudinal T1 relaxation rate (R1) captures changes in short-term Mn exposure in welders. *NeuroToxicology*, 57, 39–44. <https://doi.org/10.1016/j.neuro.2016.08.012>
- Liu, M., Cai, T., Zhao, F., Zheng, G., Wang, Q., Chen, Y., ... Chen, J. (2009). Effect of microglia activation on dopaminergic neuronal injury induced by manganese, and its possible mechanism. *Neurotoxicity Research*, 16(1), 42–49. <https://doi.org/10.1007/s12640-009-9045-x>

- Long, Z., Dyke, J. P., Ma, R., Huang, C. C., Louis, E. D., & Dydak, U. (2015). Reproducibility and effect of tissue composition on cerebellar γ -aminobutyric acid (GABA) MRS in an elderly population. *NMR in Biomedicine*, *28*(10), 1315–1323.
<https://doi.org/10.1002/nbm.3381>
- Long, Z., Jiang, Y.-M. M., Li, X.-R. R., Fadel, W., Xu, J., Yeh, C.-L. L., ... Dydak, U. (2014). Vulnerability of welders to manganese exposure – A neuroimaging study. *NeuroToxicology*, *45*, 285–292. <https://doi.org/10.1016/j.neuro.2014.03.007>
- Long, Z., Li, X.-R. R., Xu, J., Edden, R. A. E. E., Qin, W.-P. P., Long, L.-L. L., ... Dydak, U. (2014). Thalamic GABA Predicts Fine Motor Performance in Manganese-Exposed Smelter Workers. *PLoS ONE*, *9*(2), e88220. <https://doi.org/10.1371/journal.pone.0088220>
- Ma, R. E., Ward, E. J., Yeh, C.-L. L., Snyder, S., Long, Z., Gokalp Yavuz, F., ... Dydak, U. (2017). Thalamic GABA levels and occupational manganese neurotoxicity: Association with exposure levels and brain MRI. *NeuroToxicology*, *64*, 30–42.
<https://doi.org/10.1016/j.neuro.2017.08.013>
- Martinez, D., Slifstein, M., Broft, A., Mawlawi, O., Hwang, D. R., Huang, Y., ... Laruelle, M. (2003). Imaging human mesolimbic dopamine transmission with positron emission tomography. Part II: Amphetamine-induced dopamine release in the functional subdivisions of the striatum. *Journal of Cerebral Blood Flow and Metabolism*, *23*(3), 285–300.
<https://doi.org/10.1097/01.WCB.0000048520.34839.1A>
- Massano, J., & Bhatia, K. P. (2012). Clinical approach to Parkinson's disease: Features, diagnosis, and principles of management. *Cold Spring Harbor Perspectives in Medicine*, *2*(6), 1–15. <https://doi.org/10.1101/cshperspect.a008870>
- Mena, I., Marin, O., Fuenzalida, S., & Cotzias, G. (1967). Chronic manganese poisoning. Clinical picture and manganese turnover. *Neurology*, *17*(2), 128–136.
- Meyer-Baron, M., Schäper, M., Knapp, G., Lucchini, R., Zoni, S., Bast-Pettersen, R., ... van Thriel, C. (2013). The neurobehavioral impact of manganese: Results and challenges obtained by a meta-analysis of individual participant data. *NeuroToxicology*, *36*, 1–9.
<https://doi.org/10.1016/j.neuro.2013.02.003>

- Morris, E. D., Chefer, S. I., Lane, M. A., Muzic, R. F., Wong, D. F., Dannals, R. F., ... London, E. D. (1999). Loss of D2 receptor binding with age in rhesus monkeys: Importance of correction for differences in striatal size. *Journal of Cerebral Blood Flow and Metabolism*, *19*(2), 218–229. <https://doi.org/10.1097/00004647-199902000-00013>
- Morris, E., Lucas, M., & Cosgrove, K. (2013). How to Study Smoking and Drinking with PET. In *Positron Emission Tomography - Recent Developments in Instrumentation, Research and Clinical Oncological Practice*. InTech. <https://doi.org/10.5772/57414>
- Mortimer, J. A., Borenstein, A. R., & Nelson, L. M. (2012). Association of welding and manganese exposure with Parkinson disease. *Neurology*, *79*(December 2011), 1174–1180.
- Mullins, P. G., Mcgonigle, D. J., O’Gorman, R. L., Puts, N. A. J. J., Vidyasagar, R., Evans, C. J., ... Wilson, M. (2014). Current practice in the use of MEGA-PRESS spectroscopy for the detection of GABA. *NeuroImage*, *86*, 43–52. <https://doi.org/10.1016/j.neuroimage.2012.12.004>
- Narendran, R., Frankle, W. G., Mason, N. S., Rabiner, E. A., Gunn, R. N., Searle, G. E., ... Laruelle, M. (2009). Positron Emission Tomography Imaging of Amphetamine-Induced Dopamine Release in the Human Cortex: A comparative evaluation of the high affinity dopamine D2/3 radiotracers [¹¹C]FLB 457 and [¹¹C]Fallypride. *Synapse*, *63*(6), 447–461. <https://doi.org/10.1002/syn.20628>
- Nong, A., Taylor, M. D., Clewell, H. J., Dorman, D. C., & Andersen, M. E. (2009). Manganese tissue dosimetry in rats and monkeys: Accounting for dietary and inhaled Mn with physiologically based pharmacokinetic modeling. *Toxicological Sciences*, *108*(1), 22–34. <https://doi.org/10.1093/toxsci/kfn264>
- Nong, A., Teeguarden, J. G., Clewell, H. J., Dorman, D. C., & Andersen, M. E. (2008). Pharmacokinetic modeling of manganese in the rat IV: Assessing factors that contribute to brain accumulation during inhalation exposure. *Journal of Toxicology and Environmental Health. Part A*, *71*(7), 413–426. <https://doi.org/10.1080/15287390701838697>
- O’Gorman Tuura, R. L., Baumann, C. R., & Baumann-Vogel, H. (2018). Neurotransmitter activity is linked to outcome following subthalamic deep brain stimulation in Parkinson’s disease. *Parkinsonism and Related Disorders*, *50*, 54–60. <https://doi.org/10.1016/j.parkreldis.2018.02.014>

- O'Neal, S. L., Lee, J.-W., Zheng, W., & Cannon, J. R. (2014). Subacute manganese exposure in rats is a neurochemical model of early manganese toxicity. *Neurotoxicology*, *44*, 303–313. <https://doi.org/10.1016/j.neuro.2014.08.001>
- O'Neal, S. L., & Zheng, W. (2015). Manganese Toxicity Upon Overexposure: a Decade in Review. *Current Environmental Health Reports*, *2*(3), 315–328. <https://doi.org/10.1007/s40572-015-0056-x>
- Olanow, C. W. (2004). Manganese-Induced Parkinsonism and Parkinson's Disease. *Annals of the New York Academy of Sciences*, *1012*(1), 209–223. <https://doi.org/10.1196/annals.1306.018>
- Pan, D., Schmieder, A. H., Wickline, S. a, & Lanza, G. M. (2011). Manganese-based MRI contrast agents: past, present and future. *Tetrahedron*, *67*(44), 8431–8444. <https://doi.org/10.1016/j.tet.2011.07.076>
- Park, J. D., Chung, Y. H., Kim, C. Y., Ha, C. S., Yang, S. O., Khang, H. S., ... Yu, I. J. (2007). Comparison of high MRI T1 signals with manganese concentration in brains of cynomolgus monkeys after 8 months of stainless steel welding-fume exposure. *Inhalation Toxicology*, *19*(11), 965–971. <https://doi.org/10.1080/08958370701516108>
- Park, R. M., Bouchard, M. F., Baldwin, M., Bowler, R., & Mergler, D. (2014). Respiratory manganese particle size, time-course and neurobehavioral outcomes in workers at a manganese alloy production plant. *NeuroToxicology*, *45*, 276–284. <https://doi.org/10.1016/j.neuro.2014.03.015>
- Pedregosa, F., Varoquaux, G., Gramfort, A., Michel, V., Thirion, B., Grisel, O., ... Duchesnay, É. (2012). Scikit-learn: Machine Learning in Python. *Journal of Machine Learning Research*, *12*, 2825–2830. <https://doi.org/10.1007/s13398-014-0173-7.2>
- Perl, D. P., & Olanow, C. W. (2007). The Neuropathology of Manganese-Induced Parkinsonism. *Journal of Neuropathology and Experimental Neurology*, *66*(8), 675–682.
- Provencher, S. W. (1993). Estimation of metabolite concentrations from localized in vivo proton NMR spectra. *Magnetic Resonance in Medicine*, *30*(6), 672–679. <https://doi.org/10.1002/mrm.1910300604>
- R Core Team. (2013). R: A language and environment for statistical computing. Vienna, Austria: R Foundation for Statistical Computing.

- Racette, B. A., Aschner, M., Guilarte, T. R., Dydak, U., Criswell, S. R., & Zheng, W. (2012). Pathophysiology of manganese-associated neurotoxicity. *Neurotoxicology*, *33*(4), 881–886. <https://doi.org/10.1016/j.neuro.2011.12.010>
- Racette, B. A., Criswell, S. R., Lundin, J. I., Hobson, A., Seixas, N., Kotzbauer, P. T., ... Checkoway, H. (2012). Increased risk of parkinsonism associated with welding exposure. *NeuroToxicology*, *33*(5), 1356–1361. <https://doi.org/10.1016/j.neuro.2012.08.011>
- Racette, B. A., Criswell, S. R., Perlmutter, J. S., Videen, T. O., Moerlein, S. M., Flores, H. P., ... Racette, B. a. (2011). Reduced uptake of [18F]FDOPA PET in asymptomatic welders with occupational manganese exposure. *Neurology*, *76*(15), 1296–1301. <https://doi.org/10.1212/WNL.0b013e3182152830>
- Racette, B. A., Nielsen, S. S., Criswell, S. R., Sheppard, L., Seixas, N., Warden, M. N., & Checkoway, H. (2017). Dose-dependent progression of parkinsonism in manganese-exposed welders. *Neurology*, *88*(4), 344–351. <https://doi.org/10.1212/WNL.0000000000003533>
- Ramoju, S. P., Mattison, D. R., Milton, B., McGough, D., Shilnikova, N., Clewell, H. J., ... Andersen, M. E. (2017). The application of PBPK models in estimating human brain tissue manganese concentrations. *NeuroToxicology*, *58*, 226–237. <https://doi.org/10.1016/j.neuro.2016.12.001>
- Reiss, B., Simpson, C. D., Baker, M. G., Stover, B., Sheppard, L., & Seixas, N. S. (2015). Hair Manganese as an Exposure Biomarker among Welders. *Annals of Occupational Hygiene*, *60*(2), 139–149. <https://doi.org/10.1093/annhyg/mev064>
- Sabati, M., & Maudsley, A. A. (2013). Fast and high-resolution quantitative mapping of tissue water content with full brain coverage for clinically-driven studies. *Magnetic Resonance Imaging*, *31*(10), 1752–1759. <https://doi.org/10.1016/j.mri.2013.08.001>
- Saleem, K. S., Pauls, J. M., Augath, M., Trinath, T., Prause, B. A., Hashikawa, T., & Logothetis, N. K. (2002). Magnetic resonance imaging of neuronal connections in the Macaque Monkey. *Neuron*, *34*(5), 685–700. [https://doi.org/10.1016/S0896-6273\(02\)00718-3](https://doi.org/10.1016/S0896-6273(02)00718-3)
- Schroeter, J. D., Dorman, D. C., Yoon, M., Nong, A., Taylor, M. D., Andersen, M. E., & Clewell, H. J. (2012). Application of a multi-route physiologically based pharmacokinetic model for manganese to evaluate dose-dependent neurological effects in monkeys. *Toxicological Sciences*, *129*(2), 432–446. <https://doi.org/10.1093/toxsci/kfs212>

- Schroeter, J. D., Nong, A., Yoon, M., Taylor, M. D., Dorman, D. C., Andersen, M. E., & Clewell, H. J. (2011). Analysis of manganese tracer kinetics and target tissue dosimetry in monkeys and humans with multi-route physiologically based pharmacokinetic models. *Toxicological Sciences*, *120*(2), 481–498. <https://doi.org/10.1093/toxsci/kfq389>
- Seeman, P., Guan, H.-C., & Niznik, H. B. (1989). Endogenous dopamine lowers the dopamine D2 receptor density as measured by [3H]raclopride: Implications for positron emission tomography of the human brain. *Synapse*, *3*(1), 96–97. <https://doi.org/10.1002/syn.890030113>
- Seth, P., & Chandra, S. (1984). Neurotransmitters and neurotransmitter receptors in developing and adult rats during manganese poisoning. *Neurotoxicology*, *5*(1), 67–76.
- Shinotoh, H., Snow, B. J., Chu, N. S., Huang, C. C., Lu, C. S., Lee, C., ... Calne, D. B. (1997). Presynaptic and postsynaptic striatal dopaminergic function in patients with manganese intoxication: a positron emission tomography study. *Neurology*, *48*(4), 1053–1056. <https://doi.org/10.1212/WNL.48.4.1053>
- Shinotoh, H., Snow, B. J., Hewitt, K. a, Pate, B. D., Doudet, D., Nugent, R., ... Calne, D. B. (1995). MRI and PET studies of manganese-intoxicated monkeys. *Neurology*. <https://doi.org/10.1212/WNL.45.6.1199>
- Sidoryk-Wegrzynowicz, M., & Aschner, M. (2013). Manganese toxicity in the central nervous system: the glutamine/glutamate- γ -aminobutyric acid cycle. *Journal of Internal Medicine*, *273*(5), 466–477. <https://doi.org/10.1111/joim.12040>
- Sidoryk-Wegrzynowicz, M., & Aschner, M. (2013). Role of astrocytes in manganese mediated neurotoxicity. *BMC Pharmacology and Toxicology*, *14*, 1–10. <https://doi.org/10.1186/2050-6511-14-23>
- Taylor, M. D., Clewell, H. J., Andersen, M. E., Schroeter, J. D., Yoon, M., Keene, A. M., & Dorman, D. C. (2012). Update on a pharmacokinetic-centric Alternative Tier II program for MMT-part II: Physiologically based pharmacokinetic modeling and manganese risk assessment. *Journal of Toxicology*, *2012*. <https://doi.org/10.1155/2012/791431>
- Teeguarden, J. G., Gearhart, J., Clewell, H. J., Covington, T. R., Nong, A., & Andersen, M. E. (2007). Pharmacokinetic modeling of manganese. III. Physiological approaches accounting for background and tracer kinetics. *Journal of Toxicology and Environmental Health. Part A*, *70*(18), 1515–1526. <https://doi.org/10.1080/15287390701384635>

- Tran, T. T., Chowanadisai, W., Crinella, F. M., Chicz-DeMet, A., & Lönnerdal, B. (2002). Effect of high dietary manganese intake of neonatal rats on tissue mineral accumulation, striatal dopamine levels, and neurodevelopmental status. *NeuroToxicology*, *23*(4–5), 635–643. [https://doi.org/10.1016/S0161-813X\(02\)00091-8](https://doi.org/10.1016/S0161-813X(02)00091-8)
- Tsuboi, Y., Uchikado, H., & Dickson, D. W. (2007). Neuropathology of Parkinson's disease dementia and dementia with Lewy bodies with reference to striatal pathology. *Parkinson's Disease and Movement Disorders*, *13*, S221–S224. [https://doi.org/10.1016/S1353-8020\(08\)70005-1](https://doi.org/10.1016/S1353-8020(08)70005-1)
- Tuschl, K., Mills, P. B., & Clayton, P. T. (2013). Manganese and the Brain. In *International Review of Neurobiology* (pp. 277–312). <https://doi.org/10.1016/B978-0-12-410502-7.00013-2>
- Wang, G. J., Volkow, N. D., Fowler, J. S., Logan, J., Pappas, N. R., Wong, C. T., ... Netusil, N. (1999). Reproducibility of repeated measures of endogenous dopamine competition with [¹¹C]raclopride in the human brain in response to methylphenidate. *Journal of Nuclear Medicine: Official Publication, Society of Nuclear Medicine*, *40*(8), 1285–1291. Retrieved from <http://www.ncbi.nlm.nih.gov/pubmed/10450679>
- Ward, E. J., Edmondson, D. A., Nour, M. M., Snyder, S., Rosenthal, F. S., & Dydak, U. (2017). Toenail Manganese: A Sensitive and Specific Biomarker of Exposure to Manganese in Career Welders. *Annals of Work Exposures and Health*, *62*(1), 101–111. <https://doi.org/10.1093/annweh/wxx091>
- Wong, D. F., Wagner, H. N., Dannals, R. F., Links, J. M., Frost, J. J., Ravert, H. T., ... Kuhar, M. J. (1984). Effects of Age on Dopamine and Serotonin Receptors Measured by Positron Tomography in the Living Human Brain. *Science*, *226*(4681), 1393–1396. Retrieved from <http://www.jstor.org.ezproxy.lib.purdue.edu/stable/1693892>
- Wong, P. C. L., Lai, J. C. K., Lim, L., & Davison, A. N. (1981). Selective inhibition of L-glutamate and gammaaminobutyrate transport in nerve ending particles by aluminium, manganese, and cadmium chloride. *Journal of Inorganic Biochemistry*, *14*(3), 253–260. [https://doi.org/10.1016/S0162-0134\(00\)80005-7](https://doi.org/10.1016/S0162-0134(00)80005-7)
- Xiong, A., & Wesson, D. W. (2016). Illustrated review of the ventral striatum's olfactory tubercle. *Chemical Senses*, *41*(7), 549–555. <https://doi.org/10.1093/chemse/bjw069>

- Yamada, M., Ohno, S., Okayasu, I., Okeda, R., Hatakeyama, S., Watanabe, H., ... Tsukagoshi, H. (1986). Chronic manganese poisoning: A neuropathological study with determination of manganese distribution in the brain. *Acta Neuropathologica*, 70(3–4), 273–278.
<https://doi.org/10.1007/BF00686083>
- Yeh, C.-L., Ward, E. J., Ma, R., Snyder, S., Schmidt-Wilcke, T., & Dydak, U. (2016). P125 Whole-brain r1 mapping of manganese in welders - visualisation of increased mn levels in the brain. *Occupational and Environmental Medicine*, 73(Suppl 1), A161 LP-A161.
<https://doi.org/10.1136/oemed-2016-103951.442>
- Yip, S. W., Worhunsky, P. D., Rogers, R. D., & Goodwin, G. M. (2015). Hypoactivation of the ventral and dorsal striatum during reward and loss anticipation in antipsychotic and mood stabilizer-naive bipolar disorder. *Neuropsychopharmacology*, 40(3), 658–666.
<https://doi.org/10.1038/npp.2014.215>
- Yoder, K. K., Albrecht, D. S., Dzemidzic, M., Normandin, M. D., Federici, L. M., Graves, T., ... Kareken, D. A. (2016). Differences in IV alcohol-induced dopamine release in the ventral striatum of social drinkers and nontreatment-seeking alcoholics. *Drug and Alcohol Dependence*, 160, 163–169. <https://doi.org/10.1016/j.drugalcdep.2016.01.001>
- Yoder, K. K., Constantinescu, C. C., Kareken, D. A., Normandin, M. D., Cheng, T. E., O'Connor, S. J., & Morris, E. D. (2007). Heterogeneous effects of alcohol on dopamine release in the striatum: A PET study. *Alcoholism: Clinical and Experimental Research*, 31(6), 965–973. <https://doi.org/10.1111/j.1530-0277.2007.00390.x>
- Yoder, K. K., Kareken, D. A., Seyoum, R. A., O'Connor, S. J., Wang, C., Zheng, Q.-H., ... Morris, E. D. (2005). Dopamine D2 Receptor Availability is Associated with Subjective Responses to Alcohol. *Alcoholism: Clinical & Experimental Research*, 29(6), 965–970.
<https://doi.org/10.1097/01.ALC.0000171041.32716.42>
- Yoder, K. K., Wang, C., & Morris, E. D. (2004). Change in binding potential as a quantitative index of neurotransmitter release is highly sensitive to relative timing and kinetics of the tracer and the endogenous ligand. *Journal of Nuclear Medicine : Official Publication, Society of Nuclear Medicine*, 45(5), 903–911.
- Yokel, R. a. (2009). Manganese flux across the blood-brain barrier. *Neuromolecular Medicine*, 11(4), 297–310. <https://doi.org/10.1007/s12017-009-8101-2>

Zhou, Y., Chen, M. K., Endres, C. J., Ye, W., Brašić, J. R., Alexander, M., ... Wong, D. F. (2006). An extended simplified reference tissue model for the quantification of dynamic PET with amphetamine challenge. *NeuroImage*, 33(2), 550–563.
<https://doi.org/10.1016/j.neuroimage.2006.06.038>